DEVELOPMENT OF FUNCTIONAL DYE MATERIALS: SYNTHESIS AND STUDY OF SOME DYES CONTAINING RUTHENIUM POLYPYRIDYL AND SQUARAINE CHROMOPHORES

THESIS SUBMITTED TO
THE UNIVERSITY OF KERALA
IN FULFILMENT OF THE REQUIREMENTS
FOR THE DEGREE OF
DOCTOR OF PHILOSOPHY
IN CHEMISTRY
UNDER THE FACULTY OF SCIENCE

BY
V. SURESH

PHOTOCHEMISTRY RESEARCH UNIT
REGIONAL RESEARCH LABORATORY (CSIR)
TRIVANDRUM-695 019, KERALA, INDIA

DECEMBER, 2000

STATEMENT

I hereby declare that the matter embodied in this thesis is the result of investigations carried out by me at the Photochemistry Research Unit of the Regional Research Laboratory (CSIR), Trivandrum, under the guidance of Dr. Suresh Das and the same has not been submitted elsewhere for a degree.

In keeping with the general practice of reporting scientific observations, due acknowledgement has been made wherever the work described is based on the findings of other investigators.

V. Suresh

Dr. SURESH DAS
SCIENTIST

PHOTOCHEMISTRY RESEARCH UNIT
REGIONAL RESEARCH LABORATORY (CSIR)
TRIVANDRUM-695 019, INDIA

Telephone: 91-471-515318 Fax: 91-471-490186
E. Mail: das@csrrltrd.ren.nic.in

December 29, 2000

CERTIFICATE

Certified that the work embodied in this thesis entitled: **"Development of Functional Dye Materials: Synthesis and Study of Some Dyes Containing Ruthenium Polypyridyl and Squaraine Chromophores"** has been carried out by Mr. V. Suresh under my supervision and the same has not been submitted elsewhere for a degree.

SURESH DAS

(Thesis Supervisor)

ACKNOWLEDGEMENTS

It is with great pleasure that I place on record my deep sense of gratitude to Dr. Suresh Das, my research supervisor, for suggesting the research problem and for his guidance and encouragement, leading to the successful completion of this work.

I would like to express my sincere thanks to Professor M. V. George for his constant encouragement and help throughout the tenure of this work. I wish to thank Dr. G. Vijay Nair, Director, Regional Research Laboratory, Trivandrum for providing me the necessary facilities for carrying out this work.

I express my thanks to Dr. A. Ajayaghosh, Dr. K. R. Gopidas, Dr. D. Ramaiah, Dr. K. George Thomas and other members of the Photochemistry Research Unit for their suggestions and support. I acknowledge Mr. Robert Philip, Dr. E. Prasad and all my friends in the various sections of the Regional Research Laboratory for the help rendered to me during various stages of my work. I express my sincere thanks to Mrs. Sarada Nair for her secretarial help in various stages of my work.

I would like to thank Dr. P. J. Krishnan and all other teachers who have motivated me at different states of my education.

Financial assistance from CSIR, New Delhi is gratefully acknowledged.

Finally, I am deeply indebted to all the members of my family for their invaluable support and encouragement.

Trivandrum **V. Suresh**

December 2000

CONTENTS

PREFACE

Functional dyes are being increasingly used as key materials in a number of new technological applications, such as laser optical recording systems, thermal writing displays, laser printing, organic photovoltaics and photodynamic therapy. With the current availability of low cost semiconductor lasers emitting in the near infrared region (NIR), there is much interest in the development of new NIR absorbing dyes. The main objective of the present investigation was to synthesize some novel ruthenium and squaraine based dyes with improved absorption in the visible and near-infrared region capable of undergoing efficient photoinduced electron transfer. Another objective was to synthesize near-infrared absorbing dyes capable of generating singlet oxygen on photoexcitation.

Chapter 1 of the thesis presents a brief review covering some aspects of the current theoretical understanding of the structure-property relationships of dyes, with specific reference to cyanine and squaraine dyes.

Chapter 2 deals with the synthesis and photophysical characterization of the ligand, 4,4′-bis(*p*-dimethylamino)-α-styryl-2,2′-bipyridine (**7**) and some of its ruthenium complexes (**8** and **9**). The ligand (**7**) undergoes mono and di-protonation in the ground state with pKa values of 4.6 and 3.2 respectively. Excitation of the ligand results in the formation of its protonated species, due to substantial enhancement in its basicity (Δ pKa = 8.0). This may be attributed to a photoinduced intramolecular charge transfer process, which can result in enhanced charge density

on the pyridyl moiety. The strong ability of the ligand (7) to complex with transition metal ions, results in significant changes in its absorption spectrum which can be used as a method for detecting trace amounts of transition metal ions in solution. The triplet excited state properties of the ruthenium complexes as well as photosensitization of nanoporous TiO_2 films using these dyes were investigated.

The third Chapter of this thesis describes our efforts to synthesize water soluble squaraine dyes possessing high triplet quantum yields. A water soluble squaraine dye, bis(3-carboxymethylbenzselenazol-2-ylidine)squaraine and its parent compound bis(3-methylbenzselenazol-2-ylidine)squaraine were synthesized and characterized. The photophysical properties of these dyes in homogeneous and microheterogeneous media have been investigated. Compound **15** is only weakly fluorescent in aqueous media. In water, **15** forms dimer aggregates with an absorption band blue shifted to that of the monomer. The blue shift in the absorption band is indicative of formation of H-type aggregates which can be attributed to hydrophobic interaction between the chromophoric units of the dye. Heavy atom induced spin-orbit coupling due to the presence of selenium atoms within the molecular framework of the dyes, results in substantially high triplet quantum yields (ϕ_T = 0.26–0.29), in contrast to the generally low intersystem crossing efficiencies normally observed for squaraines. Photoinduced electron transfer and singlet oxygen generation from the excited triplet states of these dyes have also been investigated.

An alternative strategy for enhancing the intersystem crossing efficiency in squaraines is to use substituents possessing low lying n-π^* states, since the oscillator

strengths for $S_0 \leftharpoons T_1$ is much greater for n-π* than for π-π* transitions. The last Chapter of the thesis (Chapter 4) describes photophysical studies on such squaraine dyes possessing nitrogen heterocycles, which are expected to posses low-lying n-π* states. The effect of solvent polarity on the emission properties of bis(*N*-methylquinolin-2-ylidine)squaraine was investigated in protic and non-protic solvents. The absorption and emission maxima show a hypsochromic shift with increase in solvent polarity in both types of solvents. The fluorescence quantum yields of the dye, on the other hand, increases with solvent polarity in aprotic solvents, whereas it decreases with increase in solvent polarity in protic solvents. This effect can be interpreted to the interchange of the lowest n-π* singlet state in nonprotic solvents to a π-π* state in protic solvents, due to hydrogen bonding. The substantial triplet yields observed for some of these dyes confirm n-π* character of the lowest excited state. A novel NIR absorbing dye, bis(N-methylacridin-9-ylidine)squaraine belonging to this class of dyes has been synthesized and its photophysical properties investigated. The absorption maximum of the dye (λ_{max} = 900 nm), is substantially red shifted compared to those of squaraine dyes reported earlier in the literature. The triplet quantum yield of this dye was estimated to be 0.15.

Note: The compound numbers listed in this preface refer to those given in different Chapters of this thesis.

CHAPTER 1

FUNCTIONAL DYES

1.1. Introduction

The traditional use of dyes is to impart colour to materials. Recently the use of dyes as functional materials has led to the development of new technologies such as laser optical recording systems,[1] thermal writing displays,[2] laser printing,[3] organic photovoltaics[4-6] and photodynamic therapy of cancer.[7,8] In view of the current availability of low cost gallium-arsenic semiconductor lasers emiting in the infrared, there is much interest in the development of new infrared absorbing dyes as key materials for most of the above mentioned applications.[9,10] AlGaAs/GaAs lasers with emission wavelength of 0.78–0.85 μm, InGaAsP/InP lasers with emission wavelength of 1.1–1.6 μm are some of the semiconductor laser being produced commercially. Development of dyes for such high technology applications requires an understanding of the relationship between the chemical structures of the dyes and their functional characteristics such as absorption and excited state properties. This Chapter gives a brief description of the current understanding of the colour-property relationships of dyes, mainly with respect to cyanine and squaraine dyes.

1.2. Colour-Structure Relationship of Dyes

The π-electronic structure of the chromophore of a functional dye can be interpreted with the aid of MO theory, and such approaches may range from qualitative to the most sophisticated *ab-initio* quantitative methods.[11-17] The absorption spectra of a dye chromophore can be quantitatively calculated by the Pariser-Parr-Pople molecular orbital method (PPP MO). This method is similar to the old Hückel molecular orbital (HMO) method. Both methods deal with the π-electrons of the molecules, independently of the σ-electrons. Electron repulsion effects are included in the PPP MO method. The LCAO (Linear combination of atomic orbitals) coefficients required for this are first obtained by the HMO calculations and these are improved by iterative calculations evaluating the electron repulsion energy until no further improvement in the LCAO data is achieved. The resulting MO's are said to be self-consistent. Transition energies can then be calculated from the orbital energies and the electron repulsion terms. Further refinement involves a configuration interaction (CI) treatment. The CI treatment mixes the various excited state electronic configurations; in most cases, the five highest occupied MO's are considered for sets of configurations to give a set of the excited states.

MO calculations give a wide range of data about the energy of MO's and the form of the wavefunctions, and this data can be used for the prediction of many

functional properties. Table 1 summarizes the important functional properties of chromophores, together with the relevant data that can be calculated by MO methods.

Table 1.1 Application of MO theory to evaluate chromophoric properties

Chromophoric property	Relevant MO calculated data
Ground state	Dipole moment, electron densities and bond orders.
Light absorption	λ_{max}, oscillator strength, transition moment direction, bandwidths and intermolecular effects.
Light emission	Stoke's shift and singlet-triplet energy gaps.
Polarisation	Ground and excited state dipole moments and hyperpolarisabilities.
Photoelectrical	Ionisation potential, electron affinity, excited state dipole moment and excited state electron densities.
Photochemical	Ground and excited state electron densities, frontier orbital coefficients, total energy of ground state, singlet and triplet excited state energies.

PPP MO methods have been used for designing near-infrared dyes,[14,18] reverse saturable absorbers for use as laser shutters,[14] dichroic dyes for use in liquid crystal display systems[19,20] as well as polarizable dye molecules for nonlinear optical applications.[21] The use of PPP MO method for the design and optimization of the absorption characteristics of some cyanine and squaraine dyes is briefly described below.

The basic chromophores of cyanine dyes have been evaluated and rationalized by the PPP-MO method.[11,12,22] The chromophore for the symmetric cyanine dyes is a conjugated ionic type with two extreme resonance structures of equivalent energy. There is no C-C bond alternation in the ground and excited states. Cyanine dyes represent an odd alternant system and each atom can be divided into two groups as starred and unstarred as shown in Chart 1.1.

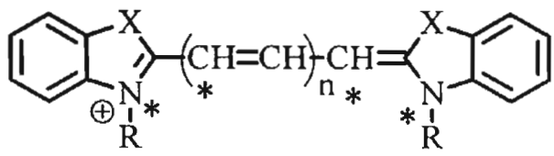

1

Chart 1.1

The π-electron densities are less at the starred position and large at the unstarred positions. Introduction of donors at starred positions and acceptors at unstarred positions results in a bathochromic shift of the λ_{max}, whereas a hypsochromic shift is produced with an electron withdrawing substituent at a starred position or an electron donating group at the unstarred position. This effect is known as the Dewar's rule.[22,23] The extent of shift is related to the donor or acceptor strength of the substituents.

It is generally known that the absorption maximum of cyanine dyes exhibits a bathochromic shift of about 100 nm with an increase in 'n', and shifts to the near-infrared for n>3. In donor-acceptor substituted dyes, the vinylene shift is

generally convergent unless a powerful acceptor group can provide the molecule with high bond uniformity. An example is provided in Chart 1.2 (**3**), which has maximum at around 860 nm whereas, the analogous symmetric cyanine **2** absorbs at lower wavelengths, with an absorption maximum around 785 nm.

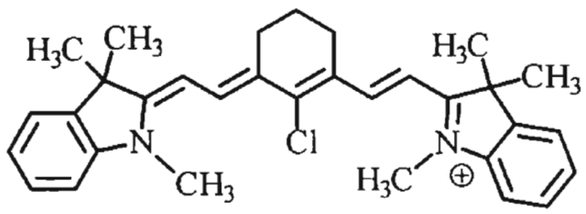

2

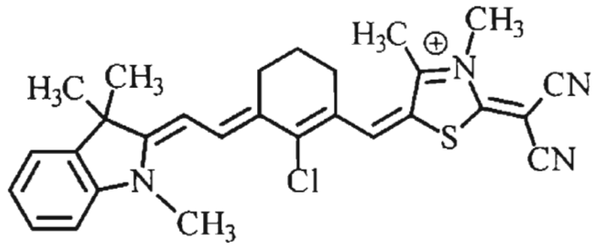

3

Chart 1.2

With the use of very strong electron donors and acceptors as terminal groups it is also possible to obtain NIR dyes with much shorter chains. Such dyes have the advantage of being chemically more stable than their long chain analogues. Examples of some powerful electron donors that can be used are shown in Chart 1.3, and the corresponding short chain NIR dyes synthesized using such donor acceptor substituents are shown in Chart 1.4.

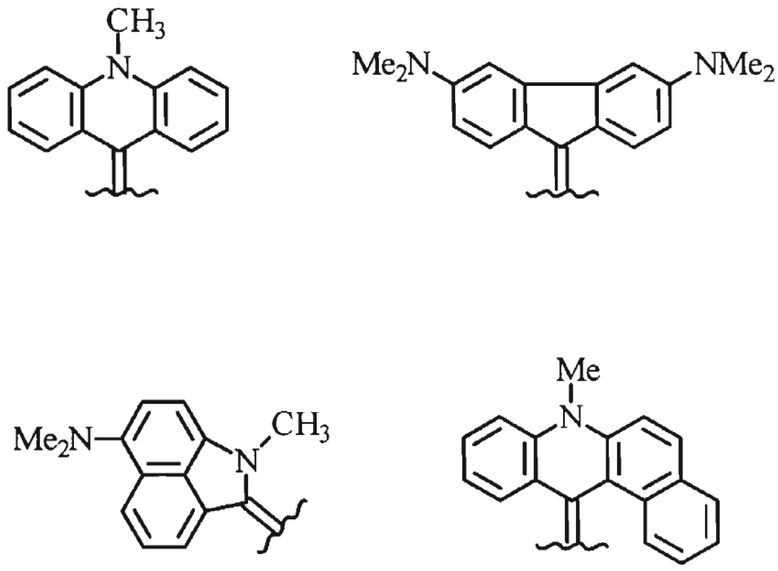

Powerful electron releasing terminal groups

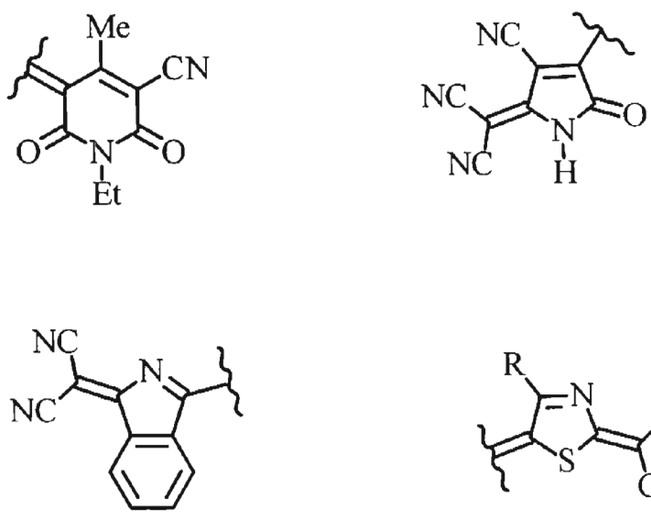

Powerful electron acceptor groups

Chart 1.3

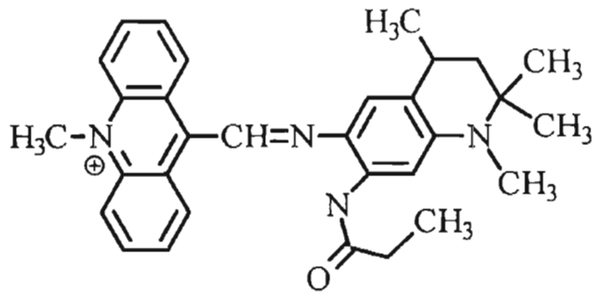

4 λ_{max}, 790 nm

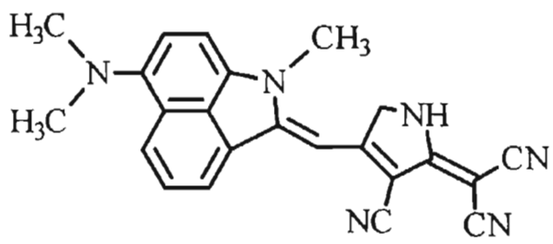

5 λ_{max}, 781 nm

Chart 1.4

Squaraines form another interesting class of dyes which find application in areas such as imaging and solar energy conversion.[24-28] These dyes have cyanine-type donor-acceptor properties and their absorption properties have been explained by PPP-MO method.[29] Chart 1.5 compares the absorption maxima of squaraines with those of the corresponding cyanine dyes. A bathochromic shift is observed for the absorption maximum of the indolinylidenemethylsquaraine derivative (**8**) compared to the corresponding cyanine derivative.

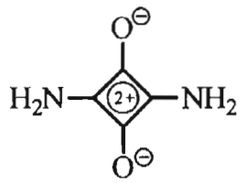

6 λ_{max}, 285 nm

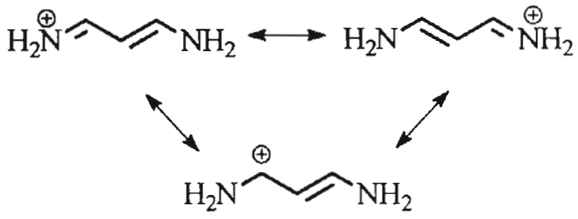

7 λ_{max}, 286 nm

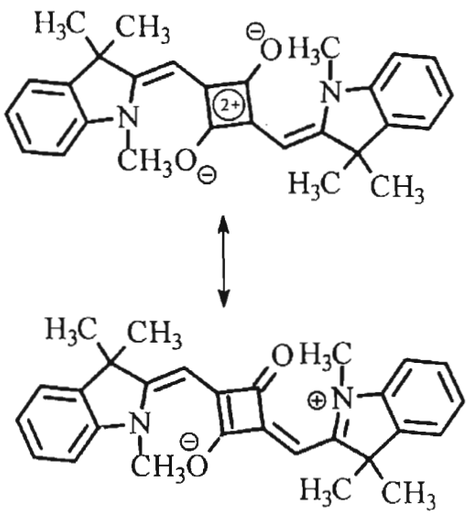

8 λ_{max}, 630 nm

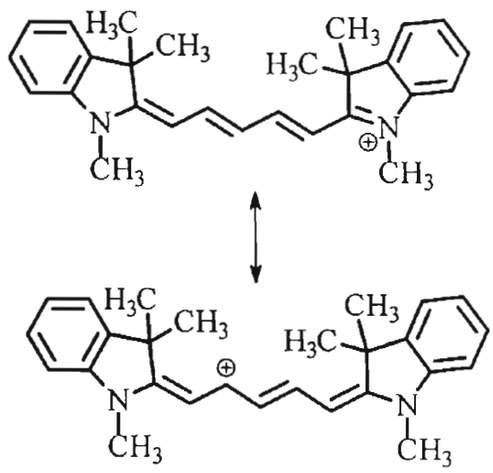

9 λ_{max}, 545 nm

Chart 1.5

The bathochromic effect can be understood on the basis of Dewar's rule, namely the introduction of an electron acceptor (carbonyl group) at the unstarred position and an electron donor (oxide group) at the starred position (Chart 1.6). Introduction of a second carbonyl group at an unstarred position (**11**, Chart 1.6) results in substantial bathochromic shifts for the croconate dye.

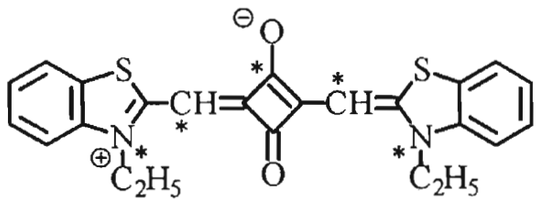

10

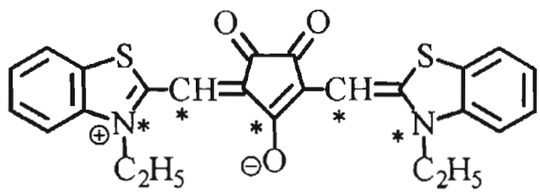

11

Chart 1.6

1.3. Structure-Excited State Property Correlation in Dyes

Complementary experimental and theoretical work in the last five years have led to a better understanding between molecular structure and excited state properties such as efficiency of internal conversion (IC) and its competition with fluorescence. In diatomic molecules, the non-crossing rule between the photochemically relevant excited state and the ground state is rigorously valid and earlier this rule had also been extended to polyatomic molecules. Recent studies however suggest that for polyatomic molecules, this rule fails, even if the two states have the same symmetry. Such crossings, which are also called as conical intersections, provide a very efficient 'funnel' for radiationless deactivation or for chemical transformation of the system. Radiationless decay can occur within the single vibrationless period when the system travels to the vicinity of such intersection points. [30,31]

Control of IC processes can play an important role in defining the functional property of dyes. Once the geometric changes occuring in the excited state which lead to the conical intersection are identified, suitable synthetic alterations can be used for blocking such channels. For cyanine type dyes which possess a number of double bonds, a large number of possibilities exist for the radiationless degradation of the excited state. An efficient experimental and theoretical tool for detecting the most probable intramolecular fluorescence quenching mechanism has been developed within the framework of the twisted-intramolecular charge-transfer model[32] and the more general theory of biradicaloid states.[30] According to this model all photochemical processes competing with fluorescence occur *via* movement of the molecule on an excited state potential energy surface until it reaches the "conical intersection" or "photochemical funnel" as discussed above. In the polymethine type dyes this intersection is proposed to occur near a 90^0 twist around one or more bonds. The approach to the "photochemical funnel" is followed by efficient radiationless decay to the corresponding ground state.[31] The high energy twisted ground state thus formed can isomerize or relax back to its original state. In addition to near 90^0 twisted conformations, conical intersections can also involve bond length changes within the main chain and in some cases, out of plane motions of hydrogen or other substituents. Determination of such conical intersections however requires a complete optimization of the excited state potential energy surface.

In an effort to simplify the procedure for making predictions and interpretation of excited state properties, Rettig and co-workers have used AM-1 CI (Austin Model-1 Configuration Interaction) method for estimating S_0-S_1 energy gaps for various possible twisted conformations of polymethine dyes.[33,34] It was proposed that the conformations yielding sufficiently small S_0-S_1 energy gap for the Frank-Condon situation will be indicative of its reduction to zero on relaxation in the S_1 state. In other words it is proposed that the proximity of a particular configuration to a possible conical intersection is inversely related to the magnitude of the corresponding Frank-Condon S_0-S_1 gap.

Using this method, the bond twists which would be most likely to bring the system closest to a conical intersection can be identified. By rigidizing these bonds, using bridging groups, the non-radiative channel available for the excited state can be blocked making the molecule fluorescent. Attempts have been made to interpret the effect of such bridging groups on some unsymmetric cyanine dyes (Chart 1.7) using theoretical modelling methods described above.

The presence of chemical bridging of flexible bonds is normally expected to increase the efficiency of fluorescence of dyes, in accordance with the so-called "loose bolt theory", due to reduction in the efficiency of non-radiative rate processes.[35] This is indeed so, for the oxygen containing derivatives **15** and its bridged derivative **16** where the fluorescence efficiency increases by a factor of 1.5 on bridging. On the other hand the same bridging pattern of the sulfur derivative, results in a decrease in fluorescence efficiency by a factor of 2 for **13**

and **14**, compared to **12**. This effect has been termed as the "inverse-loose-bolt" effect.

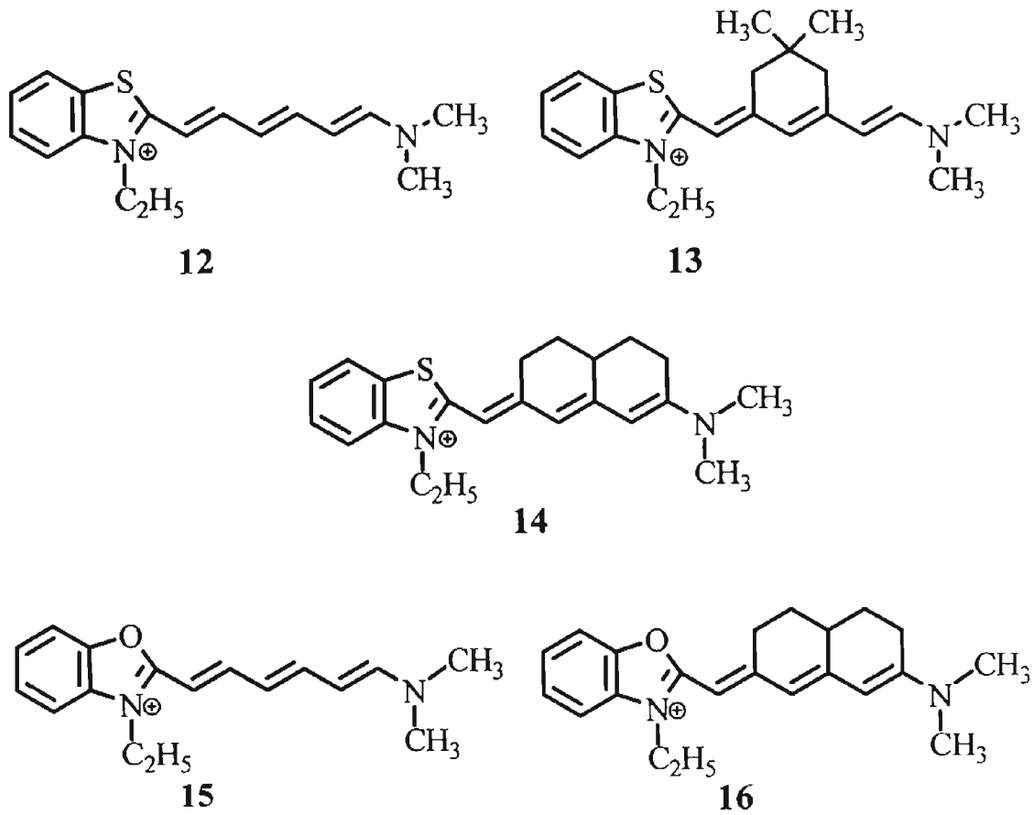

Chart 1.7

AM1 calculations also show as expected, that the S_0-BR gap magnitudes are higher for the bridged molecules compared to that of the unbridged molecule **12**.[33] This is suggestive of lowered funneling probabilities and hence increased quantum yields and larger fluorescence lifetimes. However, as mentioned above the experimentally observed results are contradictory to the expectation based on calculations. In order to explain the contradictory observation Rettig *et al.* have

invoked a three state mechanism.[33,34] They have proposed that in the unbridged model **12**, some relaxation or twisting pathway exists which can lead to a fluorescent species, as observed for some pyridinium and stilbazolium dyes.[36] Molecular rigidization can suppress the access to these fluorescent states, thereby increasing the possibility of the bridged molecules to reach the conical intersection.

The observed increase in the fluorescence of bridged oxygen derivative (**16**) compared to the unbridged one (**15**) is also not very large. This suggests that the bridges used in Chart 1.7 have not been able to block the main access to the conical intersection. The AM1-CI calculations show that the S_0-BR gaps, which are small enough to represent geometries close to a conical intersection, result specially from twists of the bonds conjugated with the heterocyclic substituent of the donor-acceptor substituted polymethine chain. These double bonds are slightly shorter than the corresponding double bond conjugated to the aniline moiety. The lack of a significant effect of bridging on the fluorescence properties shown in Chart 1.7 is therefore attributed to the double bond adjacent to the donor moiety being unbridged in all cases.[34]

The excited state properties of squaraine dyes have recently attracted increased attention.[37-42] Their excited state properties have been found to be highly sensitive to structural modifications as well as the nature of the environment. In an effort to elucidate the excited state relaxation processes in squaraines, Gude and Rettig, have compared the photophysical properties of the

squaraine dyes **8** and **18** (Chart 1.8) at various temperatures and tried to correlate them with the results of *ab-initio* quantum calculations.[43] To reduce computation time the calculations were carried out using **17** and **19** as theoretical models.

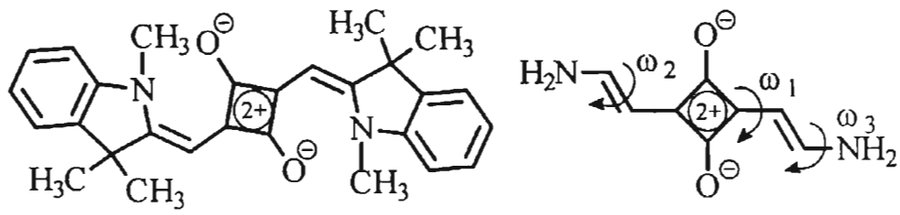

8 **17**

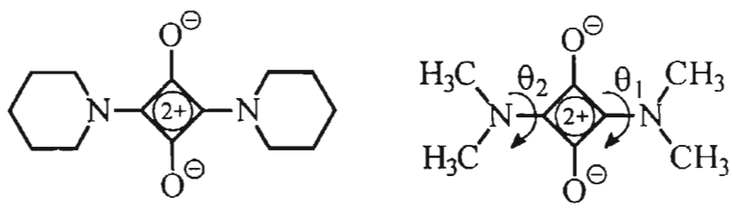

18 **19**

Chart 1.8

Compound **18** shows a weak fluorescence in non-polar solvents which decreases with increase in temperature. The extremely low fluorescence intensity of **18** has been explained on the basis of calculations, which show the strongly forbidden character of the $S_1 \rightarrow S_0$ transition. This makes the non-radiative relaxation process compete efficiently with emission. A possible non-radiative relaxation channel suggested on the basis of calculations is the rotational motion of the amino

groups as shown for **19** (Chart 1.8). This model is further supported by the increase in fluorescence intensity at low temperatures and sufficiently high solvent viscosity.

The spectroscopic behaviour of **8** differs drastically from that of **18** as it shows a sizable fluorescence in non-polar solvents. The difference can be attributed to the expanded π-system which results in a lowering of the π-π^* type transitions relative to the n-π^* type transitions. Quantitative *ab initio* calculations show that a bond-twisting process, ω_2 (**17**, Chart 1.8) is the favoured downhill relaxation process in the first excited state.

Further support for the importance of bond-twisting processes in squaraines can be found in studies of the dyes microencapsulated in β–cyclodextrin[38] and in polymers.[39] In the squaraine dye **20** (Chart 1.9) the presence of the hydroxy group brings about a two fold enhancement in the fluorescence yield, compared to the parent bis(dimethylamino)phenyl squaraine. Intramolecular hydrogen bonding in **20** can result in a reduction of the C-C bond rotation.[37]

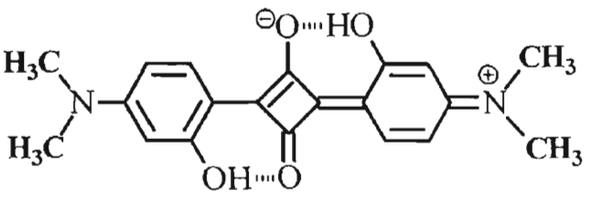

20

Chart 1.9

The constrained environment provided by such media result in significant enhancement in the fluorescence yields, and this has been attributed to restriction of the bond-twisting process in the excited state.

The fluorescence enhancement and lifetime lengthening upon binding the derivatives of **8** to bovine serum albumin can also be attributed to reduction of bond rotation, in the restricted environment.

1.4. Objectives of the Present Investigation

There is currently a considerable interest in the synthesis of new functional dyes, for a variety of applications. The theoretical understanding of the colour-structure relationship has reached a stage where it is possible to design and synthesize dyes possessing the desired absorption characteristics. The ability to make theoretical prediction of excited state properties of dyes is however far from satisfactory. The main objectives of the present investigation were to synthesize and study the photophysical properties of some novel dyes absorbing strongly in the visible and near infrared region, capable of undergoing efficient photoinduced electron transfer. Another interest was to synthesize near infrared absorbing dyes capable of generating singlet oxygen on photoexcitation in aerated media. Although cyanine and squaraine dyes are capable of undergoing efficient photoinduced electron transfer in the excited state, these processes are often accompanied by an efficient back electron transfer between the radical ions generated. A major reason for the efficient back electron transfer is that the

photoinduced electron transfer in most of these dyes occurs from the excited singlet state, which results in the formation of a singlet radical ion pair. Back electron transfer from a singlet radical ion pair can occur very efficiently. Charge separation can occur in a more efficient manner if the triplet excited state of the dyes are involved, as the triplet radical ion pair generated would be less susceptible to back electron transfer. A survey of the literature shows that except for phthalocyanines, intersystem crossing is generally inefficient in cyanine and squaraine dyes. In Chapter 2 of the thesis, we report the synthesis and photophysics of the cyanine dye 4,4′-bis(*p*-dimethylamino)-α-styryl-2,2′-bipyridine. This dye was used as a ligand for the synthesis of ruthenium complexes. The excited state properties of the cyanine and ruthenium complexes have been investigated. The ability of the ruthenium complexes to sensitize large band gap semiconductors has been compared with that of a tris(bipyridyl)ruthenium model compound. Chapters 3 and 4 deal with our efforts in synthesizing novel near infrared absorbing squaraine dyes possessing substantial triplet yields. Their photophysical and photochemical properties are reported.

1.5. References

1. Chen, D. I.; Zook, J. D., *Proc. IEEE* **1975**, *63*, 1207.
2. Sasaki, A.; Kurahashi, K.; Takagi, T., *Conf. Rec. IEEE Conf. Display Devices* **1972**, 161.
3. Schaffert, R. M., in *Electrophotography*, The Focal Press, London, **1975**.
4. Bach, U.; Lupo, D.; Cornte, P.; Moser, J. E.; Weissörtel, F.; Salbeck, J.; Spreitzer, H.; Grätzel, M., *Nature* **1998**, *395*, 583.
5. Jana, A. K., *J. Photochem. Photobiol A: Chem* **2000**, 1.
6. Hagfeldt, A.; Grätzel, M., *Acc. Chem. Res.* **2000**, *33*, 269.
7. *Photodynamic Therapy*, (Ed.: Gomer, C. J.), *Vol. 46,* Pergamon Press, Oxford, **1987**.
8. Dougherty, T. J., *Photochem. Photobiol.* **1993**, *58*, 895.
9. Kressel, H.; Butler, J. K., in *Semiconductor Lasers and Heterojunction LEDs*. Academic Press, New York, **1977**.
10. Casey.Jr, H. C.; Panish, M. B., in *Heterostructure Lasers*, Academic Press, New York, **1978**.
11. Griffiths, J., in *Colour and Constitution of Organic Molecules*, Academic press, London, **1976**.
12. Fabian, J.; Hartmann, H., in *Light Absorption of Organic Colourants*, Springer-verlag, Berlin, **1980**.
13. Griffiths, J., *Chemistry in Britain* **1986**, 997.
14. *Infrared absorbing dyes*, (Ed.: Matsuoka, M.), Plenum Press, New york, **1990**.

15. Roos, B. O., *Chem. Res.* **1999**, *32*, 137.

16. Astrand, P. O.; Ramanujam, P. S.; Hrilsted, S.; Bak, K. L.; Saver, S. P. A., *J. Am. Chem. Soc.* **2000**, *122*, 3482.

17. Roos, B. O.; Fülscher, M. P.; Malmqvist, P.-A.; Merchan, M.; Serrano-Andreas, L., in *Quantum Mechanical Electronic Structure Calculation with Chemical Accuracy*, (Ed.: Langhoff, S. R.,), Kluwer, Dordrecht, **1995**.

18. Griffiths, J., in *Chemistry of Functional Dyes*, (Ed.: Yoshida, Z., Shirota, Y.), *Vol. 2,* Mita press, Tokyo, **1992**, 1.

19. Osman, M. A. *et al*, *J. Chem. Res (S)* **1978**, *180*, 2319.

20. Blackburn, C.; Griffiths, J., *Mol. Cryst.Liq. Cryst* **1983**, *101*, 341.

21. Williams, D. J., *Angew. Chem. Int. Ed. Engl.* **1984**, *23*, 690.

22. Klessinger, M., *Theor. Chim. Acta (Berlin)* **1966**, *5*, 251.

23. Knott, E. B., *J. Chem. Soc* **1951**, 1024.

24. Law, K. Y., *Chem. Rev.* **1993**, *93*, 449.

25. Law, K. Y., *J. Imag. Sci.* **1987**, *31*, 83.

26. Tam, A. C.; Balanson, R. D., *IBM J. Res. Div* **1982**, *26*, 186.

27. Piechowski, A. P.; Bird, G. R.; Morel, D. L.; Stogryn, E. L., *J. Phys. Chem.* **1984**, *88*, 934.

28. Louffy, R. O.; Hsiao, C. K.; Kazmeier, P. M., *Photogr. Sci. Eng.* **1983**, *27*, 5.

29. Matsuoka, M., in *Infrared absorbing dyes*, (Ed.: Matsuoka, M.), Plenum Press, New york, **1990**, 19.

30. Michl, J.; Bonacic-Koutecky, V., in *Electronic Aspects of Organic Photochemistry*, John Wiley &sons, New York, **1990**.

31. Bernardi, F.; Olivucci, M.; Robb, M. A., *Chem. Soc. Rev.* **1996**, *25*, 321.

32. Rettig, W., *Top. Curr. Chem* **1994**, *169*, 253.

33. Dekhtyar, M.; Rettig, W.; Sczepan, M., *Phys. Chem. Chem. Phys.* **2000**, *2*, 1129.

34. Sczepan, M.; Rettig, W.; Bricks, Y. L.; Slominski, Y. L.; Tolmachev, A. I., *J. Photochem. Photobiol. A: Chem.* **1999**, *124*, 75.

35. Lewis, G. N.; Calvin, M., *Chem. Rev.* **1939**, *25*, 273.

36. Rocker, C.; Heilemann, A.; Faomherz, P., *J. Phys. Chem.* **1996**, *100*, 12172.

37. Law, K. Y., *J. Phys. Chem.* **1987**, *91*, 5184.

38. Das, S.; Thomas, K. G.; George, M. V.; Kamat, P. V., *J. Chem. Soc. Faraday Trans. 1* **1992**, *88*, 3419.

39. Das, S.; Kamat, P. V.; Barre, B. D. l.; Thomas, K. G., *J. Phys. Chem.* **1992**, *96*, 10327.

40. Suave, G.; Kamat, P. V.; Thomas, K. G.; Thomas, K. J.; Das, S.; George, M. V., *J. Phys. Chem.* **1996**, *100*, 2117.

41. Kamat, P. V.; Das, S.; Thomas, K. G.; George, M. V., *J. Phys. Chem.* **1992**, *96*, 195.

42. Das, S.; Thomas, K. G.; Ramanathan, R.; George, M. V.; Kamat, P. V., *J. Phys. Chem.* **1993**, *97*, 13625.

43. Gude, C.; Rettig, W., *J. Phys. Chem. A* **2000**, *104*, 8050.

CHAPTER 2

SYNTHESIS AND PHOTOPHYSICAL STUDIES OF 4,4′-BIS(*P*-DIMETHYLAMINO)-α-STYRYL-2,2′-BIPYRIDINE AND SOME OF ITS RUTHENIUM COMPLEXES

2.1. Abstract

The photophysical properties of the ligand 4,4′-bis(*p*-dimethylamino)-α-styryl-2,2′-bipyridine (**7**) have been investigated. The dye undergoes mono and di-protonation in the ground state with pKa values of 4.6 and 3.2, respectively. Excitation of **7** in neutral methanol leads to the transient formation of the monoprotonated species, which is indicative of a substantial enhancement in the basicity of the molecule in the excited state. The excited state pKa of the molecule was estimated as 12.3. The strong ability of the ligand to complex with transition metal ions, results in significant changes in its absorption spectrum which can be used as a method for detecting trace amounts of transition metal ions in solution. The ligand was used to synthesize the ruthenium complexes **8** and **9**. The excited state properties of these complexes as well as the photosensitization of nanoporous TiO_2 semiconductor films using these dyes are reported

2.2. Introduction

Photochemical approaches to the conversion of solar energy can be broadly classified into two main domains.[1-9] One area deals with the use of sunlight to

convert chemicals from one form to another, such as in the photolysis of water to hydrogen,[10] photofixation of carbon dioxide[11] and nitrogen.[12] The other approach involves conversion of sunlight to electrical energy.[13-16] For this purpose, photogalvanic cells based on photoredox reactions of dyes dispersed in solutions[17] and semiconductor based solar cells[18] have most widely been investigated. In photogalvanic cells, fast back electron transfer reactions that occur in the solution phase, following photoinduced electron transfer from the dyes limit the efficiency of charge collection at the macroelectrodes. In contrast semiconductor solar cells based on single crystal semiconductors have been shown to have good sunlight-to-electric current conversion efficiency, in the range of 15-20%. However, conventional semiconductor fabrication technology and laborious steps involved in growing single crystal silicon and cutting silicon wafers make these devices prohibitively expensive. The cost for generating electricity using photovoltaic devices can be substantially reduced by the use of polycrystalline semiconductor films. In such materials, poor conversion yields are usually observed due to charge carrier recombination at grain boundaries and at other defect sites, which reduces the minority carrier diffusion length.

Dye sensitized semiconductor cells can be used to overcome some of these problems. Such cells differ from the conventional semiconductor devices in that they separate the function of light absorption from charge carrier transport. In the case of *n*-type materials, such as TiO_2, current is generated when a dye molecule absorbs a photon and injects an electron into the conduction band of the

semiconductor from its excited state. Figure 2.1 shows such a dye sensitized nanocrystalline solar cell.[19] This system consists of the sensitizing dye adsorbed on TiO_2 and the I^-/I_3^- redox couple in the electrolyte. Nanocrystalline TiO_2 films of high internal surface area were prepared by sintering 15–30 nm colloidal titania particles on a conducting glass support. A thin layer sandwich type solar cell was prepared by placing the Pt coated counter electrode directly on the top of the dye coated transparent TiO_2 film. A thin layer of electrolyte was attracted into the interelectrode space by capillary forces. The cell voltage observed under illumination corresponds to the difference, ΔV, between the quasi-fermi level of TiO_2 and the electrochemical potential of the electrolyte.

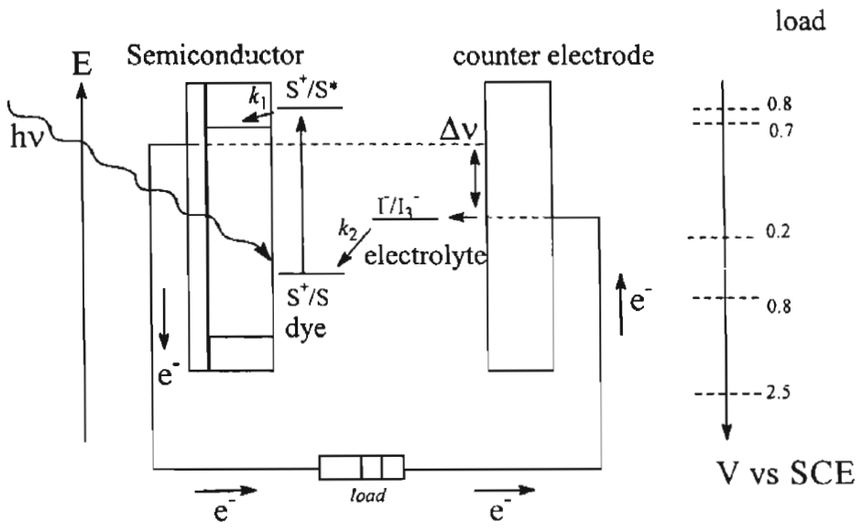

Figure 2.1. Schematic representation of the principle of a dye-sensitized photovoltaic cell to indicate the electron energy level in the different phases. Also indicated on the potential axis are the values of the different electronic levels for the photovoltaic cell.[19]

An excited sensitizer S*, injects an electron into the conduction band of the semiconductor with a rate constant 'k_1' resulting in the formation of the oxidized sensitizer. The oxidized sensitizer accepts an electron from an external electron donor such as iodide present in the electrolyte with a rate constant 'k_2'. The net process allows an electric current to be generated with light of lower energy than the semiconductor band gap. In this case, the recombination of the injected electron and radiative and non-radiative decay of the excited state of the sensitizer compete directly with photocurrent generation. Finally, the oxidised external donor will be reduced at the counter electrode making the solar cell regenerative.

2.2.1. Photosensitizing Dyes

The efficiency of such solar cells depends mainly upon the particle size of the semiconductor and on the light harvesting efficiency of the dyes. The decrease in particle size of the semiconductor surface results in an increase in the number of dye molecules, which can be directly adsorbed onto the surface, and simultaneously in contact with the redox electrolyte.[20-25]

Optimizing the photosensitizing efficiency of the dye can also enhance the efficiency of the photoelectrochemical cell. The desired properties of sensitizing dyes for applications in photoelectrochemical cells include, (i) good light absorption in the visible and near-infrared region, (ii) capability of injecting electrons from its excited state into the conduction band of the semiconductor with high efficiency, (iii) ability of the sensitizer to adsorb strongly onto the

semiconductor surface, (iv) efficient regeneration from its oxidized state and (v) photostability. For commercial viability the dye has to be able to undergo at least 10^8 oxidation-reduction cycles without degradation, which corresponds to about 20 years of exposure to natural sunlight.

Various dye sensitizers have been used in photoelectrochemical (PEC) cells.[9] Xanthenes (rhodamine B), thiazenes (thionine, methylene blue), acridines (proflavin), chlorophyll (H_2-chlorin) (Chart 2.1) are some of the most extensively studied organic sensitizers.

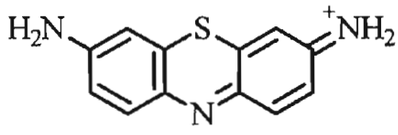

Thionine

1

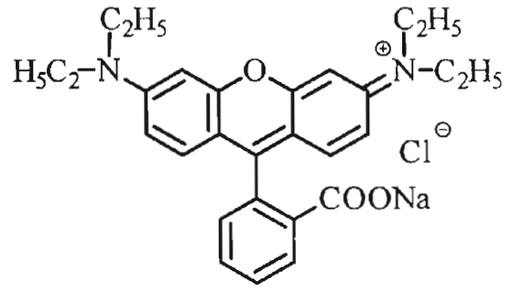

Rhodamine B

2

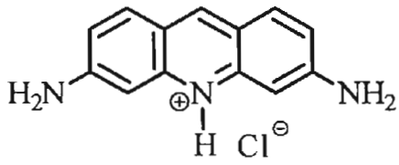

Proflavin

3

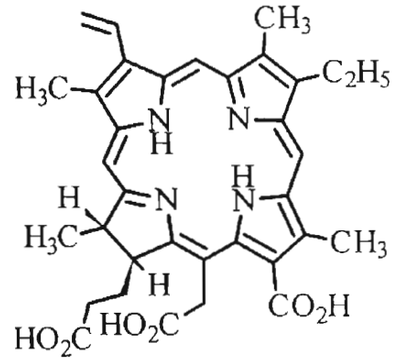

H_2-Chlorin

4

Chart 2.1

Among the various types of sensitizers investigated, polypyridine complexes of transition metal ions have proved to be the best candidates for use as sensitizers in photoelectrochemical cells.

2.2.2. Transition Metal Complexes

The photochemical properties of transition metal complexes have many similarities with that of the photochemistry of organic molecules.[26] There are also striking differences. The vibrational and electronic quanta are smaller in heavy metal complexes compared to those in most organic compounds. The more densely packed states together with generally greater spin-orbit coupling give rise to much greater level of mixing of states and thus to more rapid internal conversion and intersystem crossing processes in metal complexes. The excited state of transition metal complexes involves the promotion of 'd' rather than 's' or 'p' electrons. In organic molecules the excited states can be described as electronic transitions involving electrons of σ or π bonds and lone pairs (n). Likewise, in transition metal complexes electronic transitions fall into three categories namely ligand centered (LC), metal centered (MC), and charge transfer transitions. Charge transfer from the ligands to the coordinated metal leads to transitions that are known as ligand-to-metal charge transfer (LMCT). LMCT bands are normally observed in the UV and visible region in complexes of the type $[ML_n]^{m+}$, where M is metal and L is ligand. The number of LMCT bands decrease as 'M' becomes more oxidizing and L becomes more reducing. For LMCT transition four types of bands are possible;

$\pi_L \rightarrow \pi_M^*(t_{2g})$; $\pi_L \rightarrow \sigma_M^*(e_g)$; $\sigma_L \rightarrow \pi_M^*(t_{2g})$; $\sigma_L \rightarrow \sigma_M^*(e_g)$. In d^5 systems such as Ru (III) and Ir(IV), LMCT transitions can occur at longer wavelengths. Metal to ligand charge transfer (MLCT) transitions involve promotion of an electron from an orbital largely localized on the metal to an orbital, which is essentially ligand-localized. These are likely in compounds where M has a small ionization potential and the ligands possess an empty π^* orbital. Other transitions, which are possible are ligand-to ligand charge transfer and metal-to-metal charge transfer in the case of polynuclear complexes though these are rare.

The electronic transitions in metal complexes can be identified through an examination of the structure and bonding of the metal complexes, intensities of various transitions in the electronic absorption spectra and spin selection rules governing transitions between the states. Crystal field theory provides a general framework to analyze the bonding interactions between the electrons on the metal ion and those on the ligand during the formation of a metal complex (Figure 2.2). In a simplified picture, bonding in metal complexes can be viewed as an electrostatic attraction between the charged metal ion and a set of negatively charged ligands or the negative end of dipoles of coordinated neutral ligands. Approach of the negatively charged ligands repels the electron residing in 'd' orbitals with respect to both those residing on the ligands and those remaining on the central metal core. In an octahedral complex, the ligand cage does not destabilize all 'd' electrons equally. The electrons residing in 'd' orbitals that point towards the ligands (e_g) set are repelled more by the negatively charged ligands than those residing in the 'd'

orbitals that are directed between the ligands (t_{2g} set). The difference Δ_0 in destabilization energy leads to the splitting of the d-orbital energies.

The magnitude of the crystal field splitting parameter Δ_0 is determined by several factors such as the radius of the metal ion, the charge of the central ion and the chemical nature of the ligands. The spectrochemical series gives an energy ordering on the relative magnitudes of Δ_0 values as $CN^- > NO_2^- \sim$phen>bpy$> SO_3^{2-} >$ en $> NH_3 > CH_3CN > NCS^- \sim Cl^- > Br^- > I^-$.

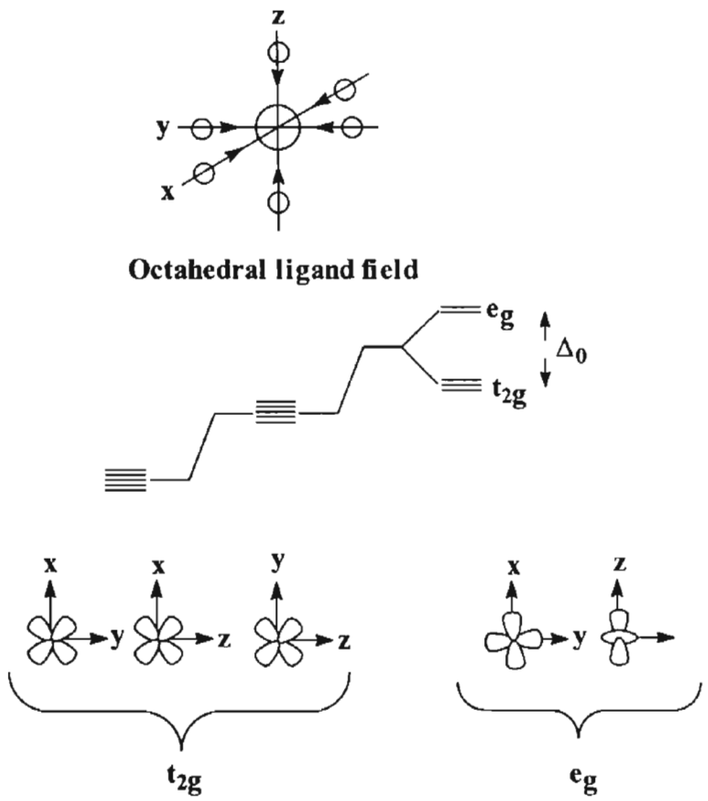

Figure 2.2. Schematic representation of splitting of metal 'd' orbitals in an octahedral ligand field.

Polypyridyl complexes in this context are strong field/ low spin complexes. Regarding the ligand electrons, those involved in ligand orbitals far away from the central metal ion, are unaffected whereas, the non-bonding electrons of the pyridines are directed towards the positively charged metal ions and are substantially lowered in energy.

Polypyridyl complexes having 'd^6' orbitals illustrate how the nature of the lowest excited state can be fine-tuned by varying the metal ion. The extent of crystal field splitting along with the relative disposition of the metal 'd' orbital with respect to ligand π orbital vary with the nature of the metal ion. Figure 2.3 shows schematically the orbital dispositions for a series of tris(bipyridine) transition metal complexes.

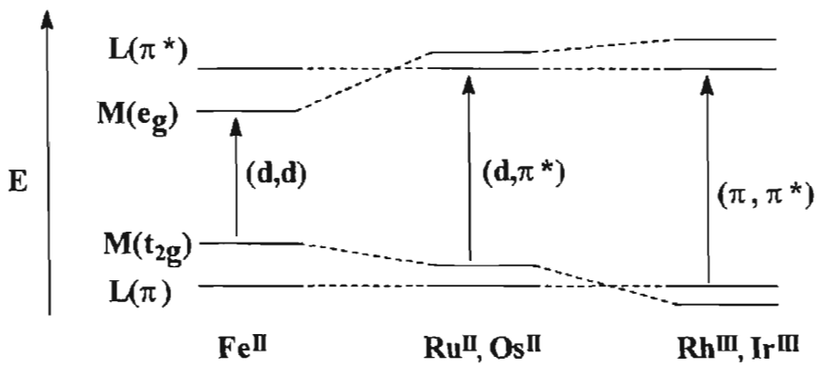

Figure 2.3. A schematic representation of electron transfer from HOMO to LUMO for different metals complexed with polypyridyl ligands.

The strong field (t_{2g}^6) configuration is common for complexes of the second and third transition series. Among the metal ions of the group VIII family, the lowest excited state of $[Fe(bpy)_3]^{2+}$ is assigned as metal-centred (MC), those of Ru(II) and

Os(II) as metal-to-ligand charge transfer and those of Rh(III) and Ir(III) as ligand centred (LC). In the first row transition metals such as Fe, the ligand field splitting Δ is such that MC transitions are of relatively low energy. Replacement of Fe(II) by Ru(II) or Os(II) leads to a progressive increase in the ligand field splitting such that $[Ru(bpy)_3]^{2+}$ and $[Os(bpy)_3]^{2+}$ have low lying MLCT excited states.

Absorption of a photon by ruthenium complexes promotes an electron from the t_{2g} orbital of M(II) to an antibonding π^* orbital on the bipyridyl system. In this charge transfer configuration one visualizes the complex as possessing a hole in t_{2g} orbital with the excited electron residing on the ligand system which can be expressed by Equation 2.1.

$$[Ru^{II}(bpy)_3]^{2+} \longrightarrow [Ru^{II}(bpy)_3]^{2+*} = [Ru^{III}(bpy)_3^{-}]^{2+} \qquad (2.1)$$

Ru(II) polypyridyl complexes exhibit a strong, long-lived luminescence between 600 to 700 nm from its triplet metal-to-ligand charge transfer (MLCT) state. From the maximum of the luminescence band, the energy of the lowest excited state is estimated to be around 2.07 eV.[27,28]

Ligand substituents in such complexes can cause considerable variations in their absorption and luminescence properties. The substituent effect on the energy of absorption and emission bands of transition metal complexes results from a combined perturbation of the LUMO (ligand π^*) and HOMO (metal t_{2g}, in octahedral symmetry) orbitals. In general, both the electron withdrawing and donating substituents stabilize MLCT excited states, with a consequent red shift on

the absorption and emission maxima. Electron withdrawing substituents increase the excited state lifetimes and the luminescence intensities at ambient temperatures.

In order to graft the sensitizer onto the semiconductor surface, a sensitizer should contain anchor groups. Anchor groups, which have been most extensively used include sulphonates[29], phosphates[30,31] and carboxylates.[32] The carboxylate group interacts directly with the surface of Ti (IV) ions resulting in a good electronic coupling of the π^* wave function of the sensitizer with the 3d orbital manifold of the conduction band of the TiO_2. As a result, electron injection from the excited sensitizer into the semiconductor membrane is extremely rapid (< ps) in such systems. In recent years, the ruthenium complex *cis* $RuL_2(NCS)_2$ (Chart 2.2, **5**), where L is 4,4'-dicarboxylato 2,2'-bipyridine, has emerged as the best model of a heterogeneous charge transfer sensitizer for nanoporous solar cells.[19] Grätzel *et al.* have used the trinuclear ruthenium complex (Chart 2.2, **6**) as the sensitizer in a photoelectrochemical cell and obtained a conversion efficiency of 7-12%.[13,14]

2.2.3. Objectives of the Present Study

The main objective of this work was to synthesize ruthenium polypyridyl complexes showing improved charge separation from their excited state. The cyanine dye 4,4′-bis(*p*-dimethylamino)-α-styryl-2,2′-bipyridine (**7**, Chart 2.3), was synthesized and used as a ligand for the synthesis of the ruthenium sensitizers **8** and **9** (Chart 2.4). This chapter describes a detailed study on the photophysical and photochemical properties of the ligand and ruthenium complexes. The

sensitization of nanocrystalline films of TiO_2 using the ruthenium complex in photoelectrochemical cells has been investigated.

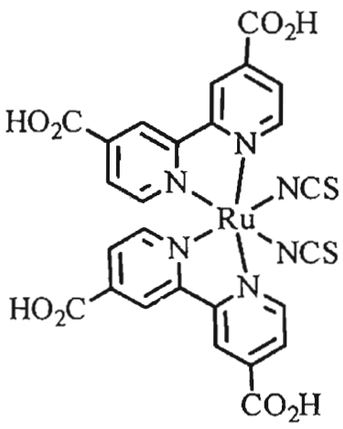

5

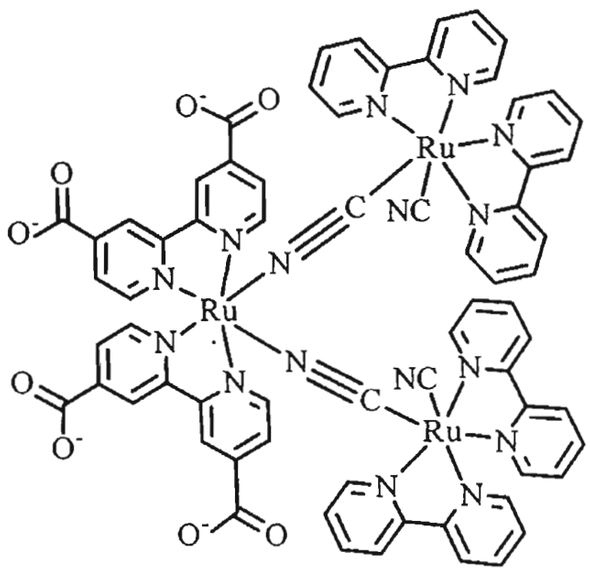

6

Chart 2.2

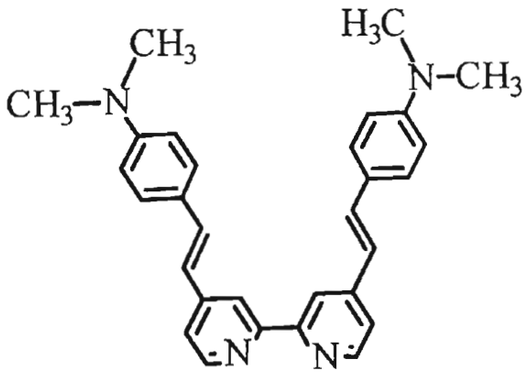

7

Chart 2.3

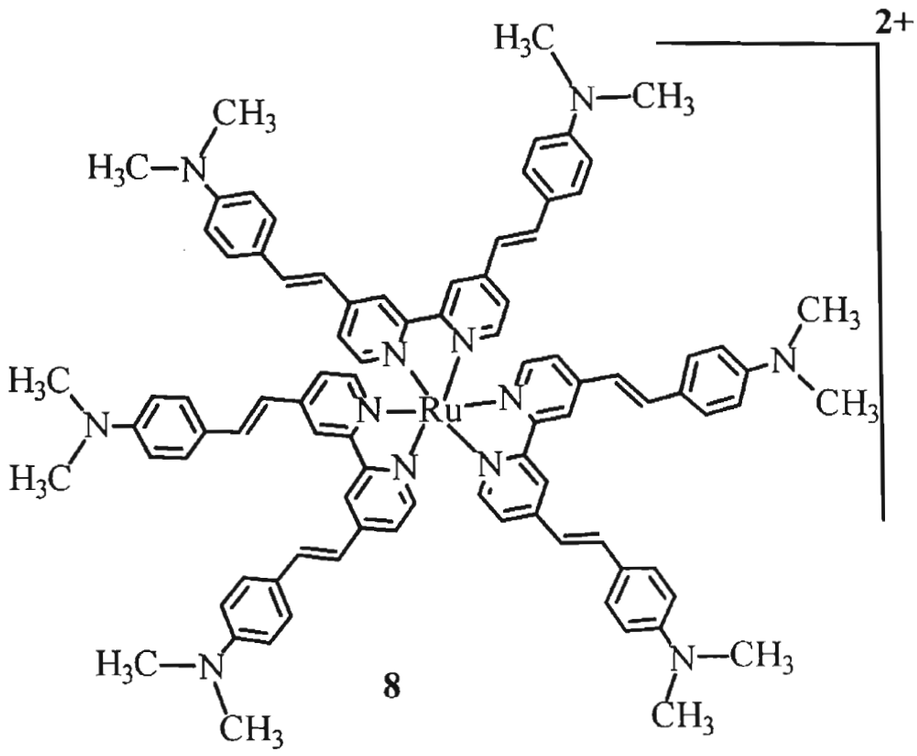

8

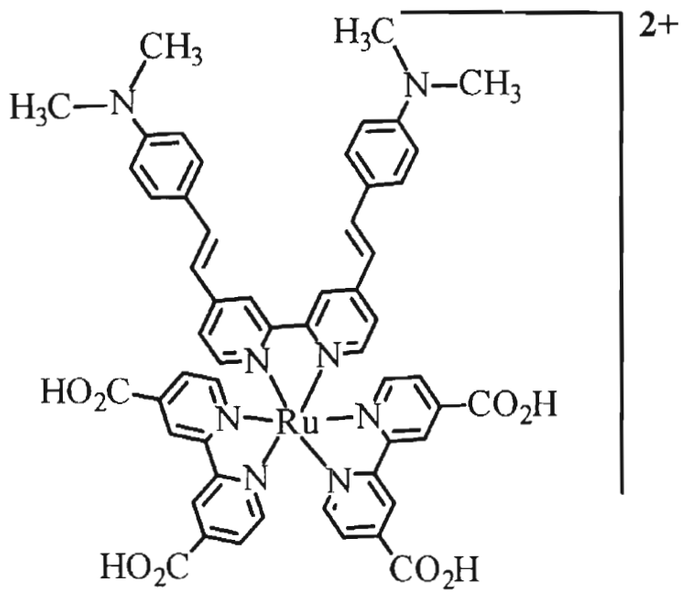

9

Chart 2.4.

2.3. Results and Discussion

2.3.1. Synthesis

4,4'-Bis(dimethylamino)-α-styryl-2,2'-bipyridine (7) was synthesized from 4,4'-dimethyl-2,2'-bipyridine and *N*,*N*-(dimethyl)aminobenzaldehyde in the presence of lithium diisopropyl amide according to a reported procedure(Scheme 2.1).[33] The complex **8** was obtained by reacting $RuCl_3.3H_2O$ with 3 equivalents of the ligand **7**. For synthesizing **9**, the intermediate **14** was first synthesized as shown in Scheme 2.2.

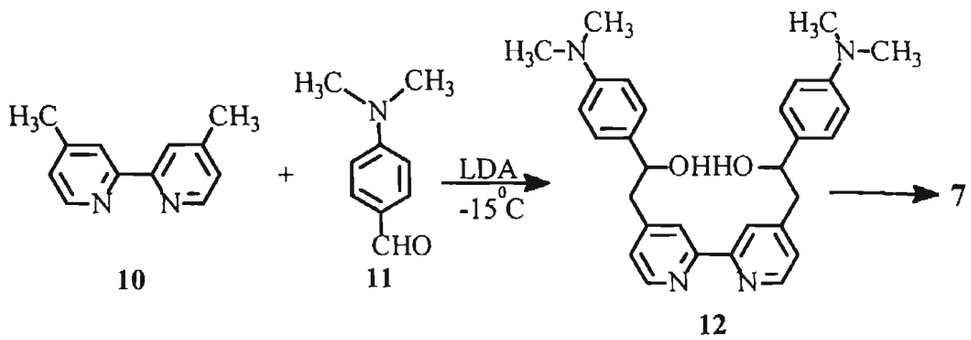

Scheme 2.1

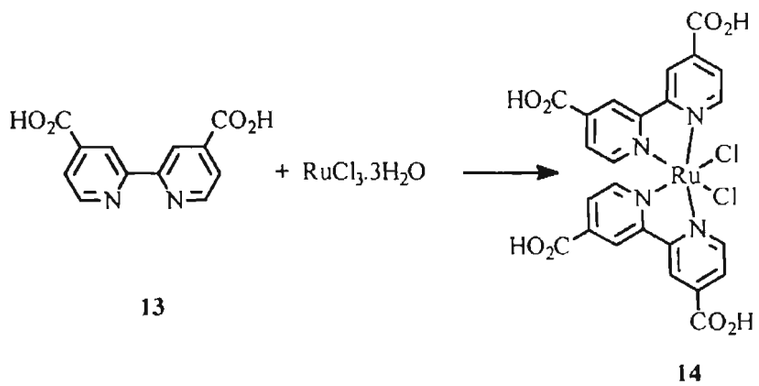

Scheme 2.2

Reaction of 7 with **14** resulted in the formation of **9**. 2,2'-Dimethyl-bipyridyl (**15**) was also reacted with **14** to yield the model compound **16**. Details regarding the experimental procedures used for synthesis and characterization of products are given in Section 2.5.

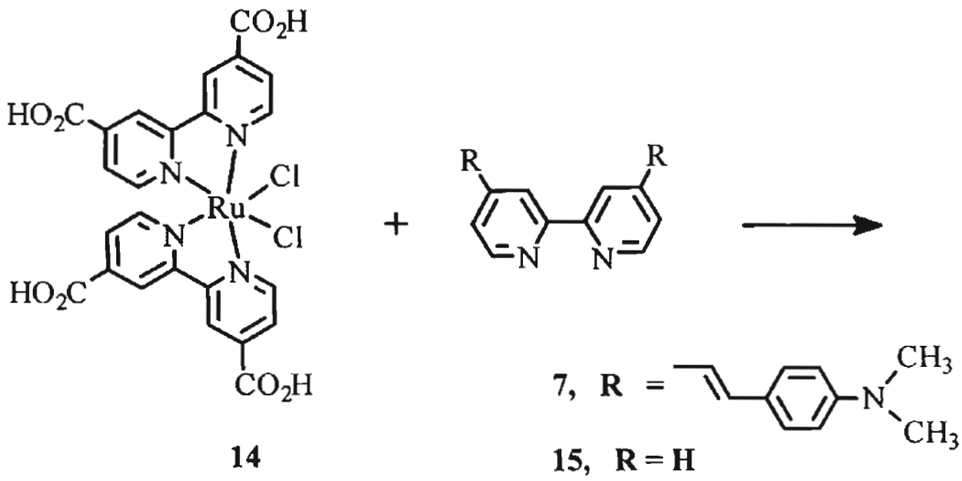

14

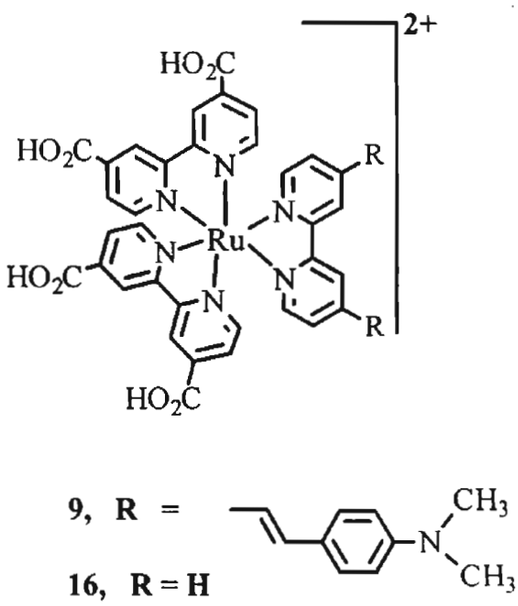

Scheme 2.3.

2.3.2. Photophysical and Photochemical Properties of 4,4′-Bis(*p*-dimethylamino)-α-styryl-2,2′bipyridine (7)

The absorption and emission spectra of 7 (Figure 2.4) show broad bands centered around 380 and 550 nm, respectively.

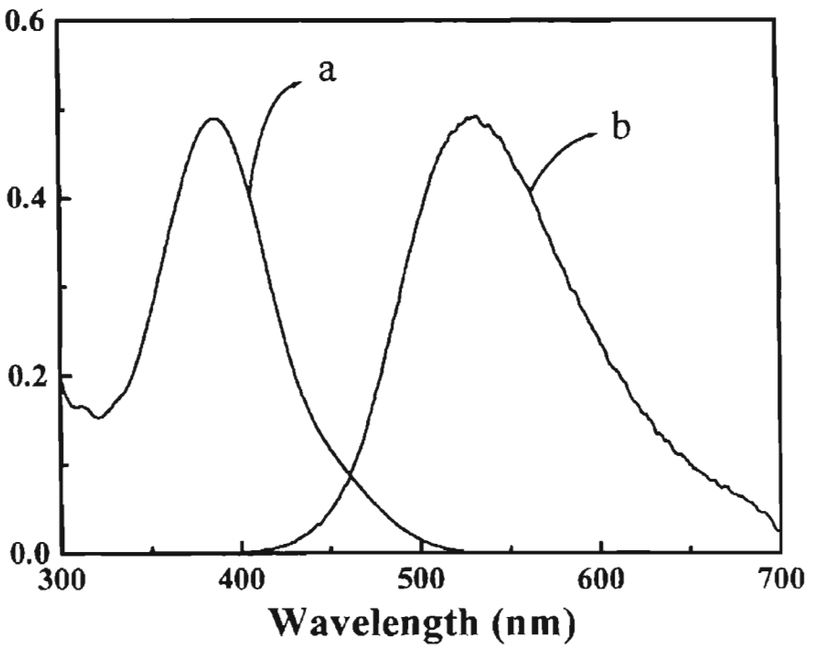

Figure 2.4. a) Absorption and b) emission spectra of 7 in methanol.

The absorption spectrum of 7 is highly sensitive to the pH of the medium. The acid-base equilibrium of the ligand was studied in 1:3 methanol water mixtures due to its limited solubility in water. On decreasing the pH of the solution new bands are formed around 310 and 480 nm, and these changes are marked by the presence of an isosbestic point at 404 nm (Figure 2.5). A plot of the absorbance at 480 nm *vs* pH indicated a pKa of 4.55 for this acid-base equilibrium (Figure 2.6).

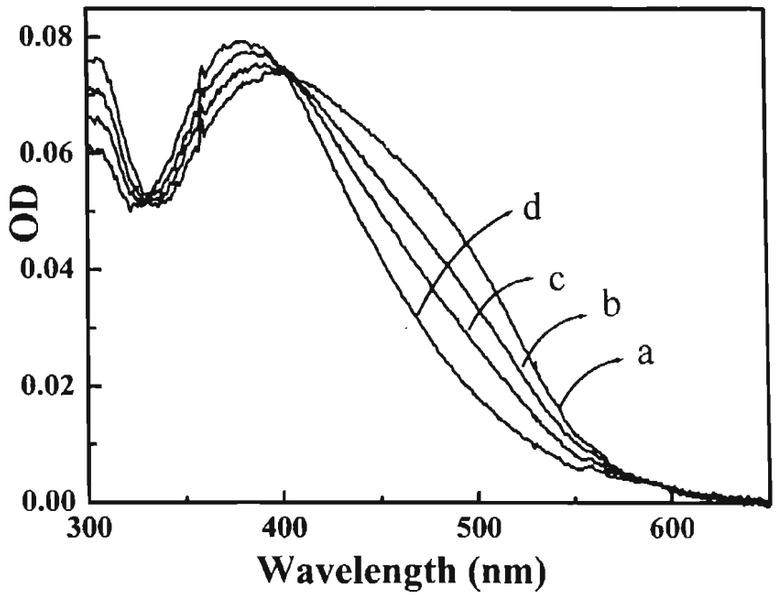

Figure 2.5. Effect of pH on the absorption spectrum of 7 in a mixture (1:3) of methanol and water. pH a)4.4; b)4.88; c)5.05; d) 5.23.

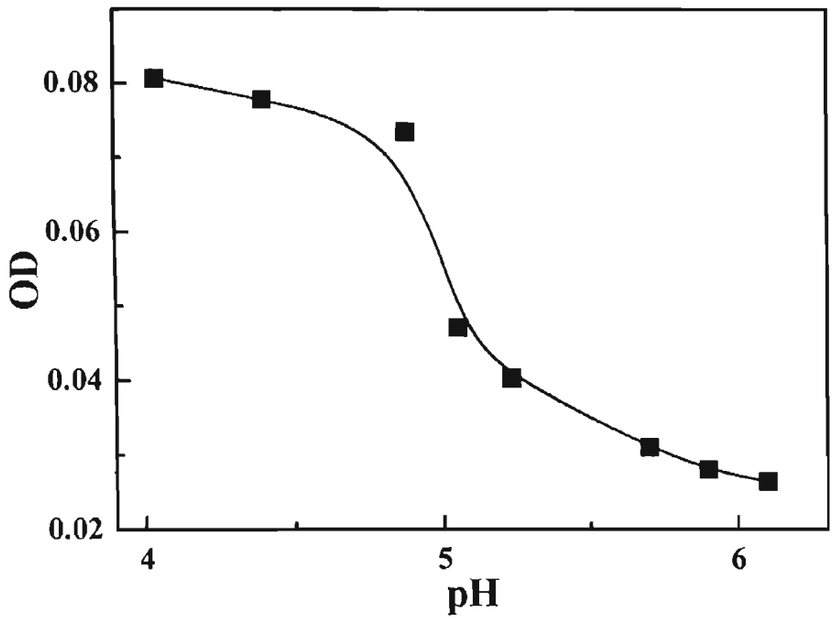

Figure 2.6. Plot of absorbance of 7 at 480 nm *vs* pH of the mixture of methanol and water (1:3) containing 7.

Further decrease in pH results in a decrease in intensity of the peak at 480 nm and an enhancement in absorption around 310 nm (Figure 2.7).

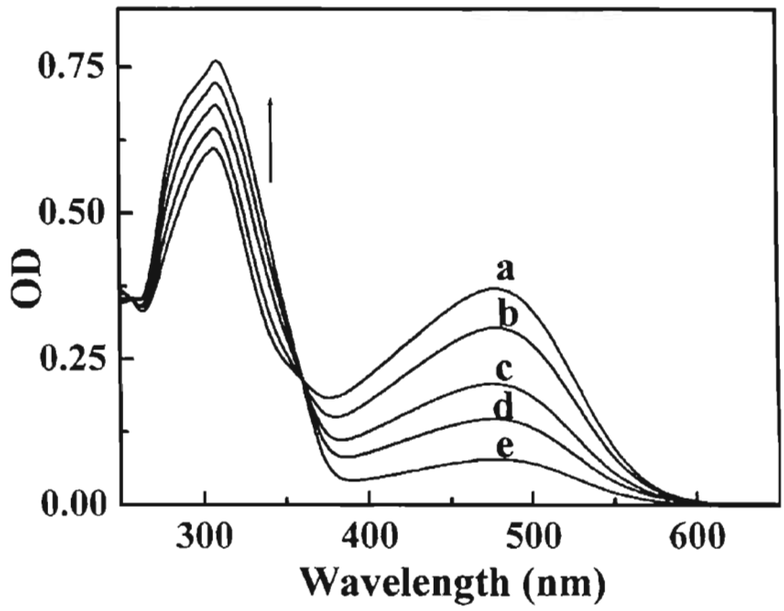

Figure 2.7. Effect of pH on the absorption spectrum of the protonated form of 7 in a mixture of (1:3) methanol and water. pH a) 2.8; b) 2.86; c) 2.95; d) 3.15; e) 3.88.

A plot of absorbance at 310 nm versus pH indicated a pKa of 3.22 for this process (Figure 2.8). The changes in absorption can be explained on the basis of the mechanism shown in Scheme 2.4. According to this Scheme, the initial protonation (pKa = 4.55) corresponds to protonation of one of the pyridyl moieties, since the pyridyl nitrogen will be more basic than the aniline nitrogen. Protonation of the pyridyl nitrogen will make it electron deficient, which could result in an enhancement and stabilization of the intramolecular charge transfer transition in these molecules.

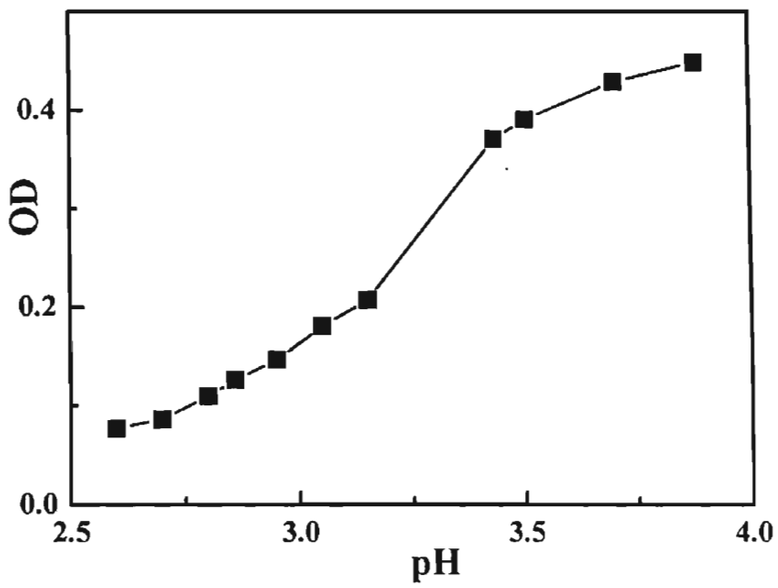

Figure 2.8. Plot of absorbance of 7 at 480 nm *vs* pH of the mixture of methanol and water (1:3) containing 7.

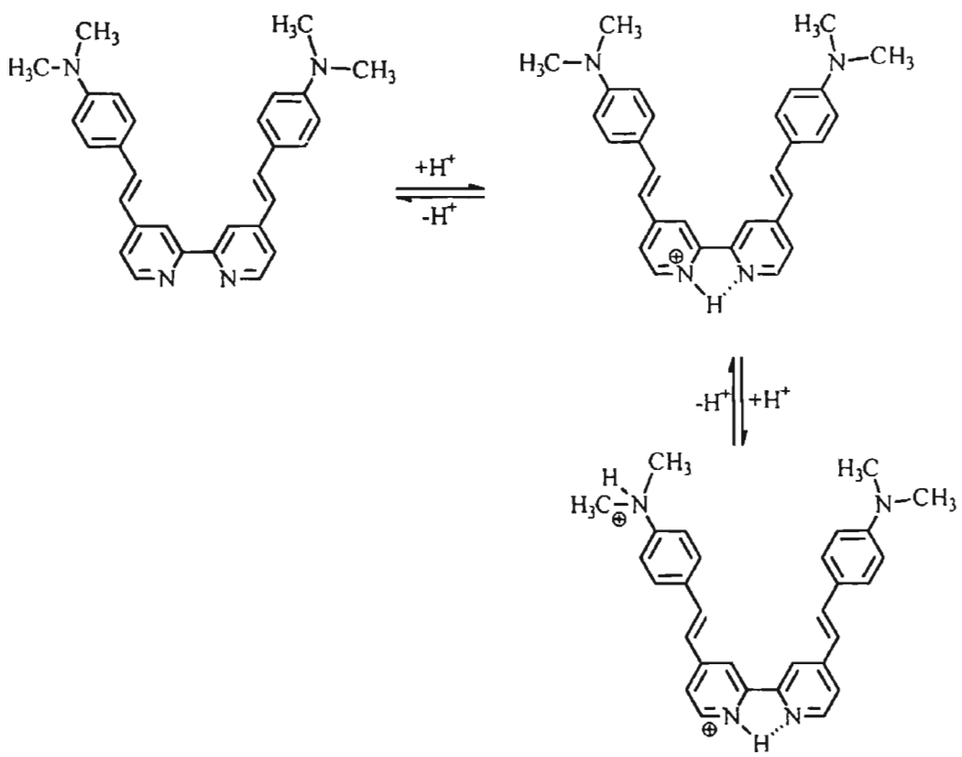

Scheme 2.4

The formation of a new band around 480 nm strongly supports this view. The site for the second protonation appears to be at the dimethylamino group. This would result in making intramolecular charge transfer more difficult due to blocking of the lone pair on the amino group. The disappearance of the long wavelength charge-transfer band (Figure 2.7) supports this.

The protonated forms are weakly fluorescent and the mono protonated form emits from 550-800 nm with a maximum around 680 nm (Figure 2.9). The absorption and emission properties of neutral and protonated forms of 7 are listed in Table 2.1.

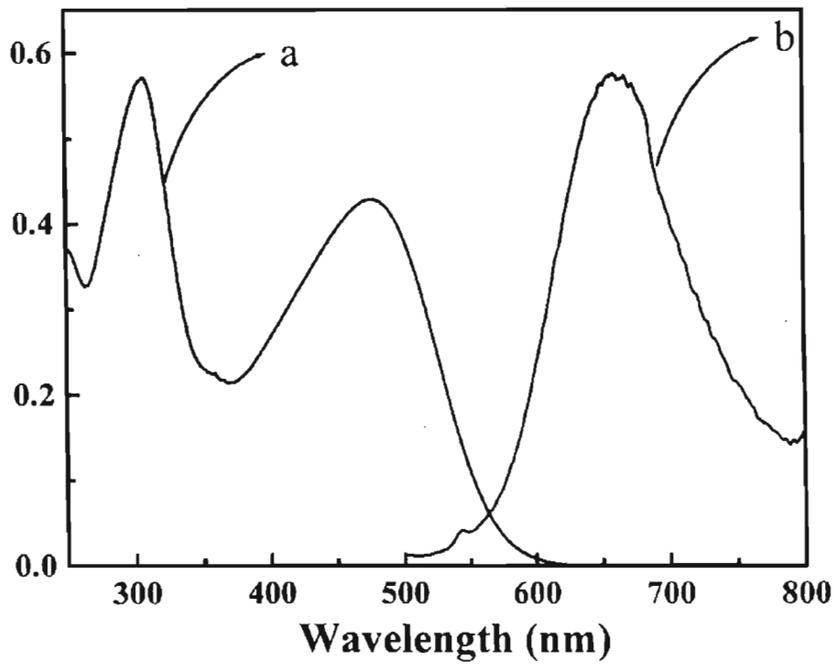

Figure 2.9. a) Absorption and b) emission spectrum of the mono protonated species of 7 in methanol.

Table 2.1. Absorption and emission properties of 7 in methanol

7	Absorption maximum (ε $M^{-1}cm^{-1}$)	Emission maximum (ϕ_f)	pKa
Neutral	380 nm (3.4 X 10^4)	550 nm (0.023)	
			4.45
Mono protonated	470 nm (3.4 X 10^4)	650 nm (4.4 x 10^{-3})	
			3.22
Di-protonated	309 nm (1.83 x 10^4)	440 nm (<1 x 10^{-3})	

2.3.2.1. Excited State pKa of 7

Nanosecond laser flash photolysis experiments were carried out to characterize the transient intermediates formed on excitation of 7. Excitation of a methanolic solution of 7 by the third harmonic of an Nd:YAG laser (355 nm, 10 ns, 60 mJ/pulse) resulted in the transient absorption as shown in Figure 2.10.

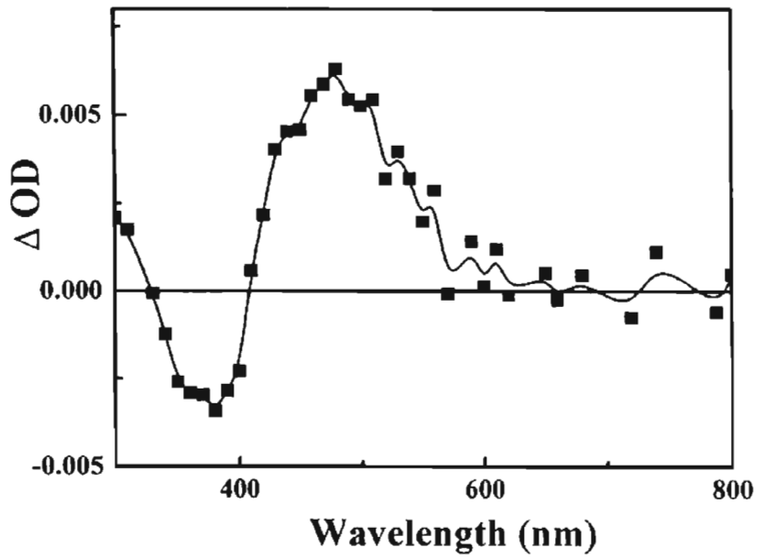

Figure 2.10. Transient absorption spectrum measured immediately after the laser pulse excitation (355 nm, 60 mJ, 10 ns) of 7 in methanol.

A bleach is observed in the region corresponding to the ground state absorption of the ligand, along with a positive transient absorption signal with a maximum centered around 480 nm. The decay of the transient absorption (Figure 2.11, trace a) is accompanied by a recovery of the ground state absorption. The transient species is not quenched by oxygen, indicating that the triplet state is not involved.

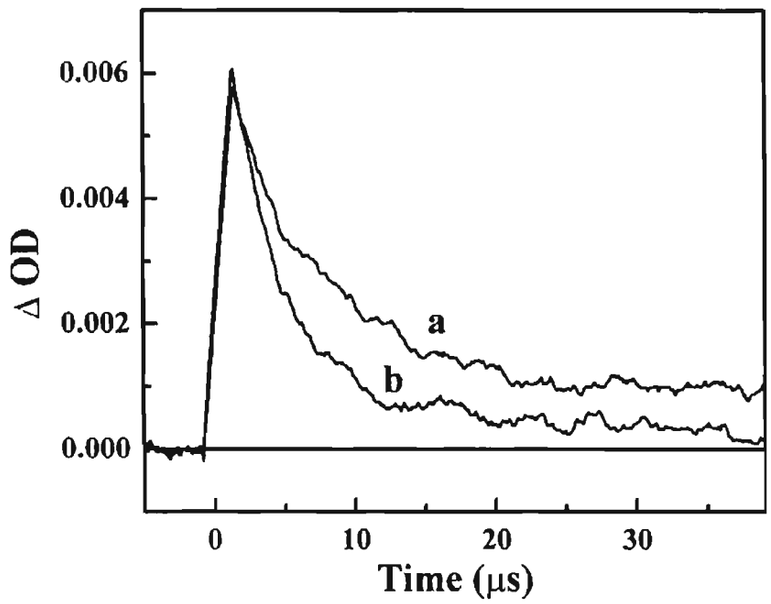

Figure 2.11. The transient decay of 7 in a) neutral, b) basic methanol, monitored at 480 nm.

The absorption maximum of the transient species corresponds to the ground state absorption maximum of the singly protonated form of the ligand. This suggests that the excited state pKa of 7 is much larger than that of the ground state. Due to the enhanced basicity of the excited state of the dye, it can pick up a proton from the solvent methanol. This change in pKa on excitation

of 7 may be attributed to an enhancement in the basicity of the pyridyl nitrogens due to an intramolecular charge transfer process. Following decay of the excited state to the ground state, deprotonation would occur in order to establish the ground state equilibrium. Addition of base results in enhancement in the decay rate of the transient and the corresponding recovery of the ground state absorption, confirming that an acid-base equilibrium process is involved (Figure 2.11, trace b). This process can be explained on the basis of the Scheme 2.5.

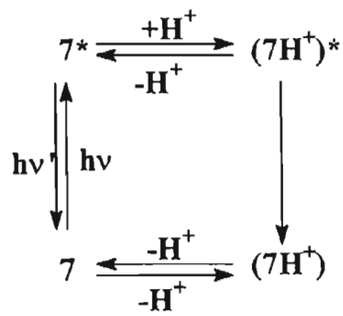

Scheme 2.5

The ability of the excited state of the ligand to abstract a proton from a solvent such as methanol suggests a substantial enhancement in its pKa in the excited state. In the excited state, the pKa values of 7 was obtained by Forster cycle equation.[34] According to this method, determination of the excited state pKa values of an acid-conjugate base system is based on the thermodynamic quantities from the equilibria which is given below (Scheme 2.6) and the energy diagram is shown in Figure 2.12.

$$ROH + H_2O \rightleftharpoons RO^- + H_3O^+$$

$$ROH^* + H_2O \rightleftharpoons (RO^-)^* + H_3O^+$$

Scheme 2.6

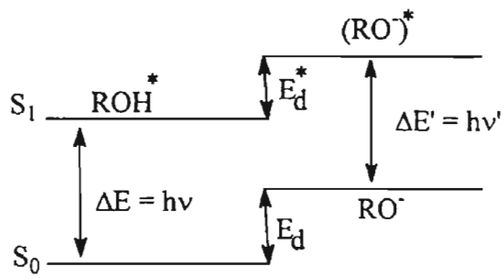

Figure 2.12. Schematic thermochemical diagram for determination of the excited state pKa values.

Based on Scheme 2.6 and Figure 2.12 the following relationship can be obtained,

$$\Delta E + E_d^* = \Delta E' + E_d \qquad (2.2)$$

where E_d and E_d^* are the heats of dissociation in the ground state and excited state and ΔE and $\Delta E'$ are the energy differences between the ground and first excited singlet states for the undissociated acid and anion or conjugate base, respectively (Figure 2.12). This Equation can be expressed as

$$E_d - E_d^* = (\Delta G - T\Delta S) - (\Delta G^* - T\Delta S^*) \qquad (2.3)$$

Assuming $\Delta S = \Delta S^*$

$$\Delta G - \Delta G^* = - RT \ln K_a/K^*_a = \Delta E - \Delta E' \qquad (2.4)$$

where the K values are the dissociation constants of the appropriate states. The difference in pKa values between the ground and excited states can then be given by Equation 2.5,

$$pKa - pKa^{*} = \frac{\Delta E - \Delta E'}{2.303RT} \qquad (2.5)$$

ΔE and $\Delta E'$ can be estimated from the 0,0 band which was obtained by using Equations 2.6 and 2.7.

$$\Delta E = h\nu = \frac{h\nu_A + h\nu_F}{2} \qquad (2.6)$$

$$\Delta E' = h\nu' = \frac{h\nu_{A'} + h\nu_{F'}}{2} \qquad (2.7)$$

where A and F refer to absorption and fluorescence respectively. Equation 2.5 can also be written as

$$pKa - pKa^{*} = 2.1 \times 10^{-3}\, \Delta\bar{\nu} \qquad (2.8)$$

where $\bar{\nu}$ is the frequency difference in cm^{-1} of the 0,0 bands of neutral and protonated forms. Using this equation and the ground state pKa value of 4.55 for **7**, the excited state pKa* of the ligand was found to be 12.3.

2.3.2.2. Complexation of 7 with Metal Ions

Colourimetric detection of cation based on changes in colour of complexation of dye reagents has recently attracted a lot of attention.[35-38] The absorption spectrum of **7** in solution was found to be very sensitive to the

presence of trace amounts of transition metal ions. Addition of copper ions to a solution of 7 in methanol at constant pH (pH 7.2) led to a decrease in the intensities of the absorption maximum at 380 nm, which was accompanied by the formation of a new band around 440 nm (Figure 2.13). Detectable changes in the absorption spectrum could be observed even in the presence of submicromolar concentrations of Cu^{2+}.

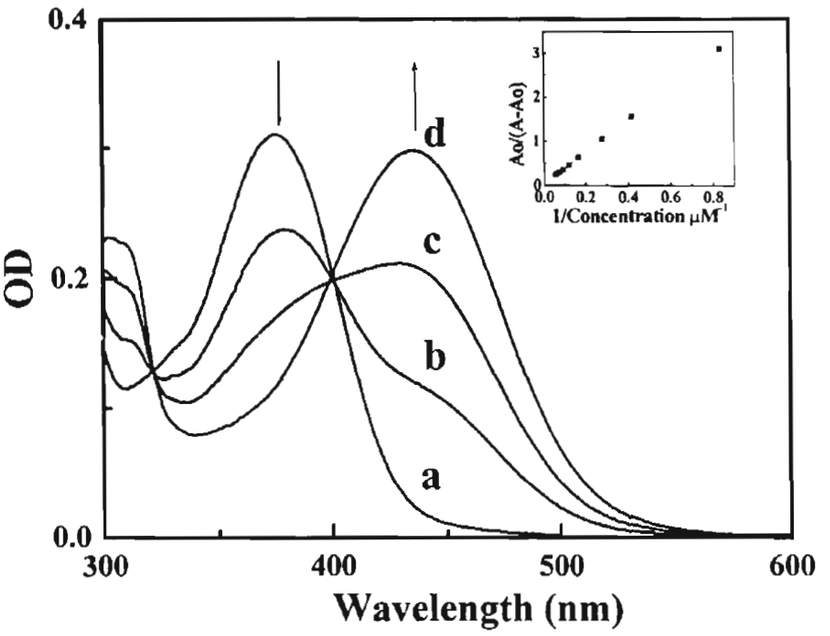

Figure 2.13. Effect of Cu^{2+} ions on the absorption spectrum of 7: a) 0 M; b) 2.4 μM; c) 6.0 μM; d) 13.45 μM: Inset shows the plot of the reciprocal of the concentration of Cu^{2+} *vs* $A_0/(A-A_0)$.

The stability constants for the complex formation of 7 with Cu^{2+} was estimated using the Benesi-Hildebrand equation (Equation 2.9) assuming a 1:1 metal to ligand complexation.

$$\frac{A}{A-A_0} = \frac{\varepsilon_L}{\varepsilon_L - \varepsilon_{ML}} \left[\frac{1}{K_s[M]} + 1 \right] \qquad (2.9)$$

where A is the absorbance of the solution containing different concentrations of metal ions, A_0 is the absorbance of the free ligand, K_s is the stability constant and [M] is the concentration of the metal ion, ε_L and ε_{ML} are the molar extinction coefficients of the free ligand and the complex, respectively. A plot of $A_0/(A-A_0)$ *vs* $1/[M^+]$ was linear confirming the 1:1 stoichiometry of the dye-metal complex at the concentrations studied. The stability constant for the complexation obtained from the slope of the plot was $2.9 \times 10^4\ M^{-1}$.

Complexation of 7 with the copper ions also leads to a reduction in the fluorescence yield of the dye (Figure 2.14). This feature of Cu^{2+}-dye complexation was analyzed using the Benesi-Hildebrand equation assuming a 1:1 metal ligand stoichiometry using Equation 2.10.

$$\frac{1}{\phi^o_f - \phi'_f} = \frac{1}{\phi^o_f - \phi_f} + \frac{1}{K(\phi^o_f - \phi_f)[\beta\text{-CD}]} \qquad (2.10)$$

where K is the stability constant, ϕ^o_f is the fluorescence quantum yield of the monomer, ϕ_f is the quantum yield of fluorescence of the dye-metal complex and ϕ'_f is the observed fluorescence. A plot of $1/(\phi_0-\phi)$ *vs* 1[M] was linear confirming the 1:1 stoichiometry of the complex at these concentrations (Figure 2.15). Using the slope of the Equation 2.10 the equilibrium constant K was obtained as $2.6 \times 10^4\ M^{-1}$ which is the same as the one obtained using absorption measurements.

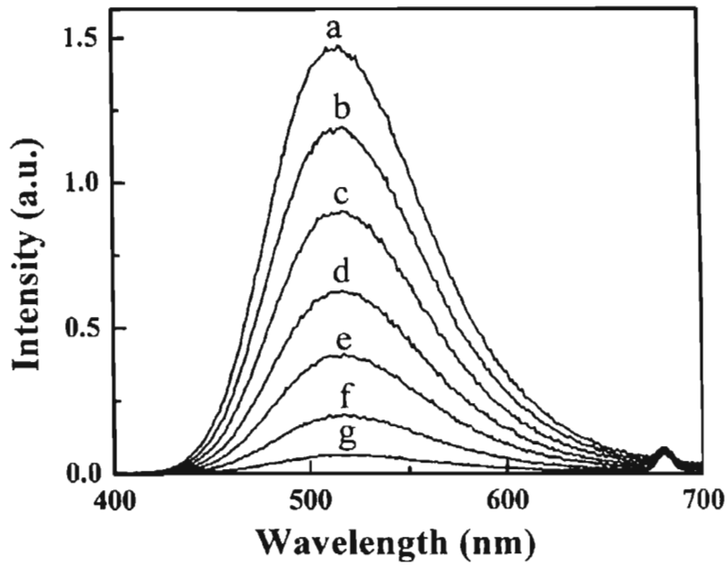

Figure 2.14. Effect of Cu^{2+} on the emission spectrum of **7**: a) 0M; b) 1.2 μM; c) 2.4 μM; d) 3.6 μM; e) 4.8 μM; f) 6 μM; g) 7.2 μM.

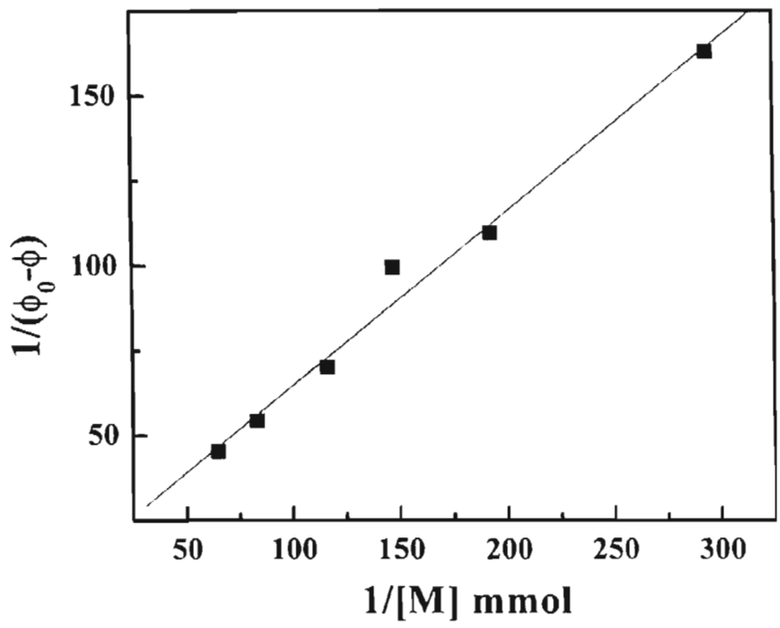

Figure 2.15. Plot of $1/(\phi_0-\phi)$ *vs* the reciprocal of the concentration of Cu^{2+} for a solution of **7** in water:methanol mixture (1:3) at pH 7.2.

Complexation of 7 with various other transition metal cations such as Hg^{2+}, Ni^{2+}, and Cd^{2+} have also been studied. The effects of Hg^{2+}, Ni^{2+}, and Cd^{2+} on the absorption spectrum of 7 are shown in Figures 2.16, 2.17 and 2.18, respectively. The absorption maxima were found to vary with the nature of the metal ion. The absorption spectrum of the dye was most sensitive to cadmium with the equilibrium constant for 1:1 complex with Cd being1.2 x 10^5 M^{-1}. The absorption maximum and equilibrium constants measured for the different metal ions have been compiled in Table 2.2.

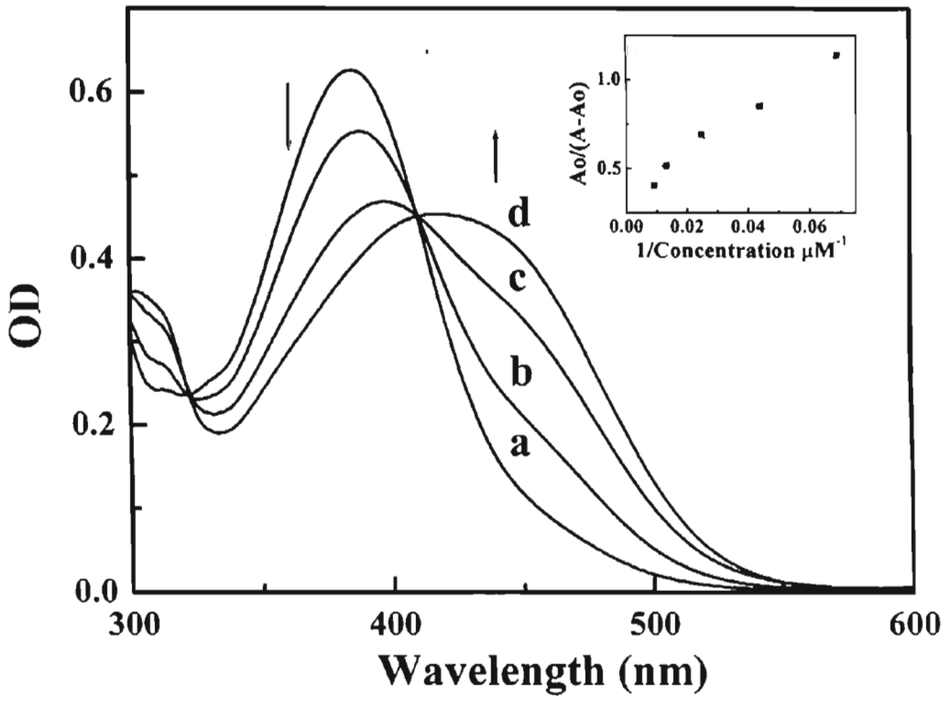

Figure 2.16. Effect of Hg^{2+} on the absorption spectrum of 7: a) 0 M; b) 5.25 μM; c) 22.8 μM; d) 110 μM. Inset shows the plot of the reciprocal of the concentration of Hg^{2+} *vs* $A_0/(A-A_0)$.

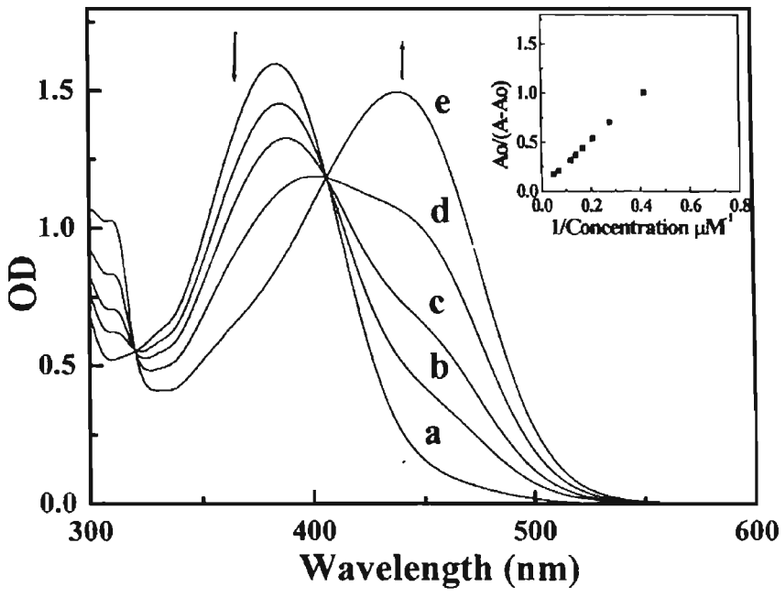

Figure 2.17. Effect of Ni^{2+} on the absorption spectrum of 7:. a) 0 M; b) 2.4 μM; c) 4.8 μM;d) 8.4 μM; e) 14.4 μM. Inset shows the plot of $A_0/(A-A_0)$ *vs* the reciprocal of the concentration of Ni^{2+} .

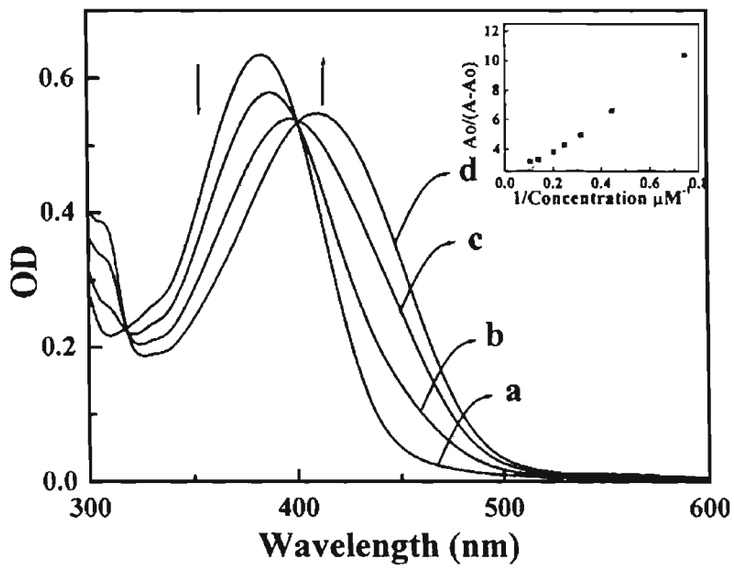

Figure 2.18. Effect of Cd^{2+} on the absorption spectrum of 7: a) 0 M; b)1.35 μM; c)4.05 μM; d)7.2 μM. Inset shows the plot of the reciprocal of the concentration of Cd^{2+} *vs* $A_0/(A-A_0)$.

Table 2.2. Stability constants for 7 with different metal cations

Cation	Cu^{2+}	Ni^{2+}	Cd^{2+}	Hg^{2+}
log K	4.2	4.6	5.1	4.6
λ_{max} nm	437	440	412	420

6/1/2013

Complexation of **7** with the metal ion involves participation of the lone pair of the electrons on pyridyl moiety. On complexation the bipyridyl moiety will become electron deficient. The resulting stabilization of the intermolecular charge state will lead to a red shift to the absorption band of the ligand.

2.3.3. Photophysical and Photochemical Properties of Ruthenium Complexes

2.3.3.1. Absorption and Emission Spectra

Absorption spectra of the ruthenium complexes (**8**, **9** and **16**) are shown in Figure 2.19. These complexes possess broad absorption in the 300-800 nm region. The broad absorption centred around 470 nm for **8**, **9**, and **16** corresponds to the MLCT transition of the ruthenium(II) polypyridyl complexes. In the symmetrically substituted ruthenium complex **8** the ligand absorption peak centred around 390 nm is clearly visible, whereas, in the unsymmetrically substituted complex **9**, only a small shoulder is observed in this region.

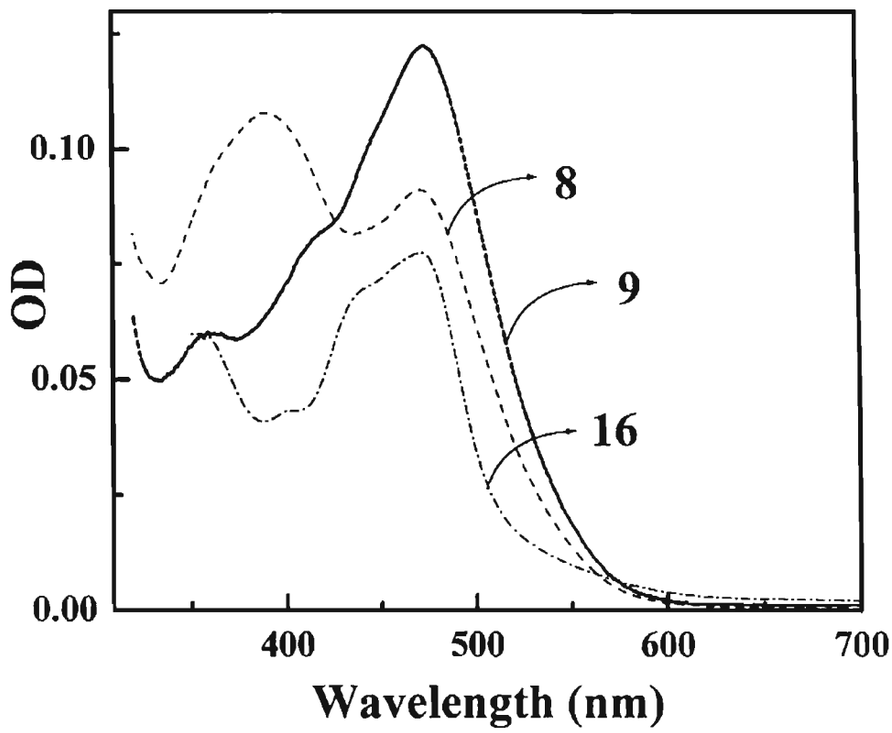

Figure 2.19. Absorption spectra of compounds **8, 9**, and **16** in methanol

Figure 2.20 shows the emission spectra of compounds **8**, **9** and **16** in deaerated methanol at ambient temperature (~27^{0}C). The emission bands have been normalized to 1 at their maximum. The emission maxima of **8** and **9** are red shifted, compared to the model ruthenium complex **16**. The radiative quantum yields of these compounds were calculated using the Equation 2.11,[39]

$$\phi_f s = \frac{\phi_f r \times A_S \times OD_r}{Ar \times ODs} \qquad (2.11)$$

where, s is sample, r is reference, A is peak area,
OD is optical density at excitation wavelength

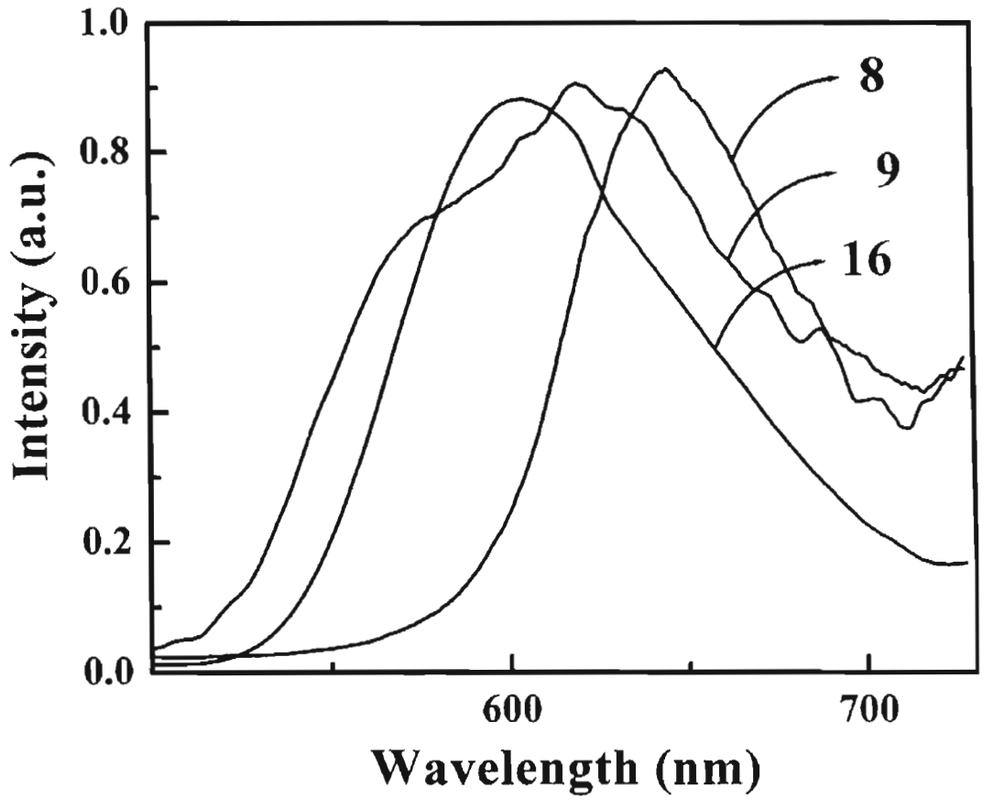

Figure 2.20. Emission spectra of **8**, **9** and **16** in deaerated methanol measured at room temperature.

Trisbipyridyl ruthenium(II) chloride hexahydrate (ϕ_f = 0.05) was used as the reference compound.[39] The extinction coefficients and radiative quantum yields of the complexes studied are listed in Table 2.3. The emission of these compounds is readily quenched by oxygen suggesting the involvement of the triplet excited state.

Table 2.3. Absorption and emission properties of compounds 8, 9 and 16

Compounds	Absorption λ_{max} (nm)	Emission	
		λ_{max}(nm)	ϕ_f
8	390($\varepsilon = 7.73 \times 10^4 M^{-1}cm^{-1}$), 471($\varepsilon = 6.7 \times 10^4 M^{-1}cm^{-1}$)	700	0.018
9	474($\varepsilon = 3.51 \times 10^4 M^{-1}cm^{-1}$)	682	0.0005
16	472($\varepsilon = 1.9 \times 10^4 M^{-1}cm^{-1}$)	663	0.12

2.3.3.2. Laser Flash Photolysis Studies of Compounds 8, 9, and 16

Nanosecond laser flash photolysis experiments were carried out in deaerated solutions of the ruthenium complexes in order to characterize the transient intermediates formed on excitation. The second harmonic of a Nd: YAG laser (532 nm, 10 ns pulse, 60 mJ/pulse) was used to excite the complexes. Figure 2.21 shows the transient absorption spectra obtained for the symmetrically substituted ruthenium complex **8**. Two negative absorption peaks with maxima centred around 430 nm and 530 nm were observed. These can be attributed to the depletion of the ground state on excitation of the complex. The complex has a strong ground state absorption below 550 nm with maxima centred around 390 nm and 471 nm. The mismatch between the maxima observed in the transient absorption spectrum and the ground state absorption spectrum may be attributed to

the presence of a transient species with strong absorption in the 400-550 nm region. A weak positive transient absorption was also observed above 560 nm. The rate of transient decay corresponds well with the recovery of the bleach at 410 nm and 530 nm (τ = 0.58 μs). The efficient quenching of the transient by oxygen suggests that it may be the triplet excited state of the complex. The triplet nature of the transient intermediate was confirmed by energy transfer to β-carotene which resulted in the formation of the triplet excited state of β-carotene.

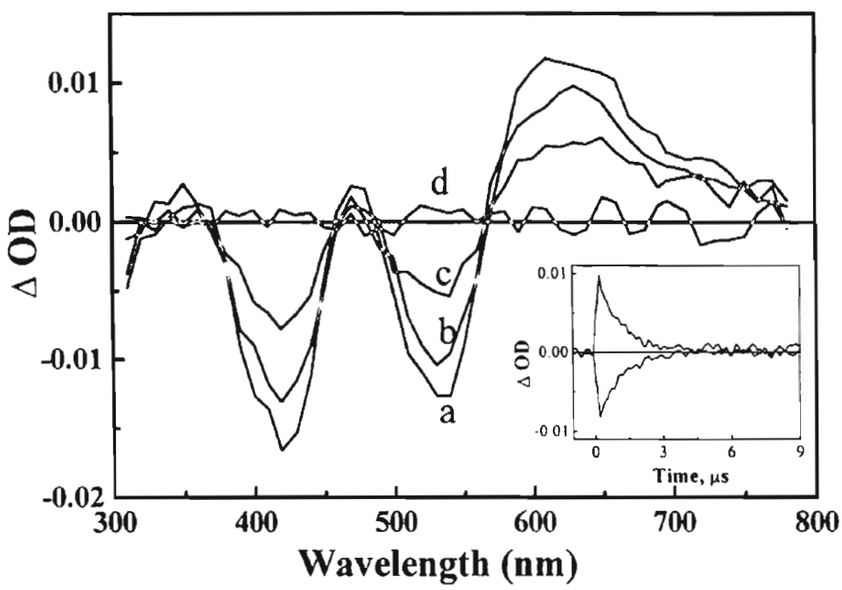

Figure 2.21. Transient absorption spectra measured following laser pulse excitation (532 nm, 10 ns, 60 mJ/pulse) of **8** in deaerated acetonitrile: a) 0.23 μs; b) 0.45 μs; c)1.05 μs; d) 2.75μs. Inset shows transient absorption profile at 590 nm and 470 nm.

The transient absorption spectra of **9** (Figure 2.22) show a bleach in the 470 nm region and a positive absorption above 560 nm region. For the model complex **16**, however, the transient absorption spectrum (Figure 2.23) shows an

additional bleach in the near infrared region with a maximum centred around 660 nm where the ground state of the complex does not absorb. This apparent bleach is attributed to phosphorescence emission from the triplet excited state of **16** which could result in additional light reaching the detector. The emission quantum yield was higher for **16** than for **8** and **9** (Table 2.3). The triplet nature of the transient species formed on excitation of **9** and **16** were also confirmed by energy transfer to β-carotene.

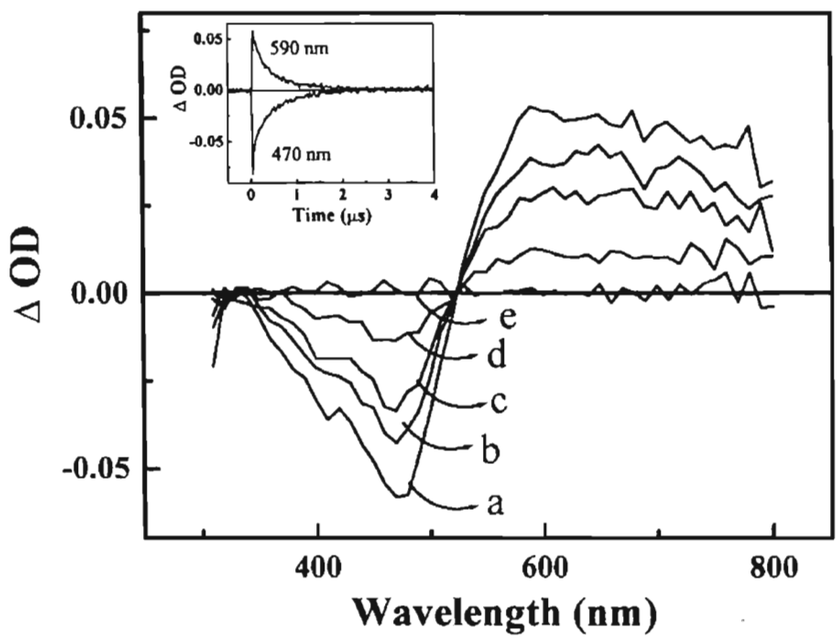

Figure 2.22. Transient absorption spectra measured following laser pulse excitation (532 nm, 10 ns, 60 mJ/pulse) of **9** in de-aerated methanol: a) 0.7; b) 1.5; c) 2.6; d) 6.9;e) 4.5μs. Inset shows transient absorption profile at 590 nm and 470 nm.

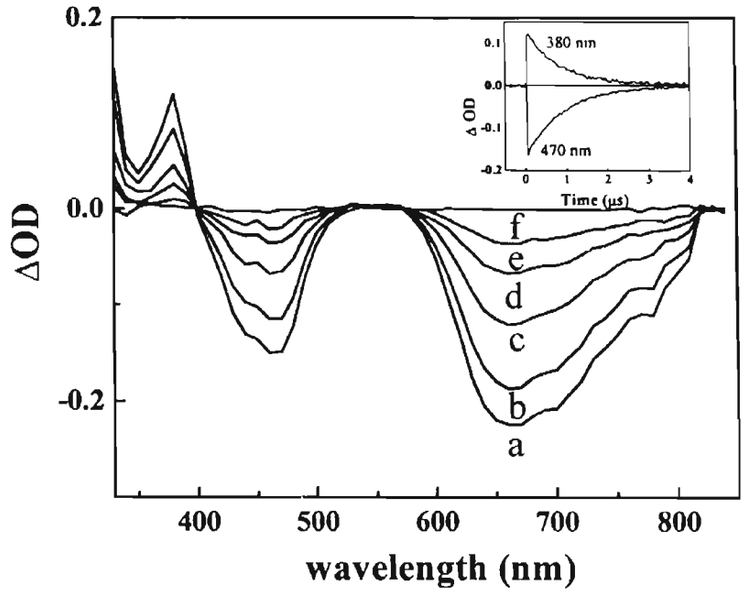

Figure 2.23. Transient absorption spectra measured following laser pulse excitation (532 nm, 10 ns, 60mj/pulse) of **16** in deaerated methanol at: a)1.1 ;b) 3.6; c) 8.6; d) 1.4; e) 2.0; f) 4.5 μs. Inset shows transient absorption profile at 380 nm and 470 nm.

The triplet yields (ϕ_T) of the compounds in deaerated methanol were measured by energy transfer to β–carotene.[40,41] Optically matched methanolic solutions of the compounds and trisbipyridyl ruthenium(II) dichloride were mixed with a known volume of a 0.1 mM solution of β-carotene in benzene. The transient absorbance of β-carotene at 520 nm was monitored and the triplet quantum yields were measured using the Equation 2.12,

$$\phi_T^S = \phi_T^R \left(\frac{\Delta A^S}{\Delta A^R}\right)\left(\frac{k_{obs}^S}{k_{obs}^S - k_o^S}\right)\left(\frac{k_{obs}^R - k_o^R}{k_{obs}^R}\right) \qquad (2.12)$$

where ϕ_T is the triplet yield, ΔA is the plateau absorbance following the completion of sensitized triplet formation, k_{obs} is the pseudo first order rate constant for the growth of the β-carotene triplet sensitized by the compounds or trisbipyridyl ruthenium (II) dichloride, and k_o is the rate constant for decay of a triplet in the absence of β-carotene. S and R denote sample and reference. The absorption maxima, lifetimes and quantum yields of the triplet state of the compounds are shown in Table 2.4.

Table 2.4. Triplet excited state properties of compounds 8, 9, and 16 in deaerated methanol

Compounds	Triplet wavelength (λ_{max})	ϕ_T	Lifetime (μs)
8	590 nm	0.19	0.58
9	590 nm($\varepsilon_T = 1.52 \times 10^4$)	0.23	0.46
16	380 nm ($\varepsilon_T = 3.18 \times 10^4$)	0.47	0.78

2.3.3.3. Excited State Redox Properties

Electron transfer processes from the excited state of sensitizers play a key role in harvesting solar energy. The ability of the ruthenium complexes (**8**, **9** and **16**) to undergo electron transfer from their excited states was investigated using methyl viologen as the electron acceptor. The one electron reduced form of methyl viologen has a characteristic absorption spectrum with maxima centred at 385 nm and 600 nm. Figure 2.24 shows the transient absorption profile at 398 nm

on laser pulse excitation of **9** in deaerated methanol containing varying amounts of methyl viologen. These results are indicative of a highly efficient electron transfer process from the excited state of the complex to the ground state MV^{2+}, as shown in Scheme 2.7. From the dependence of the observed rate constant of growth of $MV^{+\cdot}$ on the concentration of MV^{2+} a second order rate constant of 9×10^{10} $M^{-1}s^{-1}$ was obtained for the electron transfer quenching of the excited state. This value is much faster than those observed for normal diffusion controlled processes, and may be attributed to the attractive forces between the oppositely charged ruthenium complex **9** and MV^{2+}. The presence of carboxylate anion on **9** provides it with a net negative charge.

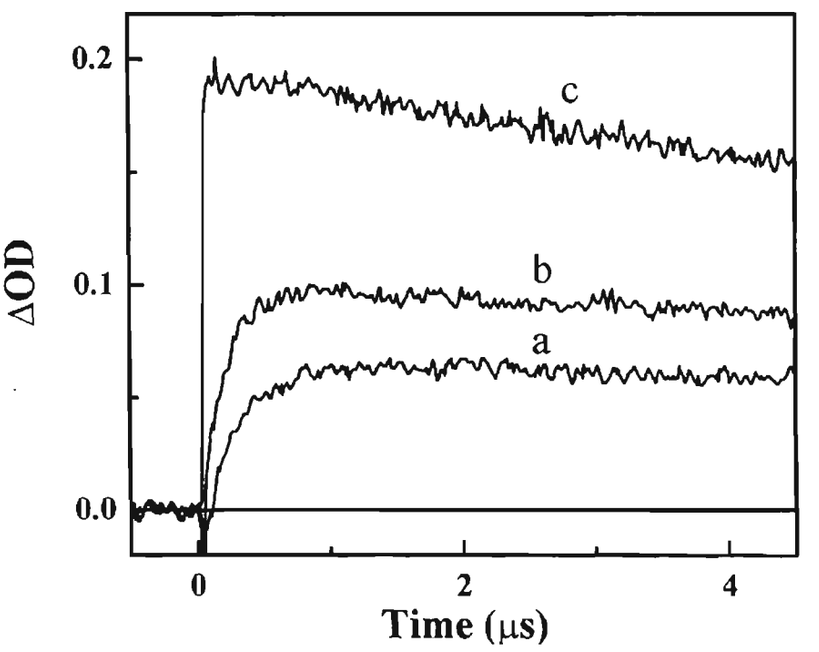

Figure 2.24. Growth of methyl viologen radical cation monitored at 398 nm, measured following laser pulse excitation (532 nm, 10 ns, 60 mJ/pulse) of **9** in deaerated methanol at different concentrations of methyl viologen: a) 17.4 μM, b) 34.8 μM, c) 0.88 mM.

$$\text{Dye} \xrightarrow{h\nu} {}^{3}\text{Dye}^{*}$$

$${}^{3}\text{Dye}^{*} + MV^{2+} \rightleftharpoons \text{Dye}^{+\bullet} + MV^{+\bullet}$$

Scheme 2.7

Figure 2.25 shows the transient decay profile at 398 nm, following laser pulse excitation of methanolic solutions of **9** (trace a) and **16** (trace b) containing 0.88 mM MV^{2+}. The optical density of the solutions at the excitation wavelength was matched for the two solutions. It becomes evident from Figure 2.25 that the excited state electron transfer process is far more efficient for **9** than for **16**.

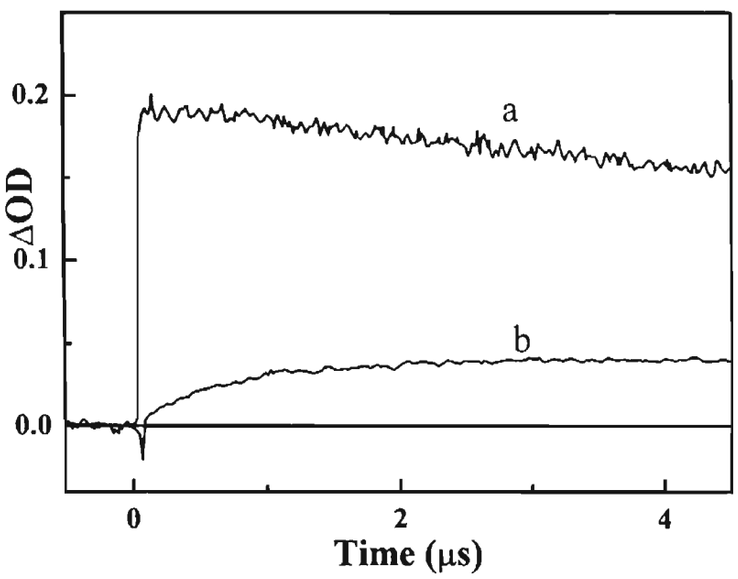

Figure 2.25. Growth of methyl viologen radical cation monitored at 398 nm measured following laser pulse excitation (532 nm, 10 ns, 60 mJ/pulse) of: a) **9**; b) **16** in deaerated methanol.

The second order rate constants for electron transfer of the excited state of **16** to the ground state of MV^{2+} was also lower (k = 2.5 x 10^9 $M^{-1}s^{-1}$). The enhanced efficiency of electron transfer for **9** compared to that from **16** may be attributed to the presence of the electron donating substituents on the bipyridyl ligand in **9**.

The rate constant for electron transfer from the ruthenium complex **8** to MV^{2+} is much lower (k = 2.09 x 10^9 $M^{-1}s^{-1}$) in spite of the presence of electron donating substituents on the bipyridyl ligand of this complex. This may be attributed to the repulsive forces between the positively charged ruthenium complex, **8** and MV^{2+}.

The $MV^{+\cdot}$ formed in these reactions decays back to MV^{2+} by a second order process, which is attributable to back electron transfer to the oxidised form of the ruthenium complex (Figures 2.26 and 2.27).

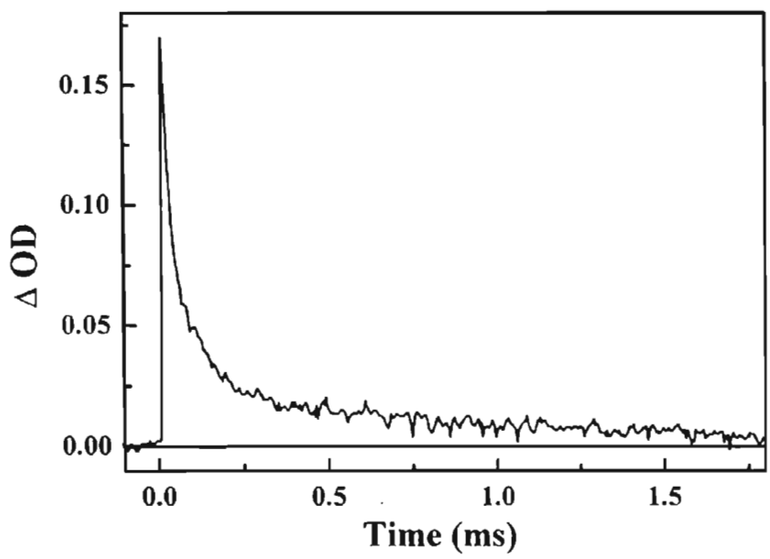

Figure 2.26. Decay of methyl viologen radical cation monitored at 398 nm measured following laser pulse excitation (532 nm, 10 ns, 60 mJ/pulse) in a methanolic solution of **9**.

The second order rate constants for the process was slightly higher for **9** (k = 6.8 x 10^9 $M^{-1}s^{-1}$) than for the model compound **16** (k = 2.5 x 10^9 $M^{-1}s^{-1}$).

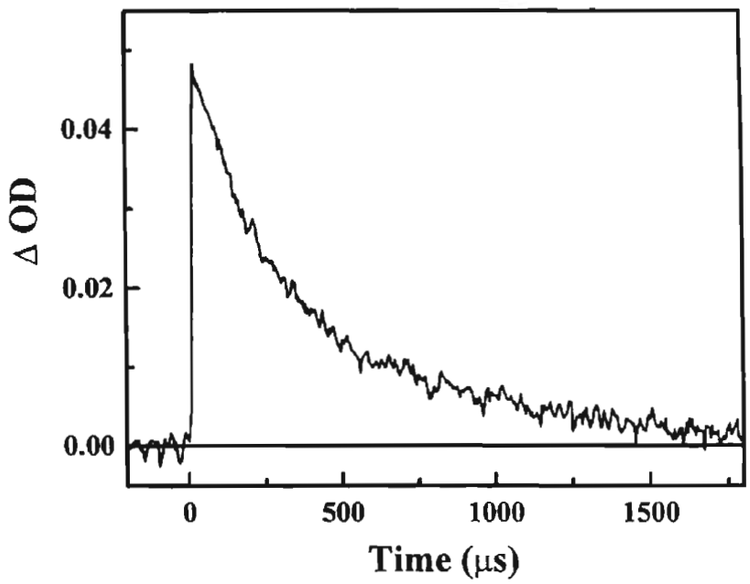

Figure 2.27. Decay of methyl viologen radical cation monitored at 398 nm measured following laser pulse excitation (532 nm, 10 ns, 60mj/pulse) in a methanolic solution of **16**.

2.3.3.4. Phosphorescence Spectra of Compounds 8, 9 and 16

The phosphorescence emission spectra of the ruthenium complex **8**, **9**, and **16** were measured in ethanol glass at 77 K. The complexes emit in the 600 nm to 800 nm region. The emission maxima, phosphorescence lifetime and energy corresponding to the short wavelength band maximum are summarised in Table 2.5.

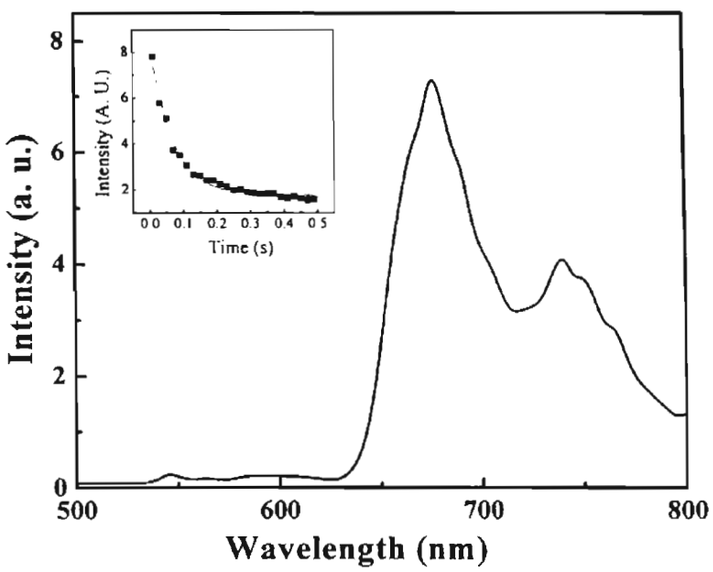

Figure 2.28. Phosphorescence spectrum of **8** in ethanol glass at low temperature Inset shows the decay profile of **8** in ethanol glass monitored at 670 nm

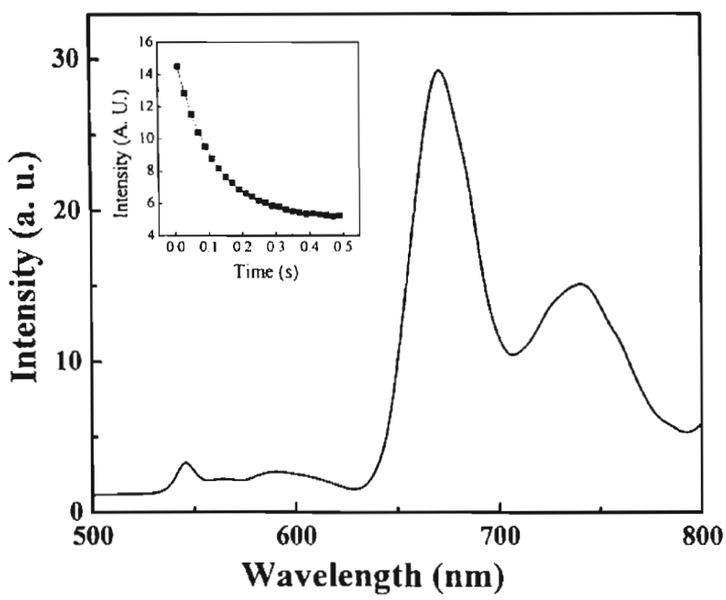

Figure 2.29. Phosphorescence spectrum of **9** in ethanol glass at low temperature. Inset shows the decay profile of **9** in ethanol glass monitored at 670 nm.

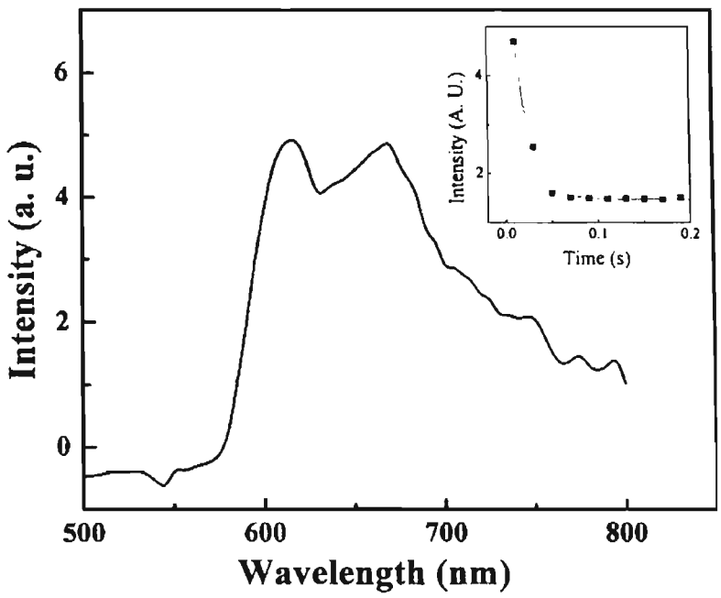

Figure 2.30. Phosphorescence spectrum of **16** in ethanol glass at low temperature. Inset shows the decay profile in ethanol glass monitored at 600 nm.

Table 2.5. Phosphorescence maximum and phosphorescence lifetime of compounds 8, 9, and 16.

Compound	Emission max	τ_p	E eV
8	675, 740 nm	66.33 μs	1.83
9	670, 740 nm	107.07 μs	1.85
16	600, 670 nm	16.46 μs	2.06

2.3.3.5. Photosensitization of Nanoporous TiO_2 Films

Colloidal TiO_2 was cast on optically transparent electrodes (Indium-tin-oxide (ITO) coated glass plates). For preparing the colloidal TiO_2 a mixture of Titanium (IV) isopropoxide (7.4 mL) and 2-propanol (2 mL) was added dropwise over a period of 30

minutes to dilute acetic acid (66 mL). The solution was then heated at 80 ^{0}C for 4 h. The nanoparticles were dispersed in solution by probe sonication for 20 minutes. [42] For preparing the nanocrystalline TiO_2 films, the ITO glass plates was covered on two parallel edges with adhesive tape to control the thickness of TiO_2 film and to provide noncoated areas for electrical contact. The colloid was applied to one of the free edges of the conducting glass and distributed with a glass rod sliding over the tape-covered edges. After air drying, the electrode was fired for 30 min at 450-500 °C in air. Transparent uniform films of TiO_2 could be obtained in this manner.

Coating of the TiO_2 surface with compounds **9** and **16** was carried out by soaking the TiO_2 film for 12 h in a 6 x 10^{-4} M solution of the ruthenium complex in dry methanol. The dye coating was carried out immediately after the high-temperature annealing in order to avoid rehydration of the TiO_2 surface or capillary condensation of water vapor from ambient air into the nanopores of the film. The presence of water in the pores can decrease the charge injection efficiency of the dye. The electrode was dipped into the dye solution while it was still hot (80 °C). After completion of the dye adsorption, the electrode was withdrawn from the solution under a stream of dry air or argon.

Photoelectrochemical experiments were carried out by incorporating the dye sensitized TiO_2 film into a thin-layer sandwich-type solar cell.[42] A light reflecting counter electrode was employed, consisting of a conducting ITO glass onto which a platinum mirror had been deposited by electrochemical method. The counter electrode was placed directly on top of the dye-coated transparent film supported by the

conducting glass sheet. Both electrodes were clamped tightly together. A thin layer of electrolyte was attracted into the interelectrode space by capillary forces. A 450W xenon light source of Spex in combination with a monochromator (SPEX 1681 0.22m) was used to irradiate the cell at all selected wavelengths.

The photocurrent-wavelength characteristics of the cells using photoelectrodes coated with **9** and **16** are shown in Figures 2.31 and 2.32, respectively. The spectrum obtained for the photocurrent generation was observed to be similar to absorption spectrum of the complexes. Maximum photocurrent generation was observed at 470 nm in both cases which corresponds to the absorption maximum of the complexes.

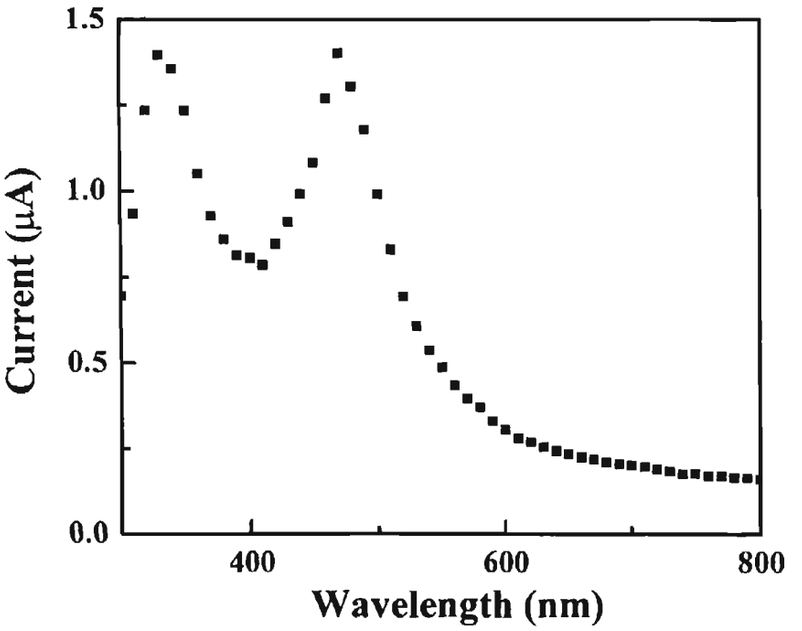

Figure 2.31. Plot of photocurrent generated by the photoelectro-chemical cell coated with **9** *vs* wavelength of excitation.

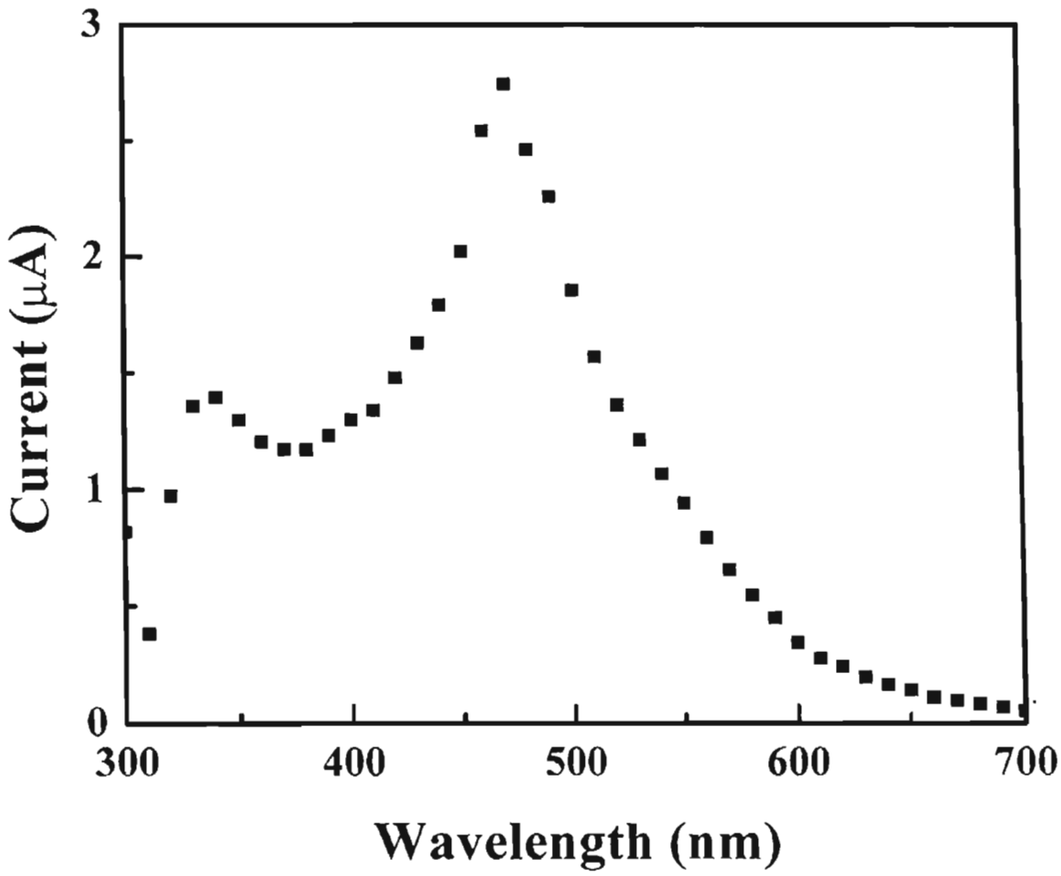

Figure 2.32. Plot of photocurrent generated by the photoelectrochemical cell coated with **16** vs wavelength of excitation.

Correction of the photocurrent generating efficiencies of the cell, for intensity of light absorbed, shows that cells employing **9** has the photocurrent generating efficiency ~40% of that for the cell using model ruthenium complex **16** as sensitizer. This appears to be contradictory with the results in the solution phase which have shown that photoelectron transfer and charge separation is more efficient for **9** than for **16**. A possible reason for the reduction in efficiency of photocurrent generation in cell employing **9** as photosensitizer may be its reduced triplet yield. The triplet

yield of **9** is roughly half of that of **16** (Table 2.4). The excited singlet state of the complexes may be too short-lived to participate in the semiconductor photosensitization process.

2.4. Conclusion

A bipyridyl ligand containing amino group as donor moiety was prepared and its photophysical properties were investigated. Two ruthenium complexes **8** and **9** were prepared using ligand **7**. Although the efficiency of charge separation from the excited state is much faster for **9** when compared to that of the model complex **16**, in solution the photocurrent generation efficiency of **9** is much less. This may be partly due to the reduced intersystem crossing efficiency of **9** compared to that of the model complex. The excited singlet state of the complexes may be too short-lived to participate in the semiconductor photosensitization process.

2.5. Experimental Section

2.5.1. Materials and Methods

General Aspects. All melting points are uncorrected and were determined using Aldrich Mel-Temp melting point apparatus. The electronic absorption spectra were recorded on Shimadzu 3101 UV-visible-NIR spectrophotometer. Radiative quantum yields were measured by relative methods using optically dilute solutions. Quinine sulphate (fluorescence quantum yield ϕ_f = 0.55) in 1N H_2SO_4, Rhodamine 6G (ϕ_f= 0.9) in ethanol and tris(bipyridyl) ruthenium(II) dichloride (ϕ_r = 0.05) in methanol were used as standard.[43] Phosphorescence emission spectra

of the compounds in ethanol glass at 77K were recorded on a SPEX 1934 D phosphorimeter. An Elico pH meter was used for pH measurements. Sodium hydroxide or HCl was used to adjust the pH. Solvents used were purified before use. All the experiments were carried out at room temperature (25 ± 1 °C).

Chemicals. β-Carotene(Aldrich) was recrystallized from a mixture of benzene and methanol. 1,3-Diphenylisobenzofuran (DPBF), and trisbipyridyl ruthenium(II) dichloride were used without further purification.

2.5.2. Synthesis

Synthesis of 4,4'-Bis[2-hydroxy-2-[*p*-(dimethylamino)phenyl]ethyl-2,2'-bipyridine

Compound 7 was prepared by adopting a reported procedure.[33] *n*-Butyllithium (9 mL, 14.4 mmol, 1.6 M in hexane) was added to a solution of diisopropylamine (1.44g, 14.4 mmoi) in dry THF (4 mL) under nitrogen atmosphere. The pale yellow solution was stirred at -0.5 ^{0}C for 20 min. Then a solution of 4,4'-dimethyl-2,2'-bipyridine (1 g, 5.4 mmol) in dry THF (20 mL) was added dropwise. The turbid reaction mixture was then stirred at 0^{0}C for 45 min. To this a solution of 4-(dimethylamino)benzaldehyde (1.61 g, 10.8 mmol) in dry THF (10 mL) was added dropwise over a period of 5 min. The mixture was stirred at 0 ^{0}C for 45 min and then at room temperature for 8 h. It was quenched with water and the product was extracted with dichloromethane (3 x 100 mL). The solvent was removed under reduced pressure and the residue on recrystallization from benzene gave 800 mg (31%) of the diol. mp 220^{0}C (decomp) IR (KBr) ν_{max} 3487, 1613,

1460, 1350, 1060, 818, 565 cm^{-1}; ^1H NMR (300 MHz, $CDCl_3$) δ 2.9 (12 H, s, -N-CH_3), 2.4 (4H, m, -CH_2CHOH), 4.9 (2H, t, -CHOH), 6.7-8.5 (14 H, m, aromatic)

Synthesis of 4-4'-Bis(p-dimethylamino)-α-styryl-2,2'-bipyridine (7)

A 10% aqueous H_2SO_4 solution (20 mL) was added to 4,4'-Bis[2-hydroxy-2-[p-(dimethylamino)phenyl]ethyl-2,2'-bipyridine and the mixture was heated at 90 ^{0}C for 2 h to yield a purple solution. The mixture was then cooled and neutralized with NaOH solution (1N) and extracted using dichloromethane and dried over $MgSO_4$. The solvent was removed under reduced pressure and the product was purified by column chromatography on silica gel (100-200) mesh using chloroform as eluent to yield 200 mg (27%) 7. IR (KBr) ν_{max} 1658, 1584, 1534, 1457, 1367, 1181, 980, 822, 575, 525 cm^{-1}; ^{1}HNMR (300MHz, $CDCl_3$) 3.0 (12H, s, N-CH_3) 6.7-8.5 (18H, m, aromatic).

Preparation of 8

A mixture of $RuCl_3.3H_2O$ (30 mg,11.4 mmol) and **7** (163 mg, 36 mmol) was heated under reflux in DMF (10 mL) for 18 h under argon atmosphere. The solvent was removed under reduced pressure. The residue was dissolved in acetone and filtered the solution for insoluble impurities. Compound **8** was finally precipitated with diethyl ether to yield 85 mg(46 %) of **8**. mp > 400 ^{0}C; IR (KBr) ν_{max} 3449, 1961, 1707, 1656, 1594, 1593, 1527, 1483, 1356, 1167, 1116, 1022, 808 cm^{-1}. UV λ_{max} (CH_2Cl_2) 435 nm (ε 77300), 491nm (ε 67000); Anal calcd. for $C_{91}H_{93}C_{12}N_{12}Ru$. C, 71.49; H, 6.0; N, 11.01; found C, 62.79; H, 6.09; N, 11.01;

Preparation of Bis(4,4'dicarboxylato-2,2'-bipyridyl)ruthenium (II) dichloride

A mixture of $RuCl_3$. $3H_2O$ (135 mg, 0.51 mmol) and 2,2'-bipyridyl-4,4'-dicarboxylic acid (250 mg, 1.03 mmol) in DMF (40 mL) was refluxed for 8 h under argon atmosphere. The contents were cooled and filtered in order to remove the insoluble impurities. The filterate was concentrated under reduced pressure. The crude product was precipated with diethyl ether. It was again dissolved in the minimum quantity of methanol and precipitated from acetone to yield 291 mg, (94 %) of bis(4,4'dicarboxylato-2,2'-bipyridyl)ruthenium (II) dichloride. mp 300 ^{0}C (dec) IR (KBr) ν_{max} 3472, 1990, 1728, 1664, 1640, 1548, 1381, 1235, 1133, 1018 cm^{-1}.

Preparation of 9.

A mixture of bis(2,2'-bipyridyl-4,4'-dicarboxylato)ruthenium(II)chloride (191 mg, 0.33 mol), **7** (147 mg, 0..33 mmol) and sodium bicarbonate (109 mg) were refluxed together in 8.6 mL of a mixture of methanol-water (1:1) solution until the bis(4,4'dicarboxylato-2,2'-bipyridyl)ruthenium (II) dichloride was used up, as indicated by the absorption spectrum. Aqueous 3M ammonium hexafluorophosphate (4 mL) was added and a red solid precipitated out. Recrystallization from acetone, yielded 40 mg (11%) of the product. IR(KBr) ν_{max} :3488, 1672, 1630, 1411, 1133, 595 cm^{-1}. Anal. calcd. for $C_{54}H_{46}F_{12}N_8O_8P_2Ru.3H_2O$ C, 48.26; H, 3.6; N, 8.34; Found: C, 42.49; H, 4.06; N, 8.89.

Preparation of 16

Bis(2,2'-bipyridyl-4,4'-dicarboxylato)ruthenium (II) chloride (104 mg, 0.16 mmol), 2,2'-bipyridine (29 mg, 0.16 mmol) and sodium bicarbonate (59 mg) were refluxed together in 8.6 ml of 1:1 methanol-water solution until the bis(2,2'-bipyridyl-4,4'-dicarboxylato)ruthenium (II) chloride was used up, as indicated by the absorption spectrum. Aqueous 3M ammonium hexafluorophosphate (4 ml) was added and a red solid precipitated out, which on recrystallization from acetone, yielded 55 mg (43 %) of the product. IR (KBr):ν_{max} 3432, 2928, 1992, 1717, 1626, 1401, 1225, 1261, 842, 763 cm^{-1}; Anal calculated for $C_{34}H_{24}F_{12}N_6O_8P_2Ru..H_2O$: C 38.76; H, 2.49; N, 7.98; Found C, 38.86; H, 2.98; N, 7.63

2.6. References

1. Piechowski, A. P.; Bird, G. R.; Morel, D. L.; Stogryn, E. L., *J. Phys. Chem.* **1984**, *88*, 934.
2. *Photochemical Energy Conversion*, (Ed.: Norris, J. R., Meisel, D.), 1989, New York, **1989**.
3. Wrighton, M. S., *Pure and Appl. Chem.* **1985**, *57*, 57.
4. Haase, M.; Weller, H.; Henglein, A., *J. Phys. Chem.* **1988**, *92*, 482.
5. E. Pelizzetti, M. S., *Photochemical Conversion and Storage of Solar Energy*, in *Proceedings of Eighth International Conference on Photochemical Conversion and Storage of Solar energy*, **1990**.
6. Liu, D.; Kamat, P. V., *J. Phys. Chem.* **1993**, *97*, 10769.
7. Heimer, T. A.; Bignozzi, C. A.; Meyer, G. J., *J. Phys. Chem.* **1993**, *97*, 11987.
8. Meyer, G. J., *J. Chem. Edu.* **1997**, *74*, 652.
9. Jana, A. K., *J. Photochem. Photobiol A: Chem* **2000**, 1.
10. Lehn, J. M.; Sauvage, P. P.; Seissel, R., *Nouceau J. De. Chemie* **1980**, 623.
11. Serpone, N.; Pelizetti, E. in *Photocatalysis:Fundamentals and Applications*, J. Wiley, New York, **1989**.
12. Ma, Y.; Yao, J. N., *J. Photochem. Photobiol. A: Chem.* **1998**, *116*, 167.
13. Regan, O.; Grätzel, M., *Nature* **1991**, *353*, 737.
14. Bach, U.; Lupo, D.; Cornte, P.; Moser, J. E.; Weissörtel, F.; Salbeck, J.; Spreitzer, H.; Grätzel, M., *Nature* **1998**, *395*, 583.
15. Kay, A.; Gratzel, M., *J. Phys. Chem.* **1993**, *97*, 6272.

16. Heimer, T. A.; Bignozzi, C. A.; Meyer, G. J., *J. Phys. Chem.* **1993**, *97*, 11987.

17. Archer, M. D.; Ferreira, M. I. in *Photochemical Conversion and Storage of Solar Energy*, Academic Press, New York, **1981**.

18. Matusyama, T.; Baba, T.; Tanaka, M.; Isomura, M.; Tsuda, S.; Nakano, S.; Kuwano, Y., *SPIE* **1993**, *2017*, 216.

19. Nazeerudin, M. K.; Kay, A.; Radicio, I.; Humphry-Baker, R.; Muller, E.; Liska, P.; Vlachopoulous, N.; Grätzel, M., *J. Am. Chem. Soc.* **1993**, *115*, 6382.

20. Tsubomera, H.; Matsumara, M.; Noyamura, Y.; Amamyiya, T., *Nature* **1976**, *261*, 402.

21. Dare-Edwards, M. P.; Goodenough, J. B.; Hammet, A.; Seddon, K. R.; Wright, R. D., *Faraday Discuss. Chem. Soc.* **1980**, *70*, 285.

22. Duonghong, D.; Serpene, N.; Grätzel, M., *Helv. Chim. Acta* **1984**, *67*, 1012.

23. Desilvestro, J.; Grätzel, M.; Kavan, L.; Moser, J. E.; Augustynski, J., *J. Am. Chem. Soc.* **1985**, *107*, 2988.

24. Matsumara, M.; Nomura, Y.; Tsubomura, H., *Bull. Chem. Soc. Japan* **1977**, *50*, 2533.

25. Willig, F.; Eichberger, R.; Sundaresan, N. S.; Parkinson, B. A., *J. Am. Chem. Soc.* **1990**, *112*, 2702.

26. Kalyanasundharam, K. in *Photochemistry of polypyridine and porphyrin complexes*, Academic press, London, **1992**.

27. Sauvage, J.-P.; Collin, J.-P.; Chambron, J.-C.; Guillerez, S.; Coudret, C.; Balzani, V.; Barigelletti, F.; Cola, L. D.; Flamigni, L., *Chem. Rev.* **1994**, *94*, 993.

28. Juris, A.; Balzani, V.; Barigelletti, F.; Campagna, S.; Bellser, P.; von Zelewsky, A. , *Coord. Chem. Rev.* **1988**, *84*, 85.

29. Schwarz, O.; Loyen, D. V.; Jockush, S.; Turro, N. J.; Durr, H., *J. Photochem. Photobiol. A: Chem.* **2000**, *132*, 91.

30. Pecky, P.; Rotzinger, F. P.; Nazeerudin, M. K.; Khole, O.; Zakeeruddin, S. M.; Humpry-Baker, R.; Grätzel, M., *J. Chem. Soc., Chem. Commun.*, **1995**, 65.

31. Yan, S. G.; Lyon, L. A.; Lemon, B. I.; Preiskorn, J. S.; Hupp, J. T., *J. Chem. Edu.* **1997**, *74*, 657.

32. Vlachopoulous, N.; Liska, P.; Augustynski, J.; Gratzel, M., *J. Am. Chem. Soc.* **1988**, *110*, 1216.

33. Juris, A.; Campagna, S.; Bidd, I.; Lehn, J. M.; Ziessel, R., *Inorg. Chem.* **1988**, *27*, 4007.

34. Becker, R. S., *Theory and interpretation of fluorescence and phosphorescence*, Wiley Interscience, New york, **1969**, 139.

35. Czarnik, A. W., *Fluorescent Chemosensors for Ion and Molecule Recognition*, *Vol. 538*, ACS Symposium Series, Washinton D. C, **1993**.

36. Lehn, J. M., *Angew. Chem. Int. Ed. Engl.* **1990**, *29*, 1304.

37. de Silva, A. P.; Gunaratne, H. Q. N.; McRoy, C. P., *Nature* **1993**, *364*, 42.

38. Thomas, K. G.; Thomas, K. J.; George, M. V., *J. Chem. Soc. Chem. Commun.* **1997**, 597.

39. Damrauer, N. H.; Boussie, T. R.; Devenney, M.; Mccusker, J. K., *J. Am. Chem. Soc* **1997**, *119*, 8253.

40. Bolleta, F.; Maestri, M.; Balzani, V., *J. Phys. Chem* **1976**, *80*, 2499.

41. C. V. Kumar; Qin, L.; Das, P. K., *J. Chem. Soc. Faraday Trans 2,* **1984**, *80*, .

42. Amadelli, R.; Argazzi, R.; Bignozzi, C. A.; Scandola, F., *J. Am. Chem. Soc.* **1990**, *112*, 7099.

43. *Kodak Laser Dyes*, Eastman Kodak Company, Kodak Publication, New York, **1987**.

CHAPTER 3

SYNTHESIS AND PHOTOPHYSICAL STUDIES OF (BIS-BENZSELENAZOL-2-YLIDINE)SQUARAINE DYES

3.1. Abstract

The strong absorption of squaraine dyes in the near infrared region makes them highly suitable for the design of sensitizers for applications in photodynamic therapy (PDT). The use of squaraines in PDT has hitherto not been explored due to their low triplet yields, which result in inefficient generation of singlet oxygen, which is thought to be the main cytotoxic species in PDT. With a view of generating squaraine dyes possessing higher triplet yields, a new water soluble squaraine dye, bis(3-carboxymethylbenzselenazol-2-ylidine)squaraine (**15**) and its parent compound bis(3-methylbenzselenazol-2-ylidine)squaraine (**14**) were synthesized and characterized. The photophysical properties of these dyes in homogeneous and microheterogeneous media have been investigated. The absorption and emission maxima of these dyes show a hypsochromic shift with increasing solvent polarity, which is accompanied by a decrease in the fluorescence quantum yield. Compound **15** is only weakly fluorescent in aqueous media. In water, **15** forms dimer aggregates with an absorption band blue shifted to that of the monomer. The blue shift in the absorption band is indicative of formation of H-type aggregates. It is proposed that the driving force for the formation of the H-type (sandwich) aggregates is the hydrophobic interaction

between the chromophoric units of the dye. Aggregate formation was not observed in the presence of β-cyclodextrin or cetyltrimethyl ammonium bromide (CTAB) micelles. Under these conditions, a red shift in the absorption and emission maxima is observed, which is accompanied by significant enhancement in the fluorescence quantum yield. These effects can be attributed to the non-polar as well as structurally restrictive environment provided by the microheterogeneous media. The dyes possess relatively high triplet quantum yields (0.26 - 0.29), in contrast to the generally low intersystem crossing efficiencies normally observed for squaraines. Photoinduced electron transfer and singlet oxygen generation from the excited triplet state have also been investigated.

3.2. Introduction

Photodynamic therapy (PDT) is fast developing as a viable method for the treatment of cancerous tissues (tumors).[1-3] Photodynamic action, which involves the lethal effect of light and oxygen on microbes in the presence of certain dyes, was discovered at the turn of the century by Raab[4] and von Tappeiner.[5] In PDT of cancer, a non-toxic photoactive drug is injected intravenously. The drug selectively concentrates in tumors after some time. This partial selectivity used in combination with specific application of light results in the necrosis of the cancerous tissues. Light of long wavelength (>600 nm), which is normally used for such applications, is harmless in the absence of the drug. The mode of action of PDT involves excitation of the drug, which is essentially a photosensitizer. The excited

singlet state of the sensitizer can undergo radiative or non-radiative transition to regenerate the singlet ground state, or undergo intersystem crossing (ISC) to generate the longer-lived triplet state (T_1) of the sensitizer. In the presence of oxygen, either energy transfer or electron transfer can occur from the triplet state. Both processes will result in the generation of cytotoxic forms of oxygen (Figure 3.1).[6]

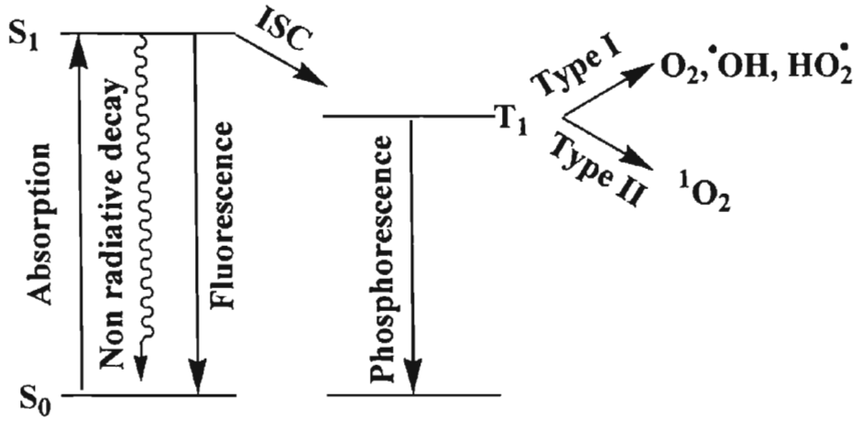

Figure 3.1. Schematic representation of the formation of cytotoxic forms of oxygen, following excitation of a photosensitizer.

Photodynamic action of a photosensitizer in the biological systems can follow two major mechanisms.[7-9] The first, which is labeled as Type I mechanism, involves electron transfer between the excited triplet state of the sensitizer and biological substrates or oxygen. The second mechanism called the Type II mechanism, involves energy transfer from the excited triplet state of the sensitizer to oxygen resulting in the formation of the singlet excited state of molecular

oxygen. Subsequent reactions of singlet oxygen with various biological substrates lead to cell damage.

3.2.1. Singlet Oxygen

The mechanism of photodamage in PDT involving most commonly used photosensitizers is believed to be predominantly of the type II nature i.e. involving the intermediacy of singlet oxygen O_2 ($^1\Delta_g$)[10] (Scheme 3.1).

The efficiency of singlet oxygen formation in such systems depends on the triplet quantum yield of the sensitizer and the quenching efficiency of the triplet by oxygen. Singlet oxygen formation by energy transfer is not always quantitative, as other mechanisms are possible in the oxygen mediated quenching of the excited triplet states.

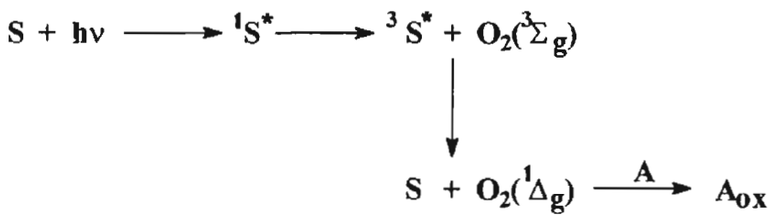

Scheme 3.1

The high reactivity of singlet molecular oxygen arises from the combination of several molecular properties, namely that it possesses an electronic energy of *ca* 1 eV,[11] is small and uncharged and that it has a lifetime of several microseconds.[12] The last two facts make $O_2(^1\Delta_g)$ distinctively different from other cytotoxic species. In particular, its ability to freely diffuse from one phase to

another in microheterogeneous systems, unhindered by coloumbic interactions or steric hindrances in bulk phases or charged interfacial regions, makes it highly suitable for PDT applications.

The high reactivity of singlet oxygen can be explained using the molecular orbital diagram illustrated in Figure 3.2.[13] Each oxygen atom has eight electrons. Four of these remain in $\sigma(1s)$ and $\sigma^*(1s)$ orbital while next four move into $\sigma(2s)$ and $\sigma^*(2s)$. The next six move into three bonding molecular orbitals: $\sigma(2p_x)$, $\pi(2p_y)$, $\pi(2p_z)$. The last pair of electrons can be accommodated either in one of the π^* orbitals (if the electrons have opposite spins) or on two MO ($\pi^*(2p_y)$ and $\pi^*(2p_z)$ if the spins are parallel. The latter configuration is energetically preferred, because of the large repulsion in energy that would occur between two electrons in the same orbital. This state of the oxygen molecule is known as the triplet sigma state ($^3\Sigma$). The configuration in which the last two electrons are located in the same $\pi^*(2p_y)$ orbital is higher in energy. This corresponds to the lower excited state of oxygen molecule, which is a singlet state because the electrons are paired. This state of oxygen molecule is denoted as $^1\Delta$ and lies 22.5 kcal/mole above $^3\Sigma$ ground state. The next excited state of oxygen ($^1\Sigma$) is 37.5 kcal/mole above the ground state. The high energy content of singlet oxygen makes it highly reactive.

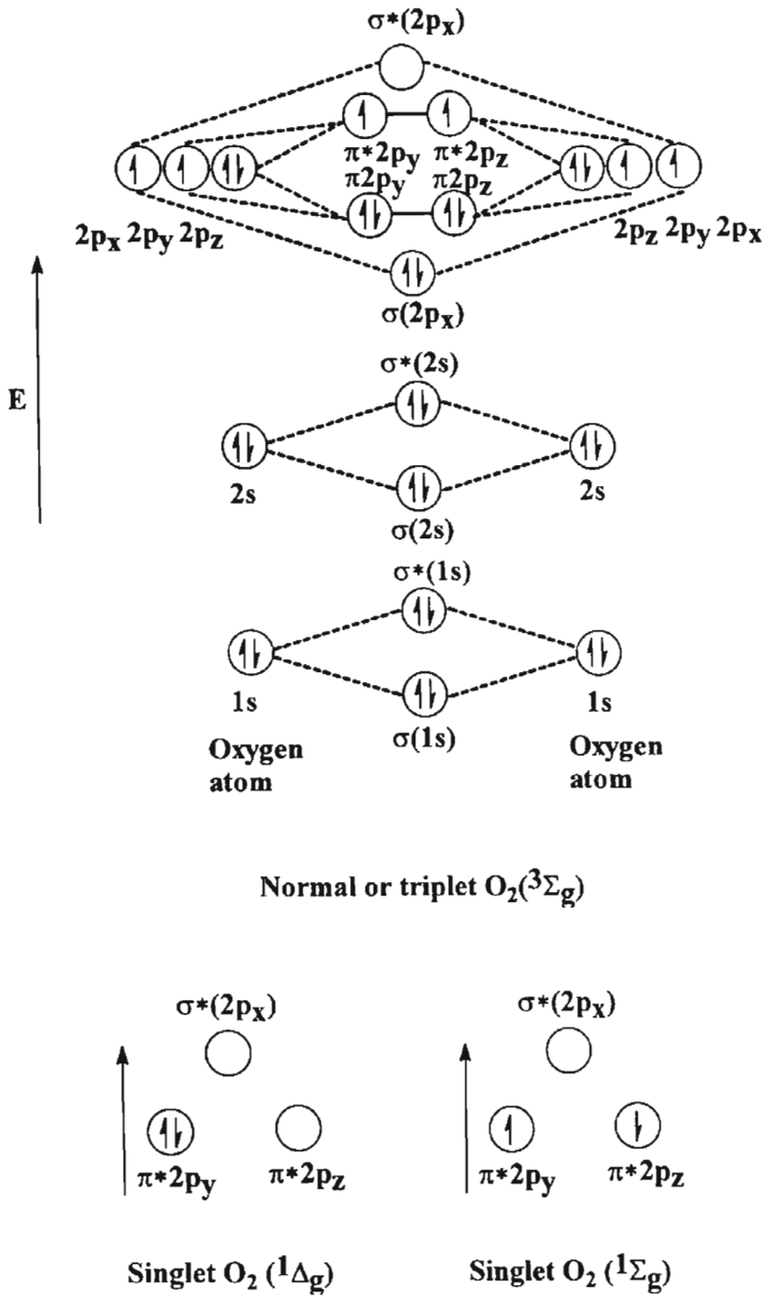

Figure 3.2. Molecular orbital diagrams of oxygen molecule illustrating the ground and excited states of oxygen.

Scheme 3.2 shows the different methods by which singlet oxygen can be generated. Although singlet oxygen generation in chemical[14] and photosensitized oxidations is well documented, it has only recently been detected in biosystems where it has been observed to form due to free radical recombination reactions,[15] phagocytosis,[16] peroxidase catalysed reactions[17] and in various medical procedures.[18]

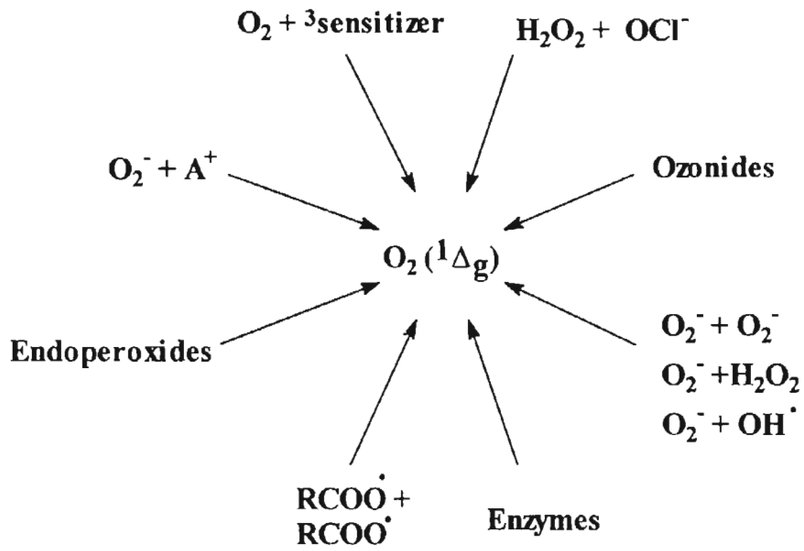

Scheme 3.2. Various pathways for the generation of singlet oxygen.

For efficient photosensitized generation of singlet oxygen, the excited triplet state of the sensitizer should possess energy >1 eV, which corresponds to the difference in energy between singlet and ground states of oxygen. This translates to absorption limit of 800 nm for porphyrin-based sensitizers. Sensitizers possessing ground state absorption at higher wavelength would not be able to generate singlet oxygen efficiently.

3.2.2. Biological Applications of Dyes

Although dyes absorbing in the ultraviolet, visible or near infrared radiation could possibly be used as photosensitizers in PDT, it is generally accepted that the use of ultraviolet radiation is disadvantageous due to its poor penetration through tissues[19] and its potential for initiating carcinogenesis.[20] Figure 3.3 shows the transmittance curve for light through a 7 mm thick layer of tissue. The dotted line represents the transmittance of human tissue in relation to the molar extinction coefficients of absorption bands of some photosensitizers. The broad feature of the dotted line at 500-600 nm is attributed to the absorption of hemoglobin.[3] It becomes evident from the figure that the transmittance of light by tissues increases with increase in wavelength.

As a result there is considerable interest in the study of dyes absorbing in the near infrared region (NIR) for a number of biological applications. For example NIR dyes, which are fluorescent, find applications in fluorescence lifetime sensing techniques for detection of H^+, O_2, K^+, or Ca^+ in biological systems.[21]

Soper *et al.* have recently reported detection sensitivities at the single molecule level in the near infrared, using pulsed laser excitation and time-gated detection for the NIR fluorescent dye IR-132. [22,23] IR-132 was observed to be superior to rhodamine 6G in spite of its lower quantum yield of fluorescence. This has been attributed to low absorption by cellular components at the higher excitation wavelength used for IR 132 compared to Rhodamine 6G, resulting in

lower background signals.[22] NIR dyes possessing high quantum yields of fluorescence are relatively unknown.

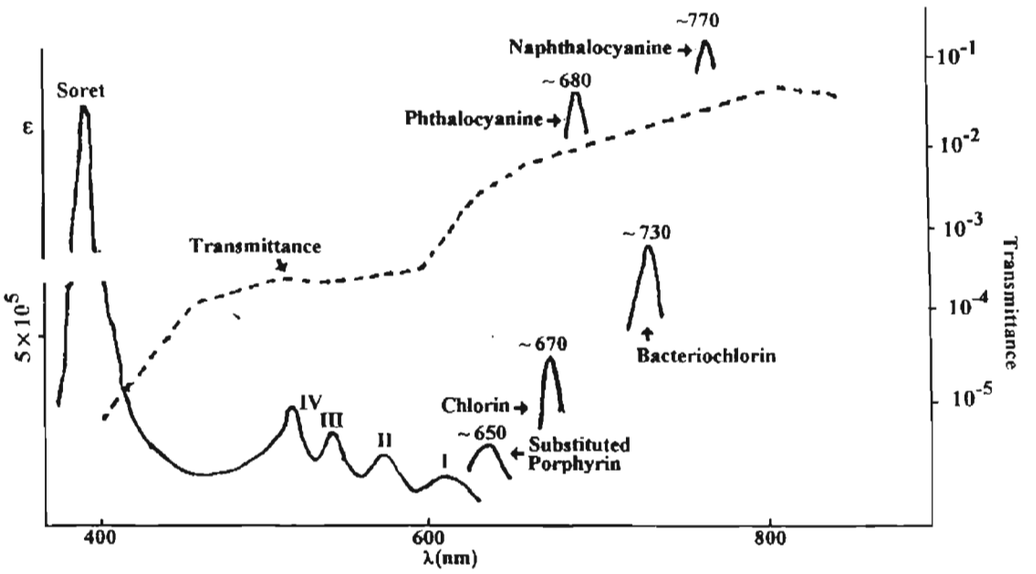

Figure 3.3. Photosensitizer absorbance in relation to tissue transmittance. The transmittance curve refers to a sample of human scrotal sac of 7-mm thickness.

From the photodynamic therapy point of view however dyes having good triplet yields are preferred.[24]

3.2.3. First Generation Sensitizers

Photosensitizers such as porphyrins have been the subject of intensive studies because of their potential use in PDT.[25-29] Photofrin®II is the commercial name for a mixture of porphyrins derived from the hematoporphyrin derivative (Hpd). Hematoporphyrin derivative (Hpd), together with its commercial variants Photofrin, Photogem and Photocarcinorin

are referred to as first generation photosensitizers.[30-34] Hpd is prepared from hematoporphyrin dihydrochloride by its reaction with acetic acid-sulfuric acid and subsequent treatment with dilute base.[35] The initial step produces a mixture of mono-and di acetates, hematoporphyrin (Hp), dehydrated products of Hp, hydroxyethyl vinyl deuteroporphyrin (HVD) and protoporphyrin.[36] This mixture upon reaction with 0.1 N NaOH solution undergoes hydrolysis and coupling reactions to produce the mixture termed Hpd. Typically the mixture consists of approximately 20% Hp, 20-30% HVD, 3-5% protoporphyrin. The remaining 50% have yet to be identified although it is proposed to consist of a mixture of ether and ester linked hematoporphyrin oligomers and protoporphyrin monomers (Chart 3.1).[37] Photofrin®II is a mixture enriched with this latter fraction to the extent of about 80-90%. This fraction is thought to be primarily responsible for the *in vivo* photodynamic activity of the drug.[28] Although Hpd and its commercial variants have been used extensively in clinical applications and have been approved for treatment of a variety of cancers in a number of countries, some disadvantages exist related with the use of these first generation photosensitizers.

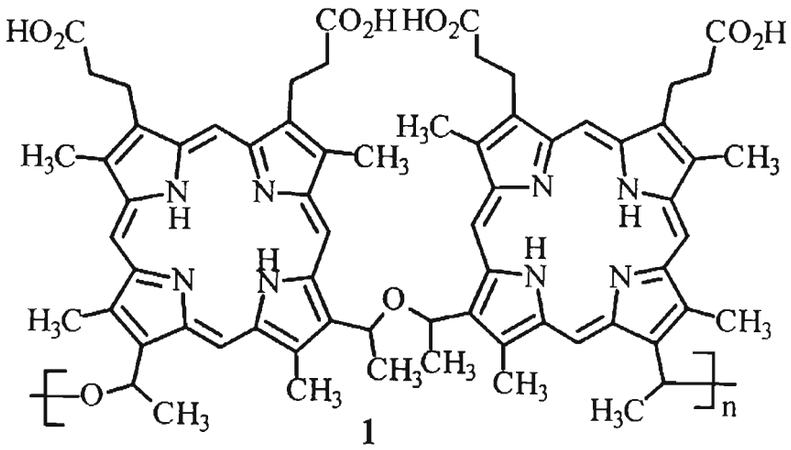

1

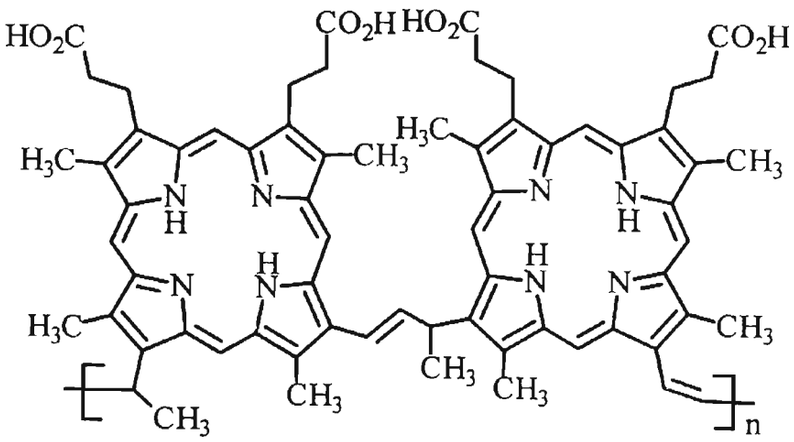

2

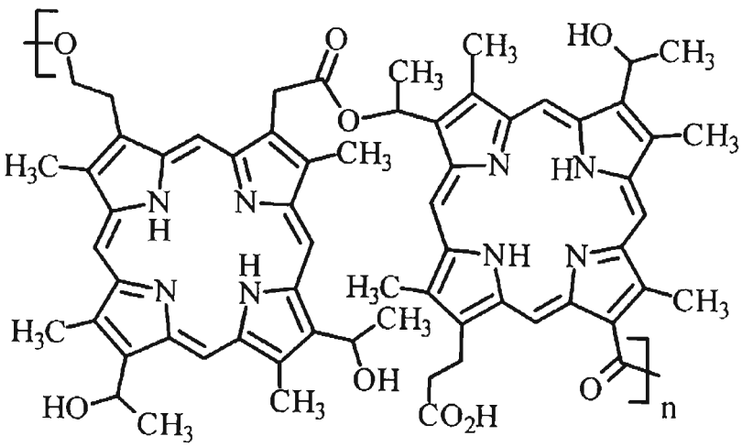

3

Chart 3.1

Hpd is a mixture of at least nine components and its preparation is highly sensitive to experimental conditions. The elucidation of mechanism by which Hpd acts has hence been hampered by the complexity of its composition. The clearance of Hpd from the body is very slow and this leads to cutaneous photosensitivity and immunosuppression for prolonged period in patients. More importantly, it has only a weak absorption in the red region of the spectrum where, as discussed before light transmission in tissues is high. It therefore becomes difficult to deliver light to some tumor sites and incomplete light penetration is observed for larger tumors for the wavelength used to excite Hpd.

3.2.4. Second Generation Sensitizers

In view of the above mentioned constraints faced with first generation sensitizers, intensive work is in progress to develop new photosensitizers for PDT applications. For a compound to be used as a sensitizer in PDT, it has to satisfy the following criteria.

(i) The sensitizer should possess a high absorption coefficient in the red region where light penetration in tissues is better.

(ii) It has to be preferentially retained in tumor tissues.

(iii) It should have a short residence time in normal tissues,.

(iv) It has to be non-toxic in the absence of light.

(v) It should have no other side effects.

(vi) It should possess a high singlet oxygen generating efficiency.

Photosensitizers can be divided into two broad classes on the basis of their charge.[38] The most commonly studied sensitizers, including Photofrin II have a net negative charge (anionic). In contrast, more recently investigated group of compounds are cationic in nature. Mechanistic studies on PDT suggest that many anionic photosensitizers including photofrin II have little or no selectivity for malignant cells *in vitro*, and that they principally target blood vessels,[39,40] rather than tumor cells *in vivo*. In contrast, cationic photosensitizers can be highly selective for carcinoma and melanoma cells *in vitro* and *in vivo*.[41-43] The basis of this selectivity is thought to be due to the differences in cellular or mitochondrial membrane potentials.

Among the second-generation sensitizers the negatively charged tetrapyrrolic macrocycles have been most widely studied. Porphyrins and their derivatives including chlorins,[44-46] glycoconjugated porphyrins,[47] purpurins,[48,49] verdins, bacteriochlorins and benzoporphyrin derivatives generate triplet states with high efficiency, from which energy transfer to ground state oxygen appears to be the most dominant process. Phthalocyanines are another class of photosensitizers which has been extensively studied for their activity in PDT. [50]

Second generation sensitizers other than porphyrins and phthalocyanines, which are extensively studied, include the positively charged xanthenes, phenothiazenes and heavy atom substituted phenoxazines (Chart 3.2).[51-53] The interaction between the positive charge on cationic photosensitizers and the cell membrane potentials leads to increased intracellular concentrations of the dye.

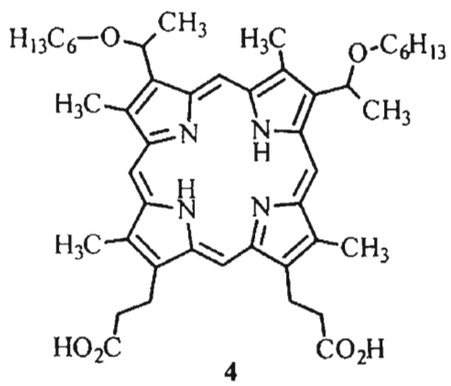

4
HP_Dihexyl ether

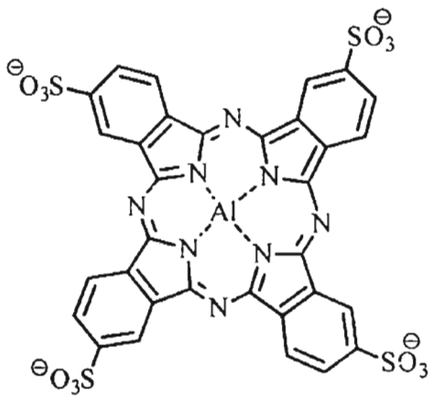

5
AlPCTS

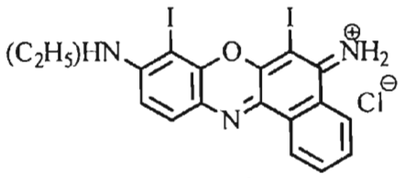

6
Cresyl Violet

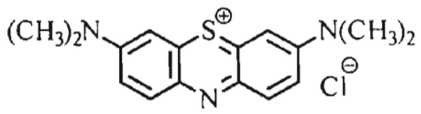

7
Methylene Blue

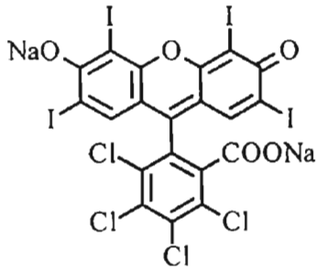

8
Rose Bengal

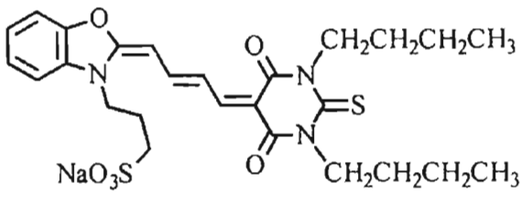

9
Merocyanine 540

Chart 3.2

Cell and mitochondrial membranes have electrical potential gradients across them, with a negative potential inside. In typical cells, there is about –60 mV across the plasma membrane and about –180 mV across the mitochondrial

membrane. A voltage gradient of 60 mV can lead to a ten-fold difference in concentration of positively charged molecules, which are sufficiently lipophilic to be able to pass through the membrane. Thus, a cationic molecule can concentrate up to ten times within the cytoplasm and up to 1000 times within the mitochondria, although these maximal concentrations are rarely achieved in biological systems. However, with suitably designed molecules, the mitochondria can become an important target for the cationic compounds.

The use of cationic dyes for chemotherapy was first demonstrated about 40 years ago by Lewis and co-workers, who studied a series of orally administered dyes for tumor inhibitory effects.[54] They found that certain cationic oxazine, diaryl- and triarylmethane compounds were moderately inhibitory and that some of them accumulated within tumors to such an extent that the malignant cells become visibly coloured. More recently in an initially serendipitous observation of mitochondrial fluorescence patterns, Chen and co-workers found that many malignant cells had a higher uptake and retention of the cationic dye rhodamine 123 than did most normal cells.[55]

3.2.5. Squaraine Dyes

Squaraine dyes[56] form a class of organic photoconducting materials, which along with other photoconductors such as phthalocyanines, naphthaquinones, cyanine and azo-pigments have been extensively studied for a variety of technical applications such as in imaging and solar energy conversion. In spite of their

strong absorption in the near-infrared region their biological applications have not been well explored Terpetsching *et al.*[57-59] have synthesized squaraine dyes **10** and **11** (Chart 3.3) and studied their interaction with bovine serum albumin (BSA). The fluorescence quantum yields and lifetimes of sq-taurine derivative increased by 28-fold and 31-fold respectively on binding to BSA.

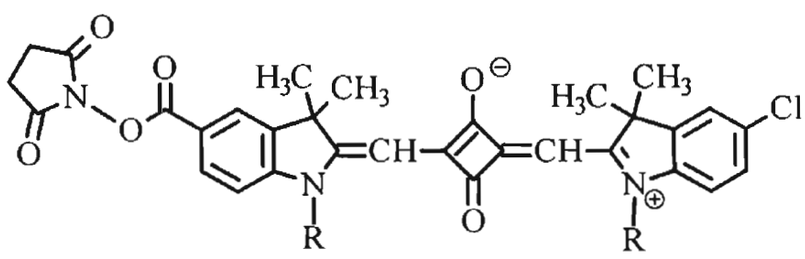

10, R = C_2H_5
11, R = $(CH_2)_4SO_3^{\ominus}$

Chart 3.3

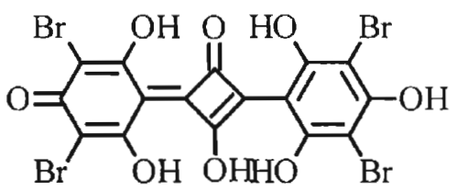

12

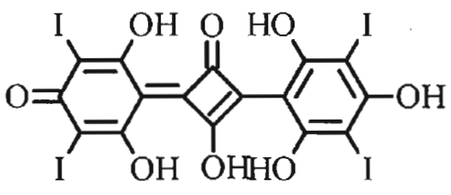

13

Chart 3.4

Squaraine dyes in general have very low intersystem crossing efficiencies and hence their application in PDT have not been explored. Recently, heavy atom substituted squaraine derivatives **12** and **13** (Chart 3.4) have been synthesized and their photophysical and photochemical properties have been explored.[60] Laser flash photolysis studies indicated triplet excited states to be the main transient intermediates for these dyes. Triplet quantum yields were found to be the highest for the neutral (ϕ_T = 0.12(**12**); 0.24 (**13**)) and deprotonated forms (ϕ_T = 0.22(**12**); 0.5(**13**)) of these dyes. Quantum yields of singlet oxygen generation by the anionic forms of **12** and **13** were found to be 0.13 and 0.47 respectively.

3.2.6. Objectives of the Present Study

As discussed above the strong absorption of squaraine dyes in the near-infrared region makes them highly suited for PDT applications. The low intersystem crossing efficiencies in these dyes can be overcome by heavy atom substitution.[61] This has been earlier reported for the bis(tri-hydroxyphenyl) squaraine derivatives **12** and **13**.[60] Although these dyes are potentially useful as sensitizers for PDT applications, they possess poor water solubility and also tend to be unstable in aqueous media. With a view to obtain stable, water soluble squaraine dyes with large intersystem crossing efficiencies, the photochemical and photophysical properties of bis(3-methyl)benzselenazol-2-ylidine squaraine (**14**) and its water soluble derivative bis(3-carboxymethyl)benzselenazol-2-ylidine squaraine (**15**) have been synthesized and their photophysical and photochemical

properties in homogeneous and microheterogeneous media have been investigated in detail. The synthesis of **14** has been reported earlier; however its spectroscopic and photochemical properties have not been studied. The triplet yields of these dyes were expected to be high due to the heavy atom effect of selenium.

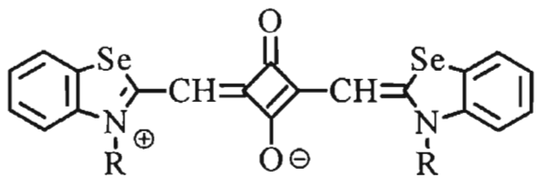

14, R = CH_3
15, R = CH_2COOH

Chart 3.5

3.3. Result and Discussions

3.3.1. Synthesis. Bis[3-(methyl)benzselenazol-2-ylidine]squaraine (**14**) was synthesized as per the reported procedures.[62] The carboxylated derivative (**15**) was synthesized as shown in Scheme 3.3and Scheme 3.4. Details regarding the synthesis and characterization of the dyes are described in Section 3.4.

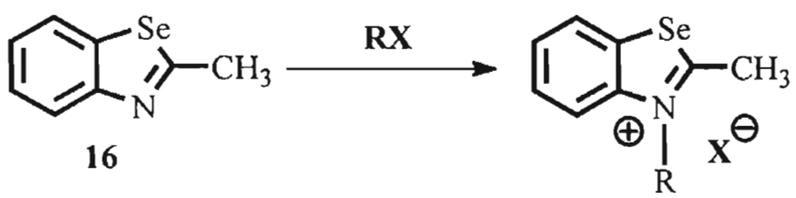

16

17, R = CH_3
18, R = CH_2CO_2H

Scheme 3.3.

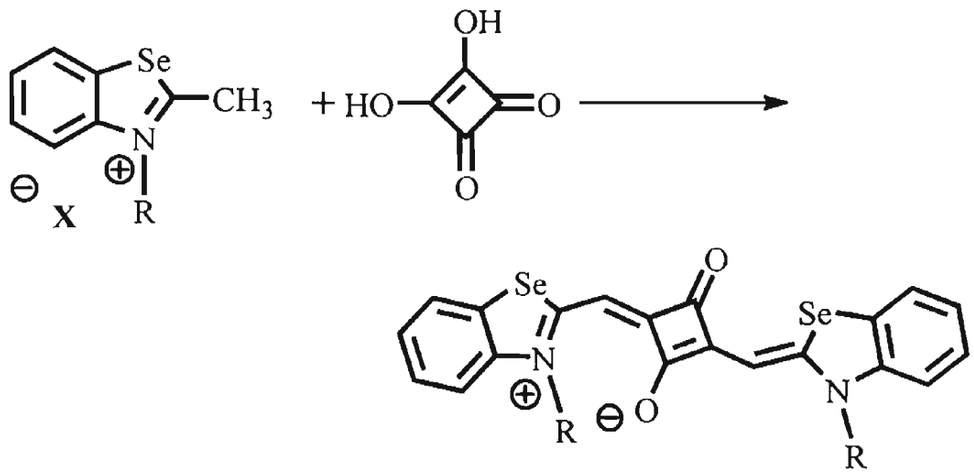

14, R = CH_3
15, R = CH_2CO_2H

Scheme 3.4.

3.3.2. Absorption and Emission Properties

The dyes are soluble in polar solvents such as dichloromethane, acetonitrile and alcohols. In addition **15** is soluble in water. Both dyes strongly absorb and emit in the near infrared region. Figure 3.4 shows the absorption and emission spectra of **14** in methanol. The absorption and emission properties of the dyes in different solvents are summarized in Table 3.1.

A hypsochromic shift in the absorption and emission maxima is observed with increasing solvent polarity, which is accompanied by a decrease in the fluorescence quantum yield. The singlet state lifetimes also decrease with increase in solvent polarity.

Table 3.1. Absorption and emission characteristics of 14 and 15 in different solvents

Solvent	14		15	
	λ_{max}(abs.), nm (ε x 10^{-5} $M^{-1}s^{-1}$)	λ_{max}(em.), nm (ϕ_f)	λ_{max}(abs.), nm (ε x 10^{-5} $M^{-1}s^{-1}$)	λ_{max}(em.), nm (ϕ_f)
Dichloromethane	682	699 (0.6)	686 (1.37)	704 (0.63)
Acetonitrile	675 (1.8)	689 (0.36)	680 (1.41)	703 (0.41)
Methanol	662 (1.3)	680 (0.21)	669 (1.51)	685 (0.29)
Water	-	-	657 ((1.08)	676 (0.016)

Using equations 3.1- 3.4, the fluorescence rate constant k_f and the sum of all nonradiative rate constants, k_{nr} have been estimated (Table 3.2). It becomes evident from Table 3.2 that k_f is fairly independent of solvent polarity, whereas k_{nr} increases significantly with increase in solvent polarity.

$$\phi_f = k_f/(k_f + k_{nr}^{tot}) \quad \textbf{(3.1)}$$

$$\tau_f = 1/(k_f + k_{nr}^{tot}) \quad \textbf{(3.2)}$$

$$k_f = \phi_f/\tau_f \quad \textbf{(3.3)}$$

$$k_{nr}^{tot} = k_f(\phi_f^{-1} - 1) \quad \textbf{(3.4)}$$

The observed results are similar to those reported earlier by Gude and Rettig for the squaraine dyes containing indolinylidine methyl groups (**19**, Chart 3.6).[63] Based on theoretical studies on simpler models, it was suggested that in the excited state, **19**

undergoes twisting relaxations which leads to a close approach of the ground and excited states, resulting in a non-radiative decay of the excited-state.

Table 3.2. The Singlet lifetimes, fluorescence rate constant k_f and the sum of all nonradiative rate constants, k_{nr} for 14 and 15 in various solvents

Solvent	14			15		
	τ_s ns	k_r (10^7 s^{-1})	k_{nr}^{tot} (10^7 s^{-1})	τ_s ns	k_r (10^7 s^{-1})	k_{nr}^{tot} (10^7 s^{-1})
Dichloromethane	5.1	11.7	7.8	4	16	9.3
Acetonitrile	2.5	15	25	2.6	16	23
Methanol	1.0	21	79	1.7	17	41

It is also proposed that increase in the dipole moment of the excited state would result in increased twisting of the C-C bonds adjacent to the squaraine ring resulting in enhancement in the non-radiative decay rates with increase in solvent polarity.

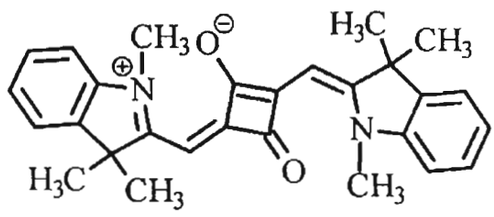

19

Chart 3.6

The hypsochromic shift observed in the absorption and emission spectra of **14**, **15** in the present study as well as that for **19** reported in the literature[63] indicate that the excited state of this class of dyes may be less polar than the ground states although the difference may not be very large. A satisfactory explanation for enhancement in the non-radiative decay with enhancement in solvent polarity in these dyes does not appear to be available at present. It is possible that interaction between polar solvents with the dye may result in vibronic coupling of close lying $^1(n,\pi^*)$ and $^1(\pi,\pi^*)$ states which, could result in enhancement of the non-radiative decay to the ground state.

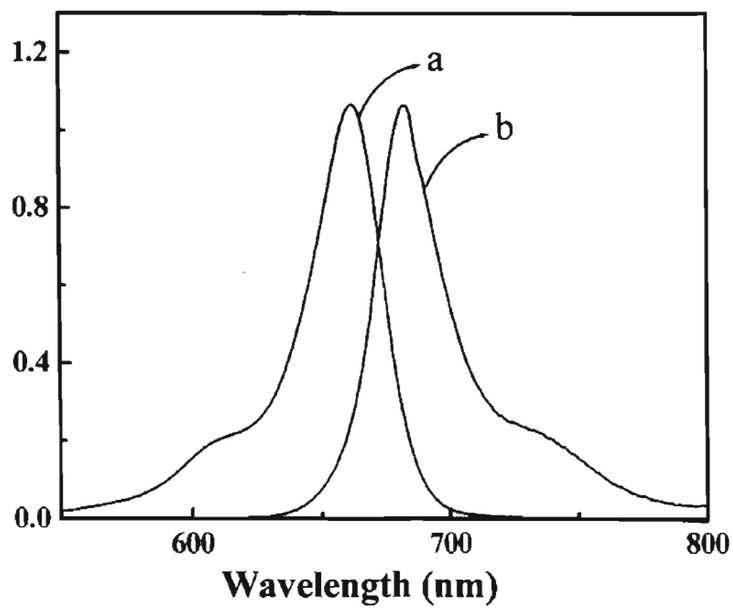

Figure 3.4. a) Absorption and b) emission spectra of **14** in methanol normalized at their maxima.

Due to the presence of two carboxylic acid groups, **15** is soluble in water at pH>7. Figure 3.5 shows the absorption spectra recorded at different concentrations

of **15** in water at pH 8.2 using a cuvette of 2 mm path length. At lower concentrations **15** shows a strong absorption band around 657 nm. A small band was also observed around 600 nm. The extinction coefficient of the monomer at 657 nm (1.1×10^5 $M^{-1}cm^{-1}$) was estimated using dilute solution of the dye (<7 μM), where it exists purely in the monomeric form. At higher concentrations the relative magnitude of the band observed at 600 nm increases significantly. This effect which is similar to that reported for the benzothiazole derivative of squaric acid[64] suggests the formation of aggregates at the higher concentrations (Figure 3.5).

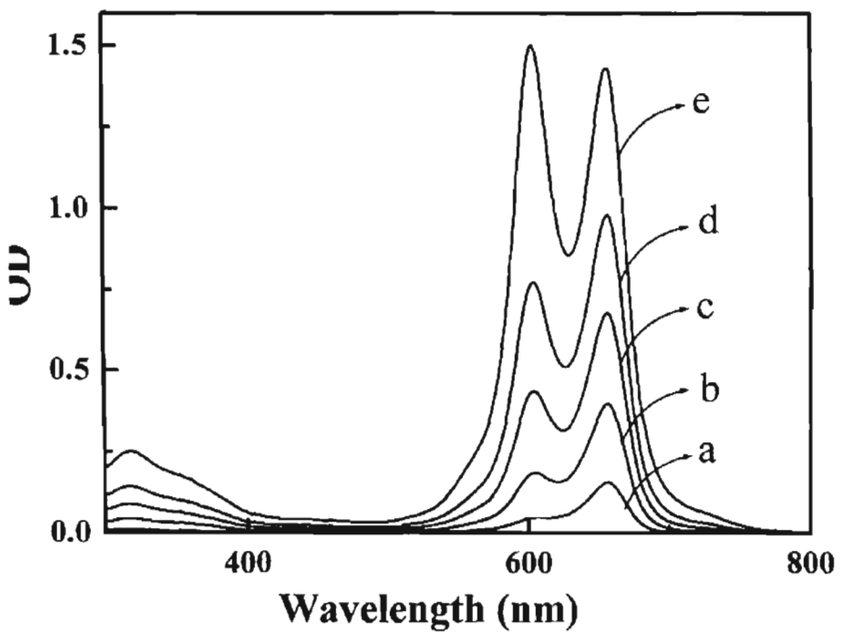

Figure 3.5. Effect of concentration on the absorption spectrum of **15** in aqueous media of pH 8.2 a)7.37 μm, b) 22.13 μm, c)44.25 μm, d) 73.75 μm, e) 132.75 μm.

Exciton theory predicts that the excited state energy level of a monomeric dye splits into two upon aggregation, one level being lower and the other higher in

energy than the monomer excited state (Figure 3.6). The transition to the higher state is forbidden for head-to-tail aggregate (J-type), whereas the lower excited state is forbidden for sandwich (H-type) aggregate. The enhancement in intensity of the maximum around 604 nm suggests that in the present case H-type aggregates are formed in aqueous solution of **15**. The extinction coefficient of **15** at 657 nm was estimated using dilute solutions where the dye exists purely in its monomeric form. Using this value the concentration of the monomer was evaluated from aqueous solutions of **15** at higher concentrations. Assuming formation of a dimer as shown in equation 3.5, the concentration of dimer was estimated using equation 3.6, where C_0 refers to the total dye concentration. The equilibrium constant for the dimerization process will be given by equation 3.7.

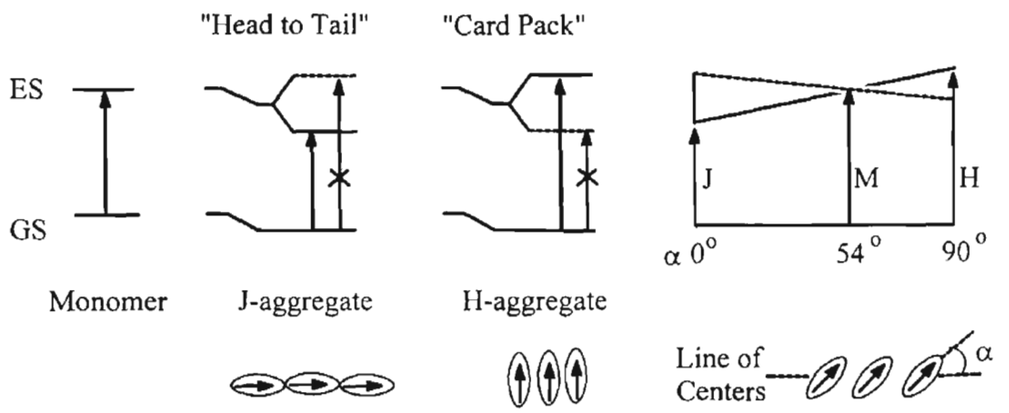

Figure 3.6. Schematic representation of splitting of the excited state during aggregation.

A plot of log [dimer] *versus* log [monomer] (Figure 3.7) was linear with a slope of 2, which confirms the dimeric nature of the aggregate. The equilibrium constant estimated from the intercept has a fairly high value ($1.59 \times 10^5 M^{-1}$).

$$2[\mathbf{15}_{monomer}] \rightleftharpoons [\mathbf{15}_{dimer}] \quad (3.5)$$

$$[\mathbf{15}_{dimer}] = (C_0-[\mathbf{15}_{monomer}])/2 \quad (3.6)$$

$$K = [\mathbf{15}_{dimer}]/ [\mathbf{15}_{monomer}]^2 \quad (3.7)$$

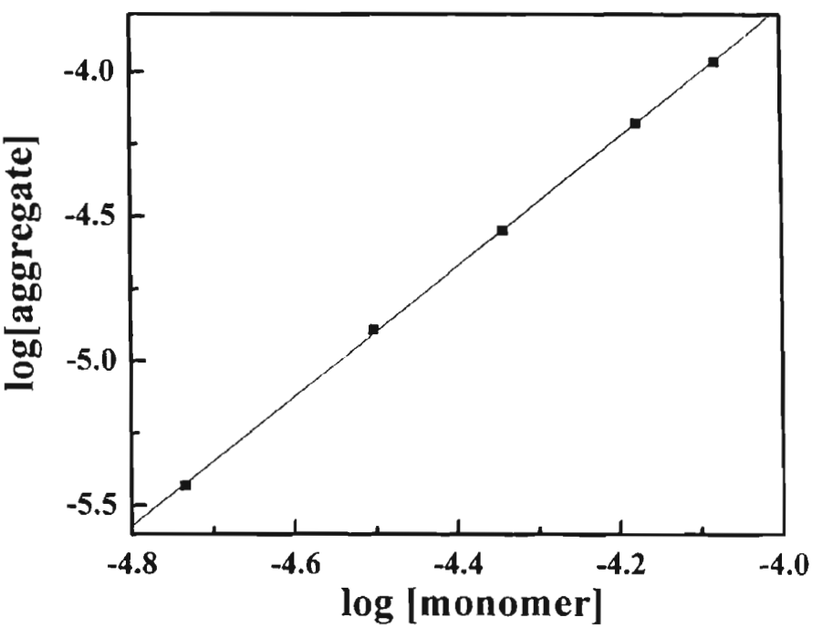

Figure 3.7. Plot of log[monomer] *vs* log[aggregate] for **15** in aqueous solutions.

3.3.3. Absorption and Emission Spectra of 15 in Microheterogeneous Media

Based on *ab initio* calculations Gude and Rettig[63] have suggested that the enhancement of non-radiative decay of methine-bridged squaraine dyes with increase in solvent polarity may be attributed to twisting of the C-C single bonds adjacent to the squaraine ring in the excited state. The twisting process in the excited state can lead to a decrease in S_0/S_1 gap resulting in an enhancement in the non-radiative decay rates.

Microheterogeneous media provided by molecules such as cyclodextrins (CD), surfactants and polymers in aqueous solutions provide a convenient method for controlling the excited state properties of molecules. Microheterogeneous medium can provide a relatively non-polar hydrophobic environment as well as an environment where conformational changes in the excited state can be restricted. Similar hydrophobic and restrictive environments are also commonly encountered in biological systems. With a view to understand the effects of such environments on the excited state properties of **15**, the photophysical properties of the dye in aqueous media containing either β-cyclodextrin (β-CD) or cetyltrimethyl ammonium bromide (CTAB) micelles have been investigated.

Cyclodextrins are cyclic, torus shaped oligosaccarides that have a central cavity capable of accommodating guest molecules in aqueous solutions (Figure 3.8). These molecules, containing six (α-CD), seven (β-CD), or eight (γ-CD) glucose units, possess different cavity diameters of approximately 4.5, 6.5 and 8.5 Å, respectively. The primary hydroxyl groups are located on the narrower side of the torus, whereas the secondary hydroxyl groups occupy the broader side. β-CD has as an internal diameter of ~ 6.5 Å on the narrower side and 7.9 Å on the broader side. The interiors of the cavities encircled by the ether oxygens provide a hydrophobic microenvironment in β-CD containing aqueous solutions. Relatively small guest molecules can be accommodated in these cavities and thereby be partially protected from the bulk water environment. The cavities also restrict the

conformational freedom of the guest molecules. Figure 3.8 shows the structure of the β-CD.

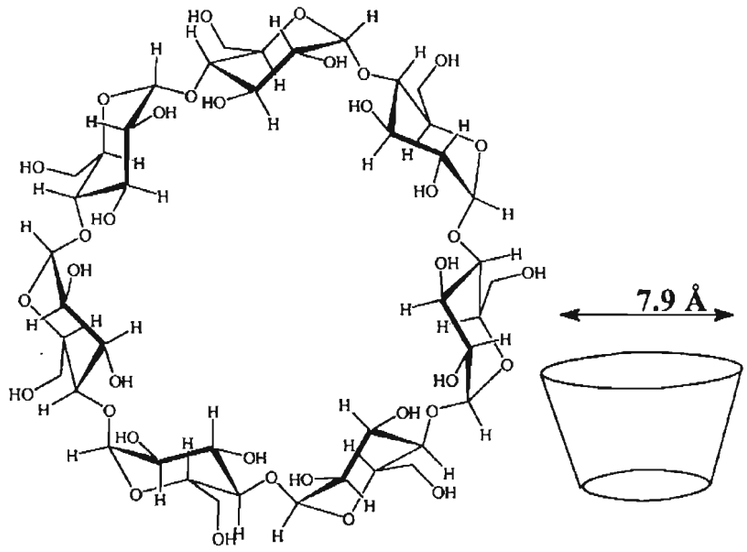

Figure 3.8 Structure and schematic representation of β-cyclodextrin.

The hydrophobic cavities of β-CDs have been used in controlling the photophysical and photochemical properties of organic guest molecules.[65-67] The effect of β-CD on intramolecular charge transfer processes in donor-acceptor substituted molecules have also been investigated. [68,69]

Figure 3.9 shows the effect of concentration of β-CD on the fluorescence intensity of **15**. Addition of β-CD to a solution of **15** in water brings about a gradual red shift in the absorption and emission maxima (Table 3.3). This was accompanied by a three-fold increase in the fluorescence quantum yield at the highest concentration of β-CD employed.

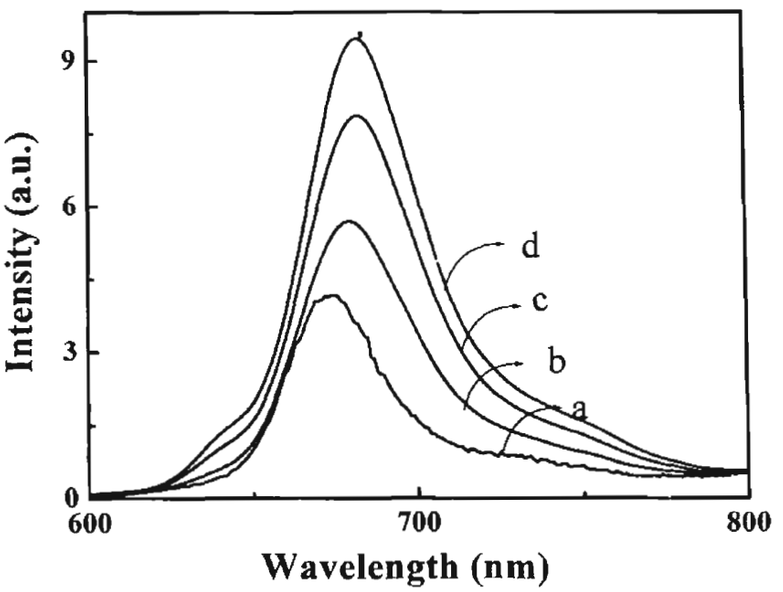

Figure 3.9. Effect of β-CD on the emission spectrum of **15** in aqueous media a) 0 M, b) 2.9 mM, c)5.8 mM, d) 8.6 mM, e) 11.6 mM, f) 14.5 mM, g) 17.4 mM.

The fluorescence enhancement of **15** on addition of β-CD was analyzed by the Benesi-Hildebrand equation (Equation 3.8) for formation of a 1:1 complex formation between the dye and β-cyclodextrin.[70]

$$\frac{1}{\phi^{o}_{f} - \phi_{f}'} = \frac{1}{\phi^{o}_{f} - \phi_{f}} + \frac{1}{K(\phi^{o}_{f} - \phi_{f})[\beta\text{-CD}]} \qquad (3.8)$$

In this equation, K is the equilibrium constant, ϕ^{o}_{f} is the fluorescence quantum yield of monomer, ϕ_{f} is the quantum yield of fluorescence of the dye-β-CD complex and ϕ'_{f} is the observed fluorescence quantum yield. The linear dependence of $1/(\phi^{o}_{f} - \phi_{f})$ on the reciprocal of concentration of β-CD (Figure 3.10) supports the formation of a 1:1 complex between the dye and β-CD. The values for the equilibrium constant (K) and fluorescence quantum yield of the β-CD-dye

complex determined from the slope and intercept of this plot were 0.013 M^{-1} and 0.073, respectively.

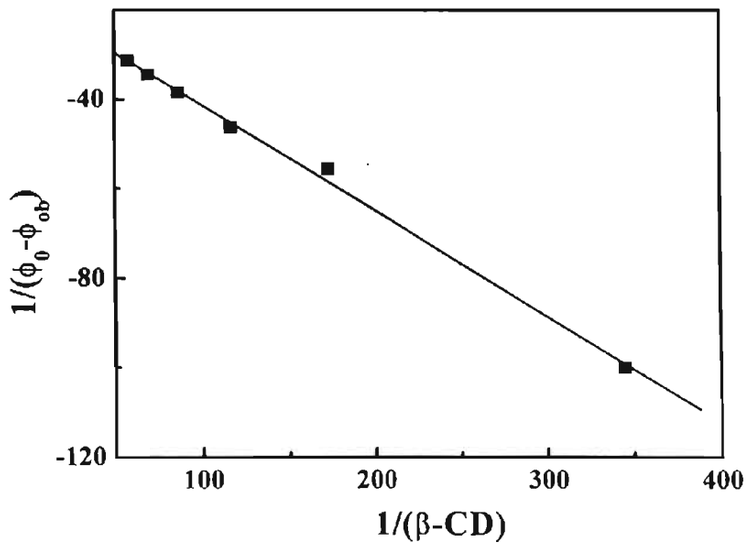

Figure 3.10. Plot of $1/(\phi_f^o - \phi_f)$ versus reciprocal of β-CD concentration for the fluorescence enhancement of **15** in water upon addition of β-CD.

Although the results clearly show that β-CD forms a 1:1 complex with the dye, the exact nature of this interaction is unclear. The distance from selenium to the carboxylic acid (6.16Å), is less than the cavity size of β-CD suggesting that it can enter into the cavity. However, due to the hydrophilic nature of the carboxylate anions this would be highly unlikely. Moreover in earlier studies of complexation of β-CD with squaraine derivatives where end-on entry into the cavity was clearly feasible, a 1: 2 dye-β-CD complex was obtained.[71] In an effort to understand the nature of this interaction the minimum energy conformation of the dye was obtained by the semiemperical PM-3 molecular modeling using

TITAN software.[72] Figure 3.11 shows the minimum energy conformation obtained using this method. Based on this structure it is proposed that β-CD complexes with the central cyclobutane moiety. The results of the *ab initio* calculations of Gude and Rettig,[63] suggest that the C-C bond twisting adjacent to the squaraine rings is responsible for the non-radiative decay of the squaraine dyes of similar structure. The partial entry of the cyclobutane ring into the β-CD cavity would provide an environment where such a bond twisting would be partially restricted.

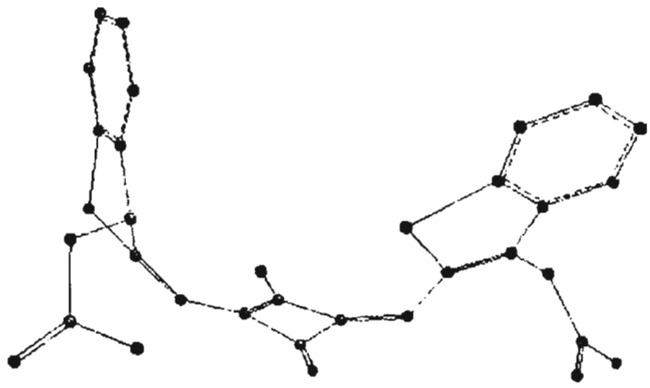

Figure 3.11. Conformation of **15** obtained by the minimum energy calculation.

CTAB forms micelles in water above its critical micellar concentration (cmc = 9.2 x.10^{-4} M), with the long alkyl chains of the surfactant forming the interior hydrophobic core and the polar heads pointing towards the bulk aqueous medium. Micellar systems therefore allow the partitioning of guest molecules between the bulk aqueous medium and the micellar structure. The addition of CTAB at concentrations higher than critical micellar concentration gave rise to bathochromic

shifts in absorption (Figure 3.12) and emission (Figure 3.13) maxima and this was accompanied by a fifteen fold enhancement of fluorescence yields (Table 3.3).

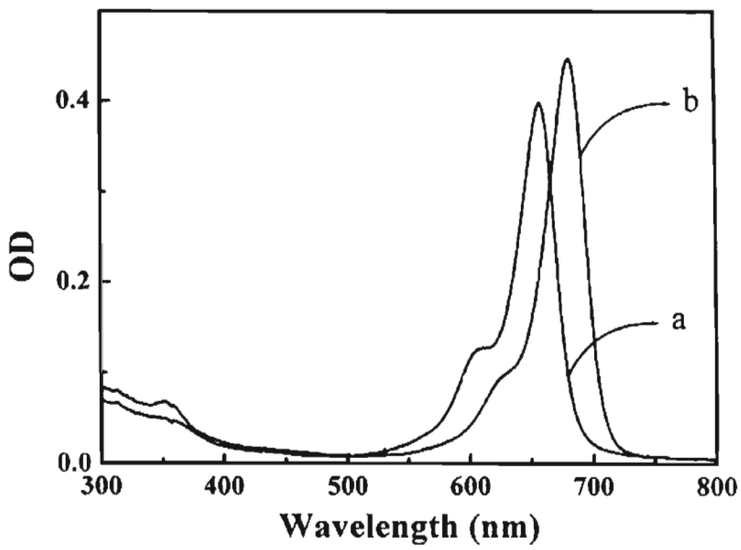

Figure 3.12. Absorption spectra of **15** in water in the presence of a) 0 M and b) 12 mM of CTAB.

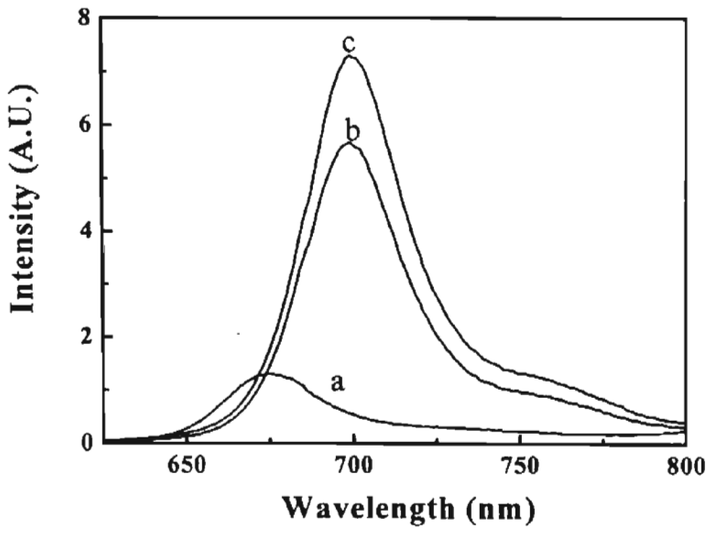

Figure 3.13. Emission spectra of **15** in water in the presence of CTAB a) 0 M, b) 4.08 mM, c) 8.16 mM, d) 12.24 mM.

The absorption and emission spectra of **15** in CTAB micelles is similar to that observed in weakly polar aprotic solvents indicating that the dye is strongly embedded into the micellar core. The enhancement in fluorescence yields can be attributed to a combination of the non-polar environment as well as reduction in the conformational freedom in the excited state of the dye. The fluorescence lifetimes as well as the non-radiative rate constants estimated using equation 3.1-3.4, are summarized in Table 3.4.

Table 3.3. Absorption and emission properties of 15 in water containing β-CD and CTAB

15	λ_{max} (abs), nm	λ_{max} (em), nm	ϕ_f
17 mM β-CD	664	676	0.048
12 mM CTAB	681	699	0.23

Table 3.4. The Singlet lifetimes, fluorescence rate constant k_f and the sum of all nonradiative rate constants, k_{nr} for 15 in water and in β-CD and in CTAB.

Solvent	**15**		
	τ_s ns	k_r x 10^7 s^{-1}	k_{nr}^{tot} x 10^7 s^{-1}
Water	0.2	80	4290
17 mM β-CD	0.33	14.54	288.4
12 mM CTAB	3.36	6.85	22.9

3.3.4. Triplet Excited State Properties

The triplet state properties of the dyes were characterized by nanosecond laser flash photolysis and by phosphorescence measurements. Figure 3.14 shows the transient absorption spectra obtained on excitation of a methanolic solution of **15** by a 355 nm pulsed laser (10 ns, 60 mJ/pulse). The transient absorption spectrum shows a bleach corresponding to the ground state absorption of the dye. A broad absorption with a maximum around 600 nm is also observed. A similar transient absorption spectrum was obtained on excitation of **14** using 355-nm laser pulse.

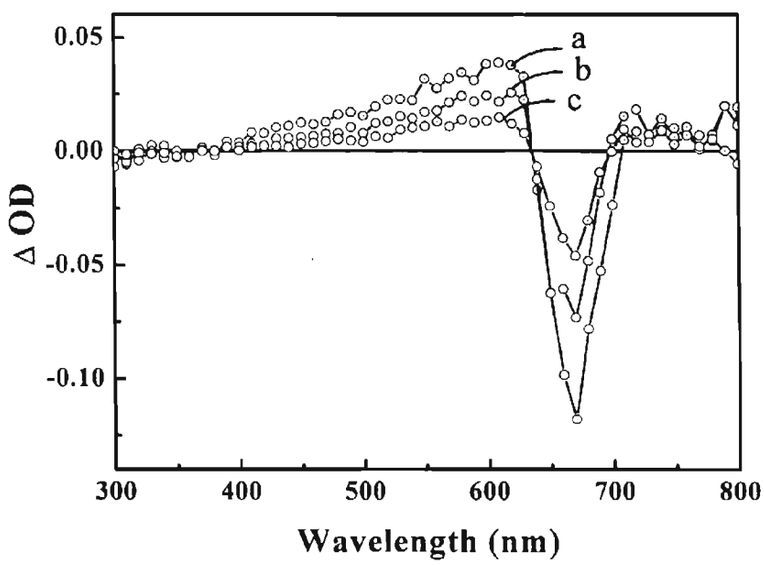

Figure 3.14. Transient absorption spectra measured following laser pulse excitation (355 nm, 10 ns, 60 mJ/pulse) of **15** in deaerated methanol at different time intervals a) 0.147 μs; 1.26 μs; 4.5 μs.

The transients of **14** and **15**, (Figures 3.15 and 3.16) which are formed within the laser pulse decay by a first order process leading to the recovery of the ground

state absorption. The recovery was complete for **14**, whereas the formation of a permanent product was observed for **15**. The transients are readily quenched by dissolved oxygen, suggesting the involvement of triplet excited states.

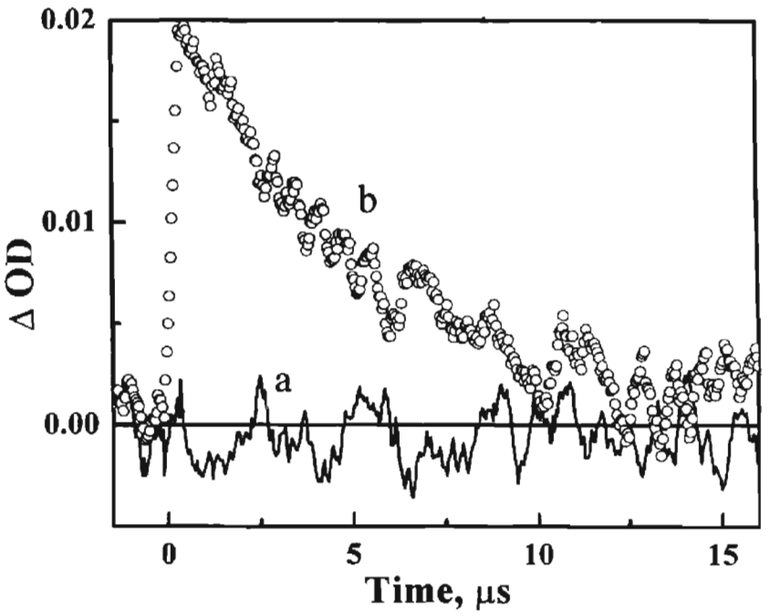

Figure 3.15. Transient decay profile of **14** in methanol monitored at 590 nm following laser pulse excitation (355 nm, 10 ns, 60 mJ/pulse): a) In the presence of oxygen and b) in the absence of oxygen.

The formation of excited triplet states was confirmed by quenching of the transients by β-carotene, which leads to the growth of the β-carotene triplet. Direct excitation of β-carotene does not lead to the formation of its triplet state, since the intersystem crossing efficiency of the β-carotene is negligible. Formation of β-carotene triplet in these systems, which can arise only via triplet energy transfer from the excited state of the dyes, confirms the triplet nature of the transient species formed on excitation of **14** and **15**.

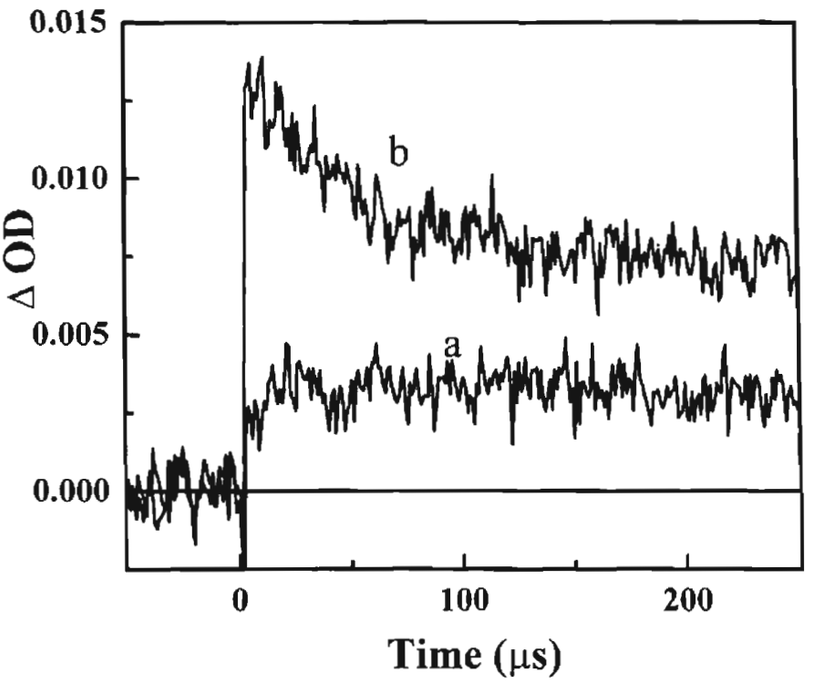

Figure 3.16. Transient decay profile of **15** in the methanol monitored at 590 nm following laser pulse excitation (355 nm, 10 ns, 60 mJ/ pulse) a) in the presence of oxygen and b) in the absence of oxygen.

The triplet yields (ϕ_T) of the compounds in methanol were determined using benzophenone as reference.[73,74] Optically matched solutions of **14**, **15** and benzophenone in methanol were mixed with known volumes of 0.1mM solution of β-carotene dissolved in benzene. The transient absorbance of β-carotene at 540 nm was monitored following 355 nm laser pulse excitation and the triplet quantum yield was measured using the following expression (Equation 3.9),

$$\phi_T^S = \phi_T^R \left(\frac{\Delta A^S}{\Delta A^R}\right)\left(\frac{k_{obs}^S}{k_{obs}^S - k_o^S}\right)\left(\frac{k_{obs}^R - k_o^R}{k_{obs}^R}\right) \qquad (3.9)$$

where ΔA is the absorbance plateau at 520 nm following the completion of sensitized triplet formation, k_{obs} is the pseudo first order rate constants for the growth of the β-carotene triplet sensitized by the dye or benzophenone, k_0 is the first order rate constants for decay of the dye or benzophenone triplet states in the absence of β-carotene and ϕ_T refers to the triplet quantum yield. S and R denote sample (**14** or **15**) and reference (benzophenone) respectively. The triplet quantum yields summarized in Table 3.5, show that the intersystem crossing efficiency of these dyes is fairly high.

The transient absorption spectrum of **15** in water (Figure 3.17) and aqueous micellar media (Figure 3.18) were similar to the one observed in methanol indicating the formation of the triplet excited state of the dye under these conditions.

Table 3.5 Triplet excited state properties of 14 and 15 in methanol

Compound	Triplet λ_{max} (nm)	τ_T μs	Phosphorescence maximum (nm)	τ_p (ms)	(ϕ_T)	($\phi_{\Delta s}$)
14	600	15	735, 750	9	0.26	0.014
15	600	15	720, 750	14	0.29	0.08

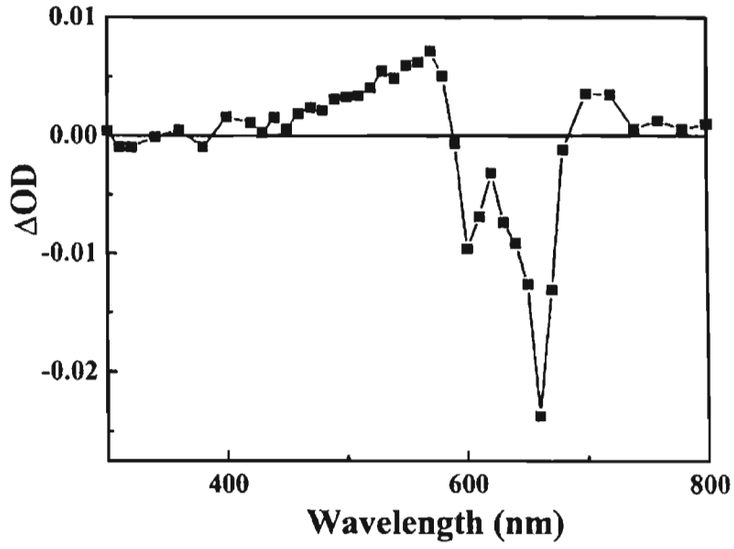

Figure 3.17. Transient absorption spectrum following laser pulse excitation (355 nm, 10 ns, 60 mJ/pulse) of **15** in deaerated water, recorded immediately after 355 nm laser pulse.

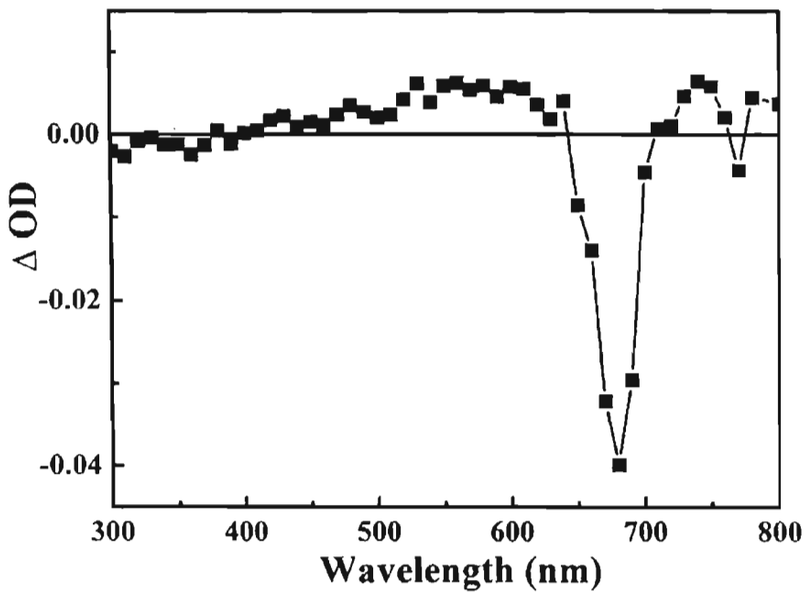

Figure 3.18. Transient absorption spectrum following laser pulse excitation (355 nm, 10 ns, 60 mJ/pulse) of **15** in deaerated water in the presence of CTAB micelles.

In order to estimate the triplet energy of the dyes, their phosphorescence were recorded in each case in alcoholic glasses at 77 K. Figure 3.19 shows the phosphorescence spectrum of **15** in ethanol glass at 77 K. The short wavelength band assigned to 0,0 transition corresponds to the triplet energy 1.7 eV. The phosphorescence lifetime of **15** in ethanol glass at 77 K was 14 ms. The phosphorescence properties of **14** and **15** are summarized in Table 3.5.

As discussed earlier intersystem crossing efficiency is generally very low in squaraine dyes.[63] Enhanced intersystem crossing in these dyes can be attributed to heavy atom induced spin orbit coupling due to the presence of selenium atoms.

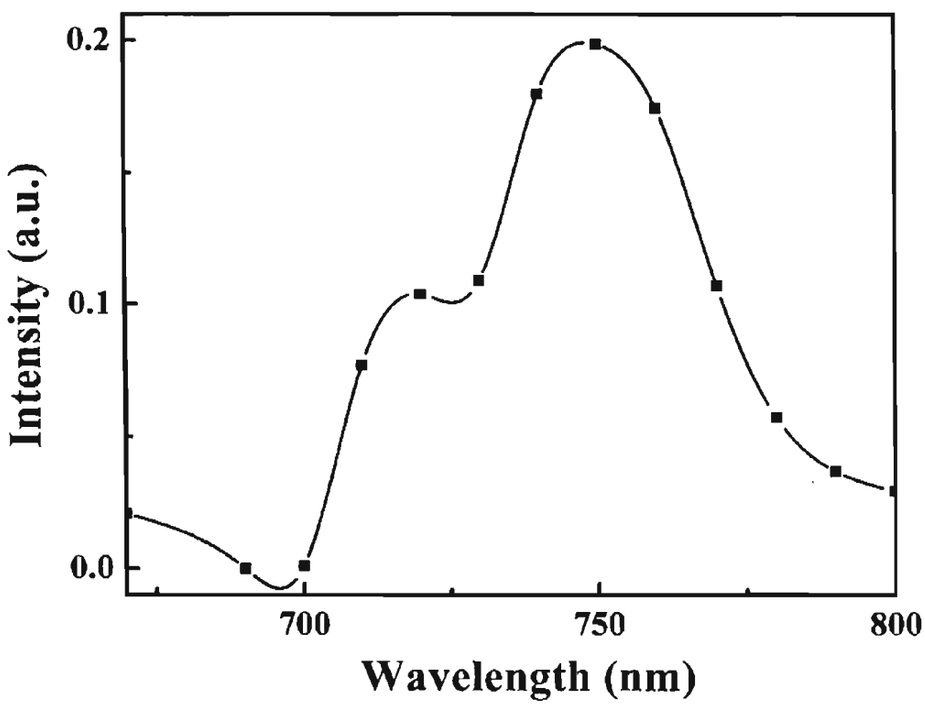

Figure 3.19. a) Phosphorescence spectrum of **15** excited at 640 nm in ethanol glass.

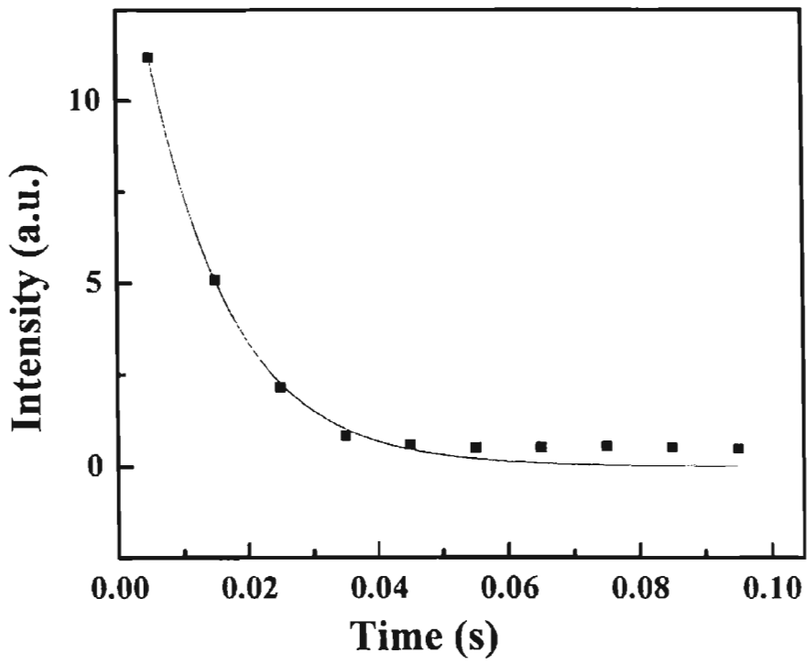

Figure 3.20. Phosphorescence decay of **15** monitored at 750 nm, in ethanol glass at 77 K.

3.3.5. Photosensitized Generation of Singlet Oxygen .

On excitation of the dyes in presence of oxygen, energy transfer from the excited triplet state can generate singlet oxygen (Scheme 3.5).

$$[\text{Dye}] \longrightarrow [\text{Dye}]^{1*}$$

$$[\text{Dye}] \longrightarrow [\text{Dye}]^{3*}$$

$$[\text{Dye}]^{3*} + O_2 \longrightarrow [\text{Dye}] + O_2^{1*}$$

Scheme 3.5

Quantum yields of singlet oxygen formation in air-saturated methanol were determined by comparing the efficiency of photooxidation of

diphenylisobenzofuran (DPBF) by the dyes, to that of a standard, namely, methylene blue ($\phi_{\Delta S}$ = 0.52).[75] DPBF was used as it absorbs in a region where the squaraine derivatives absorb weakly and it reacts rapidly with singlet oxygen to form a colorless product.[76,77] Optically dilute solutions (O.D = 0.1) of the dye or standard containing DPBF were irradiated at 660 nm using a 450 W output of Xenon arc lamp. A monochromator (SPEX 1681 0.22 m) was used to select the irradiation wavelength. Irradiation leads to a decrease in the DPBF absorption centered around 410 nm (Figure 3.21).

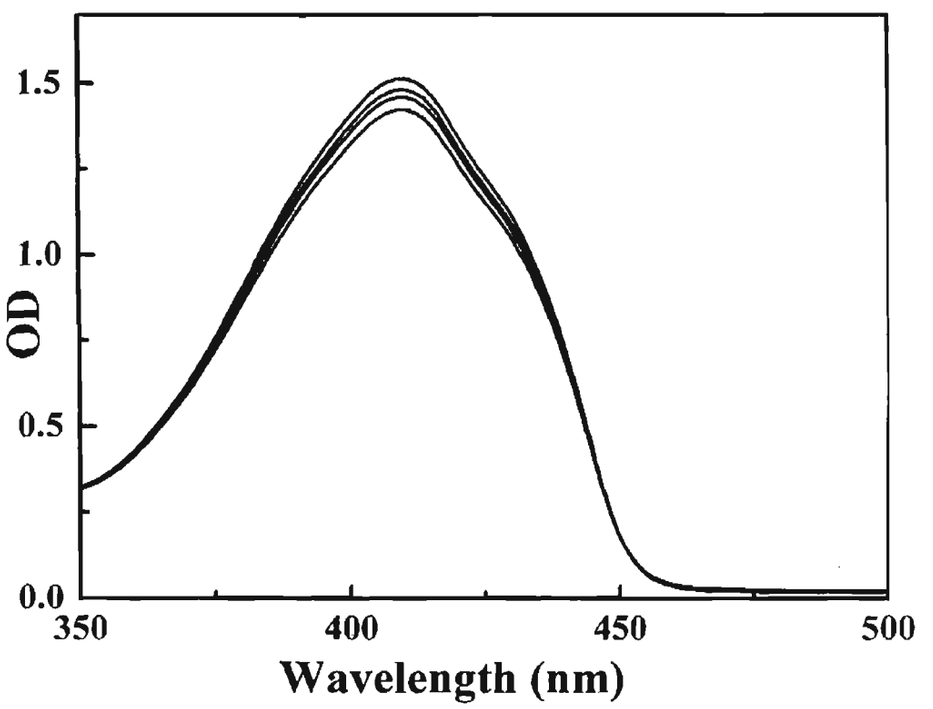

Figure 3.21 Absorption spectra of DPBF at various irradiation time intervals in the presence of **15**.

The quantum yields were measured in optically dilute solutions using Equation 3.10,

$$\phi_{\Delta S} = \phi_{\Delta R} \times \frac{m_S}{m_R} \times \frac{\left(1 - 10^{-OD}\right)_R}{\left(1 - 10^{-OD}\right)_S} \qquad (3.10)$$

where, ϕ_f refers to the quantum yield, m is the slope of a plot of change in DPBF absorbance at 410 nm with irradiation time, $1\text{-}10^{-OD}$ is the absorbance correction factor at the irradiation wavelength and S and R refer to sample (**14** or **15**), and reference (methylene blue), respectively.

Figure 3.22 shows the plot of ΔOD at 410 nm *versus* irradiation time for solutions containing the dyes under investigation and methylene blue. The quantum yields for the generation of singlet oxygen ($\phi(^1O_2)$) for **14** and **15** shown in Table 3.5, indicate that singlet oxygen formation is not very efficient for these dyes. In order to examine whether the low singlet oxygen yields are due to an alternative electron transfer mechanism occurring between the excited state of the dye and oxygen, the photostability of the dyes were examined. The dyes were found to be stable on irradiation both in the presence and absence of oxygen indicating that photodegradation or electron transfer to oxygen may not be contributing to the reduction in efficiency of singlet oxygen formation in these dyes. The low quantum yields for singlet oxygen generation may therefore be attributed to an inefficient energy transfer process from the triplet-excited state of these dyes.

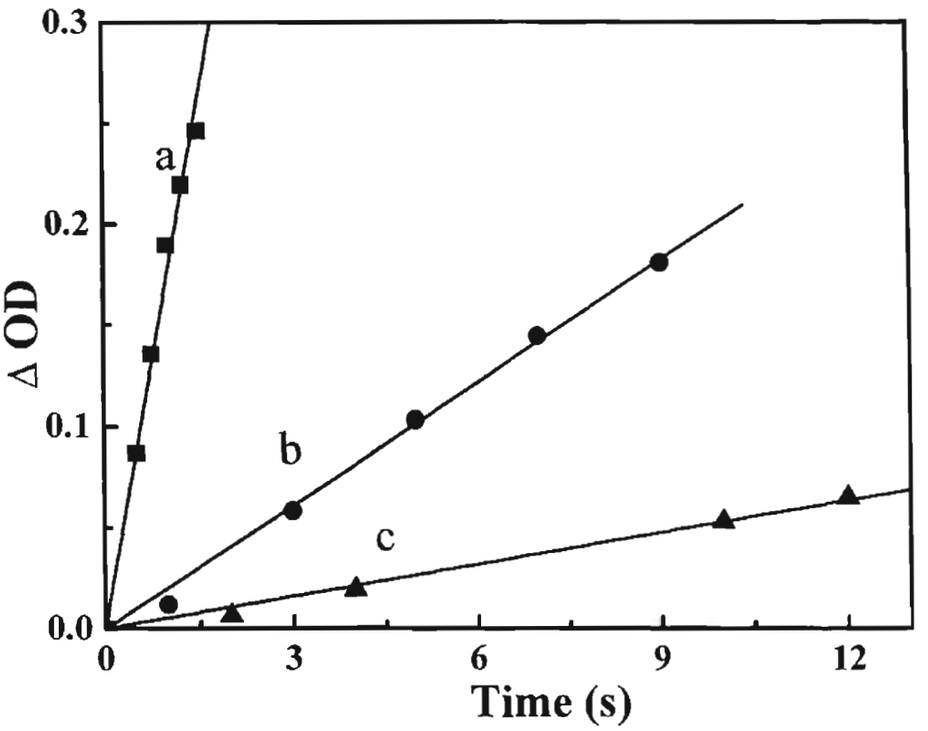

Figure 3.22. Plot of Δ OD at 410 nm *vs* irradiation time (λ_{irr} = 630 nm) for methanolic solution of (a)**14**; (b) **15** and (c) methylene blue containing 20 μM 1,3-diphenylisobenzofuran.

3.3.6. Ground and Excited State Redox Properties

Electron transfer proceses from the excited state of dye sensitizers can also play a major role in PDT applications. In view of this the oxidation characteristics of the squaraine dyes were studied using cyclic voltammetry. Due to the poor solubility of **15**, studies were carried out using the model compound **14**. Oxidation potentials of the compounds were determined in methanol using the BAS CV-50W voltammetric analyzer. The supporting electrolyte used was Bu_4NBF_4 (0.1 M). A three-electrode system with glassy carbon (working), platinum wire (auxillary),

and standard calomel electrode (reference) was used. Nitrogen was flushed through the solution, which was also stirred for homogeneity throughout the experiment except during measurement. Figure 3.23 shows the voltammogram measured for **14** in methanol. An oxidative peak is seen around 433 mV. It is evident from the figure that one-electron oxidation of this dye is reversible. Thus, in photoinduced electron transfer processes which normally involve single electron transfer, these dyes could behave in a catalytic manner under appropriate conditions.

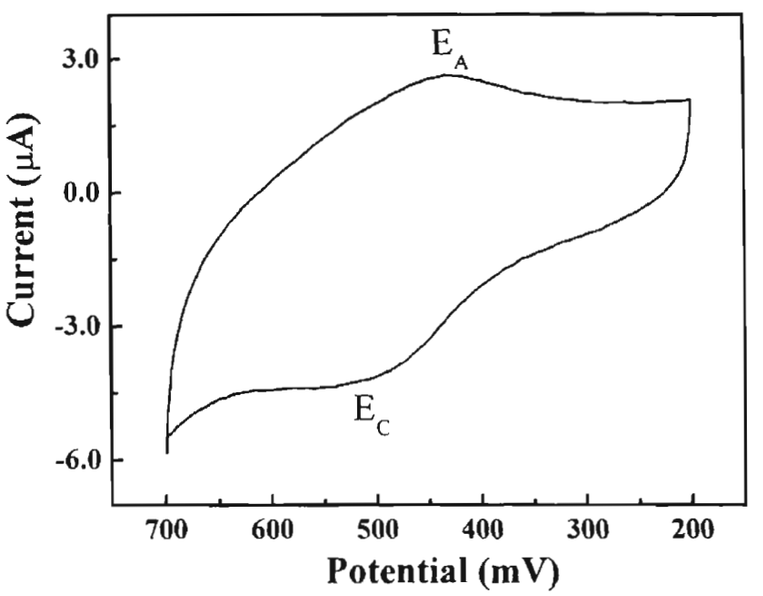

Figure 3.23. One-electron oxidation of **14** (1 mM) in acetonitrile containing 0.1 M TBAP in a three electrode cell containing Ag as the reference electrode glassy carbon as the working electrode and Pt as the auxillary electrode.

The two electron oxidation of the dye is however irreversible as indicated in Figure 3.24. The irreversible second oxidation peak of the dye occurs at 810 mV.

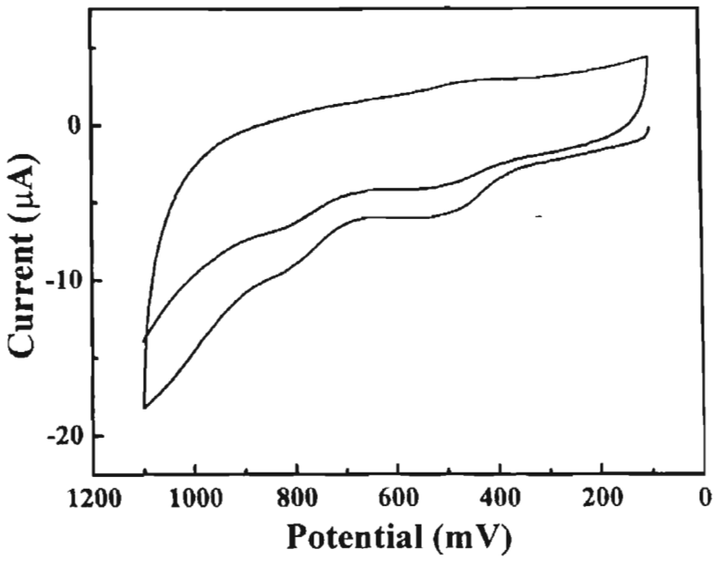

Figure 3.24. Two-electron oxidation of **14** (1 mM) in acetonitrile containing 0.1 M TBAP in a three electrode cell containing Ag as the reference electrode glassy carbon as the working electrode and Pt as the auxillary electrode.

Electron transfer reactions from the excited state of **14** and **15** were studied in methanolic solutions using methyl viologen (MV^{2+}) as the electron acceptor. Methyl viologen has a redox potential of -460 mV and is known to accept electrons from a variety of excited state electron donors, resulting in the formation of the $MV^{+\cdot}$ radical cation.[78] The $MV^{+\cdot}$ radical cation thus formed has a strong absorption peak centered on 395 nm and a weaker one centered on 590 nm. Addition of MV^{2+} (78.5 μM) to methanolic solutions of the dyes leads to a quenching of their triplet-excited states, which is accompanied by a growth around 590 nm. Figures 3.25 and 3.26 show the transient signals obtained around 590 nm on excitation of methanolic solutions of **14** and **15** containing MV^{2+} by 355 nm laser pulse.

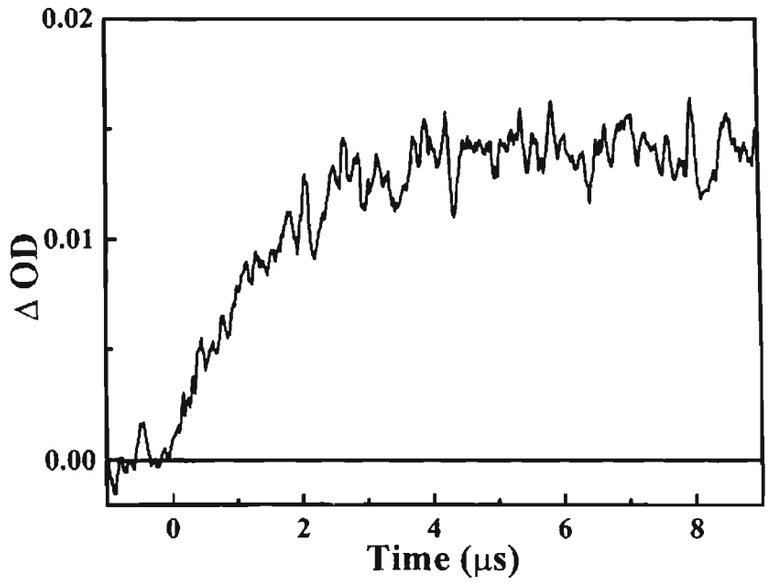

Figure 3.25. Formation of methyl viologen radical cation monitored at 590 nm following laser pulse excitation (355 nm, 10 ns, 60 mJ/pulse) which is generated by the photosensitization of **14** in presence of MV^{2+} (78.5 μM) in deaerated methanol.

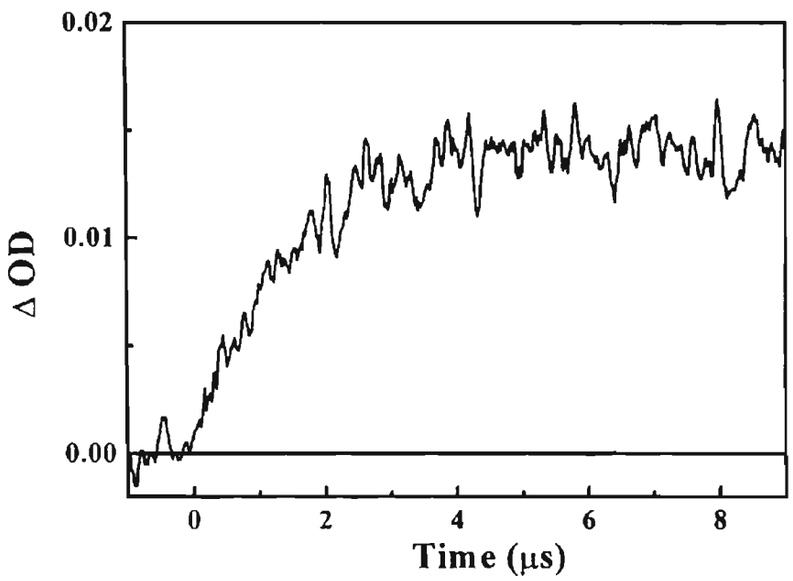

Figure 3.26. Formation of methyl viologen radical cation monitored at 590 nm following laser pulse excitation (355 nm, 10 ns, 60 mJ/pulse) which is generated by the photosensitization of **15** in presence of MV^{2+} (132.3 μM) in deaerated methanol.

The growth of the transient absorption at 590 nm can be attributed to the formation of the $MV^{+\cdot}$ radical cation according to the mechanism shown in Scheme 3.6.

$$[Dye] \longrightarrow [Dye]^{3*}$$

$$[Dye]^{3*} + MV^{2+} \rightleftharpoons [Dye]^{+\bullet} + MV^{+\bullet}$$

Scheme 3.6

The transient absorption spectrum of **14** in the presence of MV^{2+} recorded following the completion of the forward electron transfer process is shown in Figure 3.27. A sharp structured band with a peak at 395 nm clearly indicates the formation of the methyl viologen radical cation. The absorption band of the methyl viologen radical cation around 590 nm is masked by a transient signal, which may be attributed to the dye radical cation formed in the electron transfer process. The transient absorption of the dye radical cation of **14** was obtained by subtracting the absorption spectrum of methyl viologen radical cation from the transient spectrum (Figure 3.28).

Figure 3.29 shows the decay of the $MV^{+\cdot}$ radical cation monitored at 395 nm in a methanolic solution of **14** and MV^{2+}. The decay follows a second order process. The recovery of the ground state absorption also follows the same kinetics. These results indicate that the radical ion formed decay *via* back electron transfer between the dye and methyl viologen radical cations.

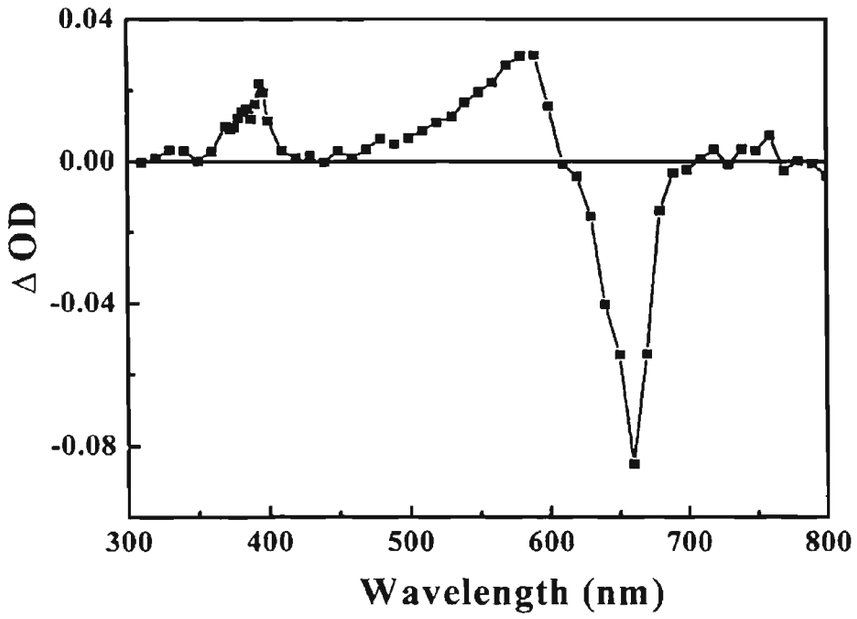

Figure 3.27. Transient absorption spectrum obtained on laser flash photolysis of a deaerated methanolic solution of **14** (3.6 μM) and MV^{2+} (78.2 μM), immediately after laser pulse (355 nm, 10 ns, 60 mJ/pulse).

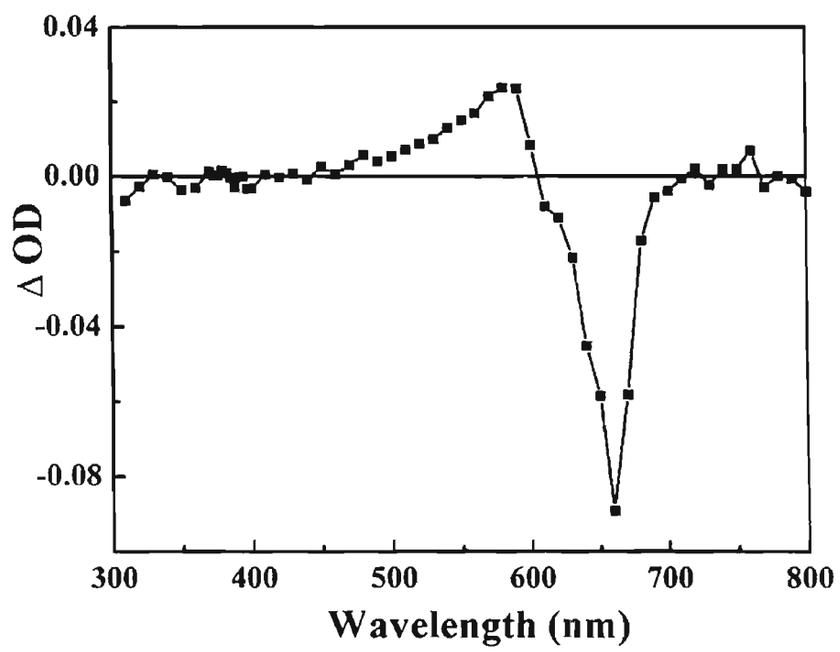

Figure 3.28. Transient absorption spectrum of the dye radical cation ($14^{+\cdot}$) obtained by subtracting the spectrum of $14^{+\cdot}$ and $MV^{+\cdot}$

Similar results were observed for the back electron transfer of the radical cation of **15** with $MV^{+\cdot}$. Efficient back electron transfer from the dye radical cation to $MV^{+\cdot}$ could also be confirmed by examining the absorption spectrum of the solutions used in the laser flash photolysis experiments, which did not indicate any degradation of the dye.

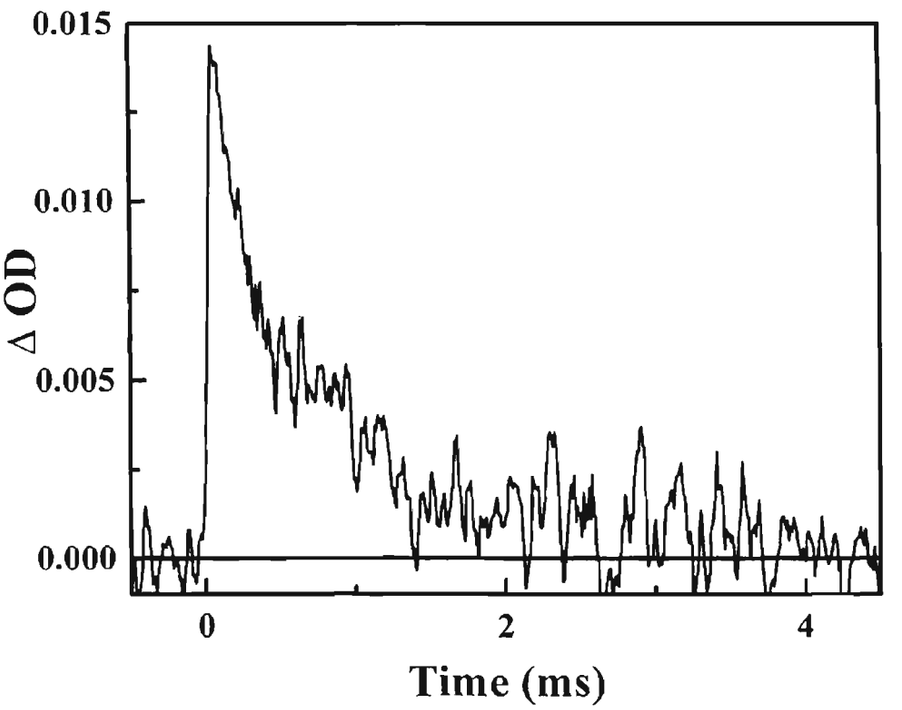

Figure 3.29. Decay of the methyl viologen radical cation observed at 395 nm , following laser pulse excitation (355 nm, 10 ns, 60 mJ/pulse)of a solution of **14** (3.6 μM) in methanol containing MV^{2+} (78.5 μM).

3.4. Conclusion

A new water-soluble squaraine dye **15** and its model compound **14** have been prepared and their ground and excited state properties were explored. These dyes posses strong absorption and emission in the near infrared region and their triplet yields are fairly high. The water soluble squaraine dye **15** generates singlet oxygen with a quantum efficiency of 0.08. This in combination with the ability of the dye to undergo reversible photoinduced electron transfer in an efficient manner make it potentially useful for PDT applications.

3.5. Experimental Section

3.5.1. Materials and Methods

All melting points are uncorrected and were determined using Aldrich Mel-Temp melting point apparatus. The electronic absorption spectra were recorded on Shimadzu 3101 UV-visible-NIR spectrophotometer. Quantum yields of fluorescence were measured by relative methods using optically dilute solutions. DOTC iodide (fluorescence quantum yield ϕ_f = 0.49) in ethanol was used as standard.[79] An Elico pH meter was used for pH measurements. Sodium hydroxide or HCl are used to adjust the pH. Solvents used were purified before use. All experiments were carried out at room temperature.

2-Methylbenzselenazole, and squaric acid (Aldrich) were used without further purification for the synthesis of **14** and **15**. β-Carotene(Aldrich) was recrystallized from a mixture of benzene and methanol. 1,3-Diphenylisobenzo-

furan (DPBF), methylene blue, β-cyclodextrin, cetyltrimethyl ammonium bromide (CTAB) and benzophenone were used without further purification.

3.5.2. Synthesis.

2-Methylbenzselenazolium methiodide was synthesized[80] by heating a mixture of 2-methylbenzselenazole (2g, 10.1 mmol) and methyl iodide (2g 14.1 mmol) for 20 h. The product was recrystallized from methanol to give 3.05g, (87%) of a pure sample.

3-(Carboxymethyl)-2-methylbenzselenazolium bromide was synthesized [80] by heating a mixture of 2-methylbenzselenazole (2g, 10.1 mmol) and bromoacetic acid (2g, 15.2 mmol) for 20 h. The product was recrystallized from methanol to give (2.5 g, 72.5 %) of a pure product, mp 193°C (decomp).

Synthesis and characterization of 14 and 15. Compounds **14** and **15** (Scheme 3.4) were synthesized by refluxing the appropriate methylbenzselenazolium salt (2.95 mmol) and squaric acid (1.5 mmol) in a solvent mixture (1:2.5) of benzene and 1-butanol in presence of quinoline accompanied by azeotropic distillation of water.[62]

Compound **14** was purified by chromatography over silica (100-200 mesh) using a mixture (1:10) of methanol and chloroform as eluent to give 21% of **14**. mp >250 °C. ^{1}HNMR ($CDCl_3$): δ 3.3 (s, 3H, N-CH_3), 6.2 –7.9 (m, aromatic); IR ν_{max} (KBr) 3472, 1733, 1696, 1654, 1571, 1515, 1424, 1304, 1229, 1085, 743 cm^{-1}.

Compound **15** was dissolved in water and precipitated at its isoelectric point. It was then repeatedly washed with water and methanol to give the pure sample (yield 27%), mp >250 °C. ^{1}H NMR (D_2O): δ 4.2 (s, 2H, N-CH_2COOH), 5.4 (s, 1H, styryl), 6.9-7.6 (m, 4H, aromatic); ^{13}C NMR (D_2O): δ 49.96, 88.29, 113.589, 124.395, 125.162, 127.501, 127.877,.142.472, 163.079, 169.292, 172.302; IR ν_{max} (KBr) 3442, 1741, 1687, 1656, 1643, 1551, 1265, 1192, 1105, 751, 623 cm^{-1}.

3.5.3. Laser Flash Photolysis

The laser flash photolysis experiments were carried out using the third harmonic (355 mm, 60 mJ/pulse) of a Nd: YAG laser GCR-12 series, Quanta Ray of 10 ns pulse width. The kinetic absorption spectrophotometer used to detect the optical density changes after laser excitation (LKS-20, Applied photophysics) has been described earlier.[81] The analyzing and laser beams were fixed at right angles to each other.

3.6. Reference

1. Kessel, D. in *Photodynamic Therapy of Neoplastic Disease*, *Vol. 2*, CRC Press, Boca Raton; Florida, **1990**.
2. *Photodynamic Therapy*, in (Ed.: Gomer, C. J.), *Vol. 46*, Pergamon Press, Oxford, **1987**.
3. Bonnet, R., *Chem. Soc. Rev.* **1995**, *24*, 19.
4. Raab, O., *Zeit. Biol.* **1900**, *39*, 44.
5. Tappeiner, A. v.; Jodlbauer, A., *Dtsh. Arch. Klin.Med.* **1904**, *80*, 427.
6. Laustiat, G., *Biochemie* **1986**, *68*, 771.
7. Dougherty, T. J.; Kaufman, J. E.; Goldfarb, A.; Weishaupt, K. R.; Boyle, D.; Mittleman, A., *Cancer Res.* **1978**, *38*, 2628.
8. Kessel, D., *Photochem. Photobiol.* **1984**, *39*, 851.
9. Moan, J., *Photochem. Photobiol.* **1986**, *43*, 994.
10. Redmond, R. W.; Heihoff, K.; Braslavsky, S. E.; George, T., *Photochem. Photobiol.* **1987**, *45*, 209.
11. Kasha, M.; Brabham, D. E., in *Singlet Oxygen*, (Ed.: Wasserman, H. H., Murray, R. W.), Academic Press, New York, **1979**, 2.
12. Wilkinson, F.; Brummer, J. G., *J. Phys. Chem. Ref. Data* **1981**, *10*, 809.
13. Kaplan, M. L., *Chem. Technol.* **1971**, 621.
14. Shinkarenko, N. V.; Aleskovskii, V. B., *Russ. Chem. Rev.* **1981**, *50*, 406.
15. Howard, J. A.; Ingold, K. U., *J. Am. Chem. Soc.* **1968**, *90*, 1056.
16. Tauber, A. J.; Barbier, B. M., *Photochem. Photobiol.* **1978**, *28*, 701.

17. Krinsky, N. I., in *Singlet Oxygen*, (Ed.: Wasserman, H. H., Murray, R. W.), Academic Press, New York, **1979**, 597.

18. Foote, C. S., in *Free Radicals in Biology*, (Ed.: Pryor, W. A.), *Vol. II*, Academic Press, New York, **1976**, 112.

19. Wan, S.; Parrish, J. A.; Anderson, R. R.; Madden, M., *Photochem. Photobiol.* **1981**, *34*, 679.

20. Tyrrell, R. M.; Pidoux, M., *Cancer Res.* **1987**, *47*, 1825.

21. Lakowicz, J. R., *Laser Focus World* **1994**, *28*, 60.

22. Soper, S. A.; Mattingly, Q. L., *J. Am. Chem. Soc.* **1994**, *116*, 3744.

23. Soper, S. A.; Mattingly, Q. L.; Vengula, P., *Anal. Chem.* **1993**, *65*, 740.

24. Takemura, T.; N.Ohta; Nakajima, S.; Sakata, I., *Photochem. Photobiol.* **1989**, *50*, 339.

25. Milanesi, C.; Biolo, T.; Jori, G.; Schaffner, K., *Lasers in Med. Sci.* **1991**, *6*, 437.

26. Guardino, M.; Biolo, R.; G, J.; Schaffner, K., *Cancer Lett.* **1989**, *44*, 1.

27. West, C. M. L.; Moore, J. V., *Photochem. Photobiol.* **1989**, *49*, 169.

28. Dougherty, T. J., in *Porphyrin Localization and Treatment of Tumours*, (Ed.: Doiron, D. R., Gomer, C. J.), Alan R. Liss, New York, **1984**, 75.

29. Kessel, D.; Chang, C. K.; Musselman, B., in *Methods in Porphyrin Photosensitization*, (Ed.: Kessel, D.), Plenum Press, New York, **1985**, 213.

30. Ben-Hur, E.; Rosenthal, I., *Photochem. Photobiol.* **1985**, *42*, 129.

31. Morgan, A. R.; Garbo, G. M.; Kreimer-Birnbaum, M.; Keck, R. W.; Chaudhuri, K.; Selman, S. H., *Cancer Res.* **1987**, *47*, 469.

32. Moan, J.; Nerg, K., *Photochem. Photobiol.* **1991**, *55*, 931.

33. Henderson, B. W.; Dougherty, T. J., *Photochem. Photobiol.* **1992**, *55*, 145.

34. Dougherty, T. J., *Photochem. Photobiol.* **1993**, *58*, 895.

35. Dougherty, T. J.; Lawrence, G.; Kaufman, J. E.; Boyle, D.; Weishaupt, K. R.; Goldfarb, A., *J. Natl. Cancer. Inst.* **1979**, *62*, 231.

36. Bonnet, R.; Ridge, R. J.; Scourides, P. A., *J. Chem. Soc (Perkins I)* **1981**, 3135.

37. Lightner, D. A.; Donagh, A. F. M., *Acc. Chem. Res.* **1984**, *17*, 417.

38. Oseroff, A. R., in *Photodynamic Therapy: Basic Principles and Clinical Applications*, (Ed.: Henderson, B. W., Dougherty, T. J.), Marcel Dekker Inc, New York, **1992**, 79.

39. Henderson, B. W., in *Photochemotherapy*, (Ed.: Kessel, D.), CRC Press, Boca Raton, **1990**.

40. Selman, S. H.; Birnbaum, M. K.; Klaunig, J. E.; Goldblatt, P. J.; Keck, R. W.; Britton, S. L., *Cancer Res.* **1984**, *44*, 1924.

41. Oseroff, A. R.; Ohuoha, D.; Ara, G.; McAuliffe, D.; Foley, J.; Cincotta, L., *Proc. Natl. Acad. Sci. USA* **1986**, *83*, 9729.

42. Oseroff, A. R.; Ara, G.; Ohuha, D.; Aprille, J. R.; Bommer, J. C.; Yarmush, M. L.; Foley, J.; Cincotta, L., *Photochem. Photobiol.* **1987**, *46*, 83.

43. Cincotta, L.; Foley, J. W.; Cincotta, A. H., *Photochem. Photobiol.* **1987**, *46*, 751.

44. Krattinger, B.; Nurco, D. J.; Smith, K. M., *Chem. Commun.* **1998**, 757.

45. Mettah, S.; Shibata, M.; Alderfer, J. L.; Senge, M. O.; Smith, K. M.; Rein, R.; T. J. Dougherty; Pandey, R. K., *J. Org. Chem.* **1998**, *63*, 1646.

46. Kozyrev, A. N.; Suresh, V.; Das, S.; Senge, M. O.; Shibata, M.; Dougherty, T. J.; Pandey, R. K., *Tetrahedron* **2000**, *56*, 3353.

47. Bai, S.; Liu, C.; Guo, Z., *Proc. SPIE* **1993**, *1616*, 275.

48. Garbo, G., *J. Photochem. Photobiol. A: Chem.* **1996**, *34*, 109.

49. Kozyrev, A. N.; Zheng, G.; Zhu, C.; Dougherty, T. J.; Smith, K. M.; R. K. Pandey, *Tetrahedron Lett.* **1996**, *37*, 6431.

50. Ben-Hur, E., in *Photodynamic Therapy: Basic Principles and Clinical Applications*, (Ed.: Henderson, B. W., Dougherty, T. J.), Marcel Dekker Inc, New York, **1992**, 63.

51. Wadwa, K.; Smith, S.; Oseroff, A. R., *Advances in Photochemotherapy*, in *SPIE*, (Ed.: Hasan, T.), **1989**, 154.

52. Foley, J. W.; Cincotta, L.; Cincotta, A. H., *Advances in Photochemotherapy*, in *SPIE*, (Ed.: Hasan, T.), *Vol. 997*, **1989**, 90.

53. Gandin, E.; Lion, Y.; van de Vorst , *Photochem. Photobiol.* **1983**, *37*, 271.

54. Lewis, M. R.; Goland, P. P., *Cancer Res.* **1953**, *13*, 130.

55. Chen, L. B., *Ann. Rev. Cell. Biol.* **1988**, *4*, 155.

56. Schmidt, A. H., in *Oxocarbons*, (Ed.: West, R.), Academic Press, New York, **1980**.

57. Terpetschnig, E.; Szmacinski, H.; Lakowicz, J. R., *Proc. SPIE-Int.Soc. Opt. Eng.* **1994**, *2137*, 608.

58. Terpetsching, E.; Lakowicz, J. R., *Dyes. Pigm.* **1993**, *21*, 227.

59. Terpetsching, E.; Szmacinski, H.; Ozinskas, A.; Lakowicz, J. R., *Anal. Biochem.* **1994**, *217*, 197.

60. Ramaiah, D.; Joy, A.; Chandrasekhar, N.; Eldho, N. V.; Das, S.; M. V. George, *Photochem. Photobiol.* **1997**, *65*, 783.

61. Detty, M. R.; Merkel, P. B., *J. Am. Chem. Soc.* **1990**, *112*, 3845.

62. Sprenger, H. E.; Ziegebien, W., *Angew. Chem. Int. Ed. Engl.* **1967**, *6*, 553.

63. Gude, C.; Rettig, W., *J. Phys. Chem. A* **2000**, *104*, 8050.

64. Das, S.; Thomas, K. G.; Thomas, K. J.; Madhavan, V.; Liu, D.; Kamat, P. V.; George, M. V., *J. Phys. Chem.* **1996**, *100*, 17310.

65. Cox, G. S.; Turro, N. J.; Yang, N. C.; Chen, M. J., *J. Am. Chem. Soc.* **1984**, *106*, 422.

66. Duveneck, G. L.; Sitzmann, E. V.; Eisenthal, K. B.; Turro, N. J., *J. Phys. Chem.* **1989**, *93*, 7166.

67. *Photochemistry in Organized and Constrained Media*, (Ed.: Ramamurthy, V.), VCH, New York, **1991**.

68. Nag, A.; Dutta, R.; Chattopadhyay, N.; Bhattacharyya, K., *Chem. Phys. Lett.* **1988**, *157*, 83.

69. Cho, W. D.; Kim, Y. H.; Kang, S. G.; Yoon, M.; Kim, D., *J. Phys. Chem.* **1994**, *98*, 558.

70. Benesi, H. A.; Hildebrand, J. H., *J. Am. Chem. Soc.* **1949**, *71*, 2703.

71. Das, S.; Thomas, K. G.; George, M. V.; Kamat, P. V., *J. Chem. Soc. Faraday Trans. 1* **1992**, *88*, 3419.

72. Evaluated using semi-empirical PM3 method of TITAN Software. Version 1., Wavefunction Inc; Schrödinger Inc, **1999**.

73. Kumar, C. V.; Qin, L.; Das, P. K., *J. Chem. Soc. Faraday Trans 2* **1984**, *80*, 783.

74. Carmichael, I.; Hug, G. L., *J. Phy. Chem. Ref. Data* **1986**, *15*, 1.

75. Scaiano, J. C., *Handbook of Organic Photochemistry*, CRC Press, **1989**, 229.

76. Foote, C. S. in *Singlet Oxygen*, Academic Press, New York, **1979**.

77. Merker, P. B.; Kearns, D. R., *J. Am. Chem. Soc* **1975**, *97*, 462.

78. Bock, C. R.; Connor, J. A.; Gutierrez, A. R.; Meyer, T. J.; Whitten, D. G.; Sulliven, B. P.; Nagle, J. K., *J. Am. Chem. Soc.* **1979**, *101*, 4815.

79. *Kodak Laser Dyes*, Eastman Kodak Company, Kodak Publication, New York, **1987**.

80. Mills, W. H., *J. Chem. Soc.* **1922**, *121*, 455.

81. Ramaiah, D.; Cyr, D. R.; Barik, R.; Gopidas, K. R.; Das, P. K.; George, M. V., *J. Phys. Chem.* **1992**, *96*, 1271.

CHAPTER 4

SYNTHESIS AND PHOTOPHYSICAL PROPERTIES OF SOME SQUARAINE DYES CONTAINING *N*- HETEROCYCLIC SUBSTITUENTS

4.1. Abstract

The synthesis and characterization of a novel squaraine dye bis(*N*-methyl-acridin-9-ylidine)squaraine (**5**), absorbing strongly in the NIR region is reported. The absorption maximum of the dye (900 nm) is substantially red shifted compared to that of squaraine dyes reported earlier. The photophysical properties of these dyes as well as some other squaraine dyes containing *N*-heterocyclic substituents have been investigated. The fluorescence quantum yield of one of these dyes bis(*N*-methylquinolin-2-ylidine)squaraine (**3**) shows an interesting solvent dependence. Whereas, in aprotic solvents the fluorescence quantum yield increases slightly with increase in solvent polarity, in protic solvents a drastic decrease in fluorescence quantum yield with increase in solvent polarity is observed. These effects are attributed to a change in the lowest emitting state for an n-π^* state in non-protic solvents to π-π^* in protic solvents, due to hydrogen bonding. The triplet excited states properties of these dyes have also been investigated.

4.2. Introduction

The strong absorption of squaraine dyes in the visible and near infrared region make them highly suitable for a number of applications such as a xerographic

photoreceptors,[1] optical recording devices[2] and solar cells.[3,4] In many of these applications, a particular requirement is that the dye should be able to undergo efficient photoinduced charge separation. Extensive work in this laboratory as well as in other groups have shown that although squaraine dyes undergo photoinduced electron transfer, the efficiency of charge separation is limited, due to very fast back electron transfer.[5-7] A principal reason for this is that the photoactive state of most of the squaraine dyes studied so far is the singlet excited state, since their intersystem crossing efficiencies are low. Photoinduced electron transfer from the singlet state results in the formation of a singlet radical ion pair. Back electron transfer between the radical ion pairs thus formed is a spin allowed process, and therefore occurs very efficiently. Charge separation following photoinduced electron transfer is hence expected to be better when triplet excited states are involved. In Chapter 3 of this thesis, we have shown that efficient charge separation occurs in photoinduced electron transfer between the triplet excited state of bis(3-methyl)benzselenazol-2-ylidine squaraine and MV^{2+}. It is therefore of interest to search for new squaraine dyes possessing good triplet quantum yields. The studies described in Chapter 3 of the thesis as well as earlier studies[8,9] from this laboratory have shown that, substitution of the heavy atoms in the molecular framework of the dyes can be utilized for enhancing the triplet yields.

An alternative strategy for enhancing the triplet quantum yields of these dyes would be to synthesize squaraine dyes with substituents possessing low lying n-π^* states. The oscillator strengths of spin allowed (S_0-S_1) transitions range from

$1\text{-}10^{-4}$, while that of a spin forbidden (S_0-T_1) transient range from 10^{-5}-10^{-9} for π-π^* excitation. However for n-π^* transitions the oscillator strength for a spin forbidden electronic excitation can be higher.[10] Most studies on the photophysics of squaraine dyes reported in the literature have dealt with molecules possessing aniline donors, an example of which (**1**) is shown in Chart 4.1. The lowest excited state of these dyes is the π-π^* state.

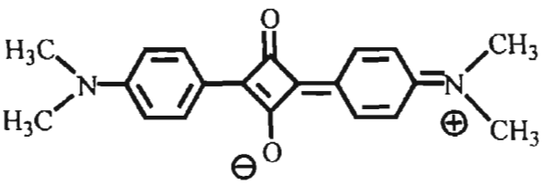

1

Chart 4.1

There are several reports on the synthesis and absorption spectra of cyanine type squaraine dyes possessing *N*-heterocyclic substituents, which can possess low lying n-π^* states. However, study of the photophysical properties of this class of dyes have been limited to bis(3-methylbenzothiazolium-2-ylidine)squaraine[11] and bis(3-methylindolinin-2-ylidine)squaraine,[12] both of which do not possess measurable triplet quantum yields. The bis(3-carboxymethylbenzselenazol-2-ylidine)squaraine, discussed in Chapter 3 also belongs to this class of dyes, but its high triplet quantum yield may be attributed mainly to the presence of a heavy atom such as selenium.

In this Chapter we describe some preliminary work carried out on the photophysical properties of a few squaraine dyes (**2-5**, Chart 4.2) belonging to this

class of dyes. Some aspects of the photophysical properties of bis(3-methyl-indolinin-2-ylidine)squaraine (**2**) have been reported recently by Gude and Rettig.[12] The new squaraine dye, bis(3-methylacridin-9-ylidine)squaraine (**5**) has been synthesized which absorbs strongly in the NIR region with a maximum centered around 900 nm. The absorption spectrum of this dye is substantially more red shifted than those of squaraine dyes reported earlier in the literature.[5]

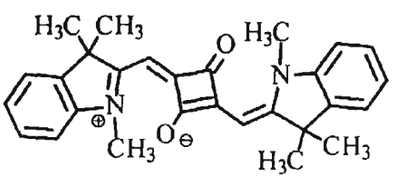

2

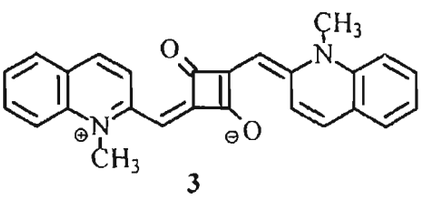

3

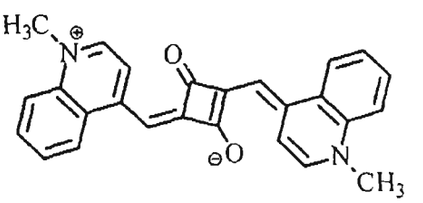

4

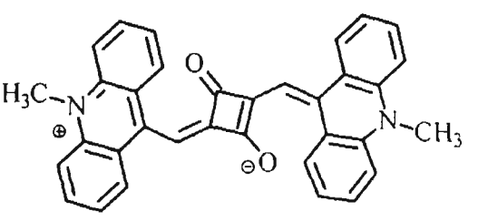

5

Chart 4.2

4.3. Results and Discussion

4.3.1. Synthesis

Compounds **2-5** were prepared by condensation reactions of the corresponding salts of the nitrogen containing heterocycles with squaric acid in the presence of a weak base, using procedures reported in the literature.[13] A typical example is shown in Scheme 4.1, for the synthesis of bis(3-methylacridin-9-ylidine)squaraine. The iodide salt used in the reactions were prepared by methylation of *N*-heterocycles by methyl iodide using reported procedures.[14] Details regarding the synthesis and characterization of these squaraine dyes are described in Section 4.5.

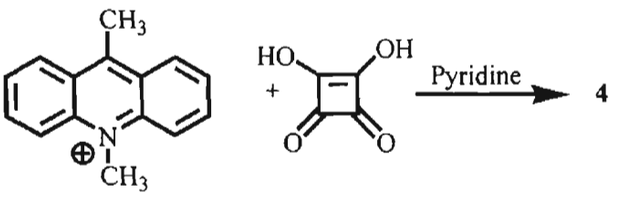

Scheme 4.1

4.3.2. Absorption and Emission properties

Figure 4.1 shows the absorption spectra of the dyes (**2-5**) in methanol. A systematic bathochromic shift in the absorption bands is observed with increase in the extent of conjugation. A shift of nearly 80 nm in the absorption maximum is observed on changing the *N*-heterocyclic substituent from 2,3,3-trimethyl indolinine (**2**) to quinoline(**3**). A further shift of 100 nm occurs when the quinoline moiety is linked to the rest of the molecule through a *para*-substituted methylene group (**4**). This may be attributed to an increase in the conjugation

length in **4** compared to that of **3**. Introduction of an additional double bond is known to bring about 100 nm shift in the absorption maxima of cyanine type dyes.[15]

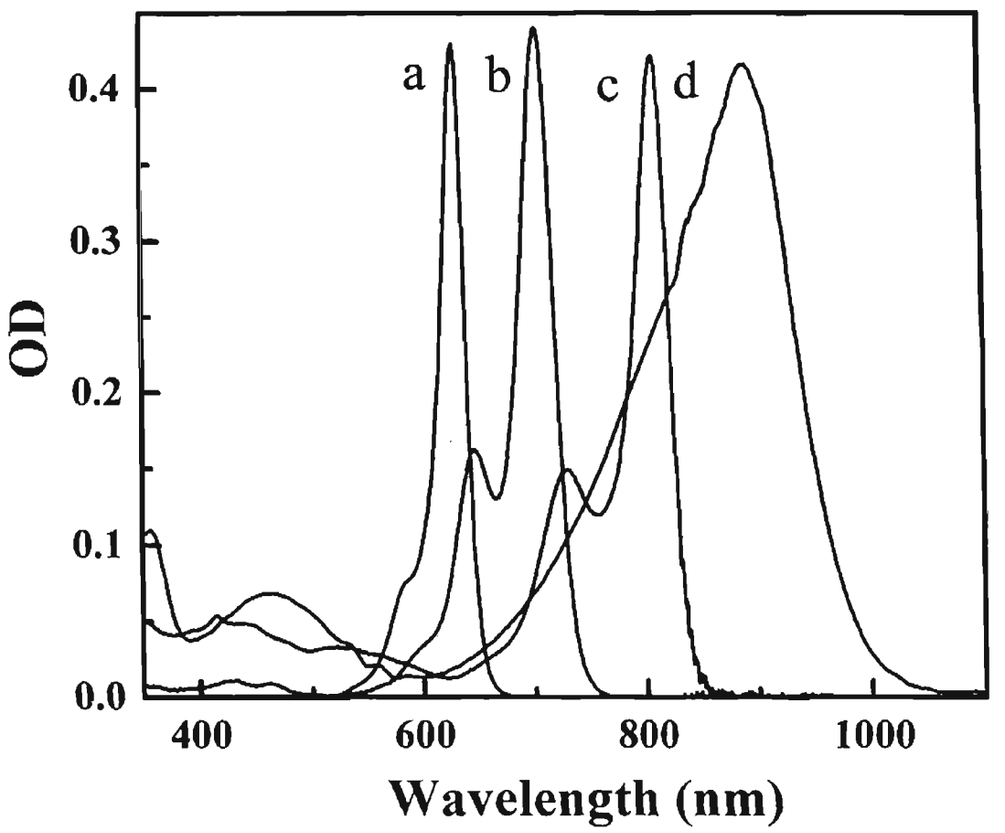

Figure 4.1. Absorption spectra of a) **2**; b) **3**; c) **4**; and d) **5** in methanol, normalized at their maxima

Interestingly, an additional shift of 100 nm is observed for the absorption maximum of **5**, although the conjugation length remains the same. The absorption band of **5** with a maximum centred on 900 nm is substantially more red-shifted than that of squaraine dyes reported in the literature.[5] The shift may be attributed

partly to the acridinium moiety being a much stronger electron donor than the quinolinium moiety.[16] Apart from a few dyes possessing absorption maxima in the 800-820 nm region, absorption maxima of most squaraines reported in literature fall in the 500 – 800 nm region. The spectral band half widths of these dyes were 342 cm^{-1}, 415 cm^{-1}, and 307 cm^{-1}, for **2**, **3**, and **4**, respectively whereas for **5**, the half band width is much larger (842 cm^{-1}).

Figure 4.2 shows the absorption spectra of **5** in solvents of varying polarity. A small hypsochromic shift in the absorption maximum with increase in the solvent polarity is indicative that the ground state of the dye is more polar than the excited state.

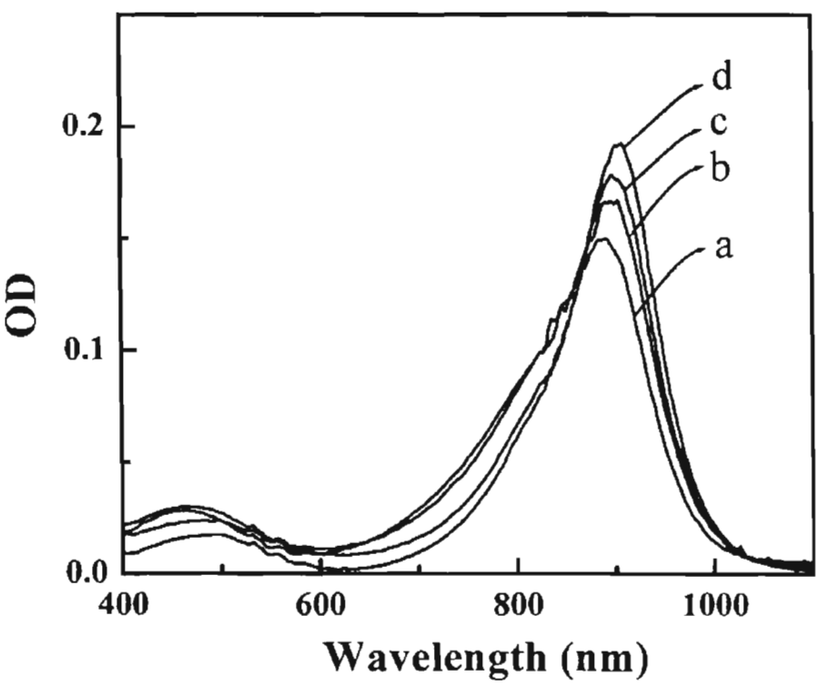

Figure 4.2 Absorption spectra of **5** in a) methanol, b) ethanol, c) 2-propanol and d) 1-butanol

A similar observation was made for the other dyes. Squaraine dyes containing methylene spacer groups are known to show hypsochromic shifts in their absorption and emission spectra with increasing solvent polarity.[12,17] The absorption properties of **5** in various solvents are listed in Table 4.1.

Table 4.1. Absorption properties of 5

Solvent	λ_{max} (abs nm)	ε ($M^{-1}cm^{-1}$)
Acetonitrile	891	45000
1-Butanol	907	52400
Dichloromethane	910	69400
Ethanol	903	46500
2-Propanol	898	53300
Methanol	892	41000

The fluorescence spectra of **2-4** in methanol are shown in Figure 4.3. The dye **2** shows a weak fluorescence band (ϕ_f = 0.036) in methanol with a maximum centred on 633 nm.[12] The shoulder in the red region is interpreted as a vibronic band, similar to the shoulder in the blue region of the absorption band. Gude and Rettig have shown that the fluorescence quantum yield of this dye decreases with increase in solvent polarity. From a ϕ_f value of 0.378 in a relatively non-polar solvent such as toluene, ϕ_f drops to 0.036 in methanol.[12] The quinolinium derivatives **3** and **4** are very weakly fluorescent (Figure 4.3). The fluorescent

quantum yield of **3** is 3 x 10^{-4} in methanol. Due to the poor spectral response of the fluorescence spectrometer beyond 750 nm the fluorescence quantum yields of **4** as well as the fluorescence spectrum of **5** could not be measured.

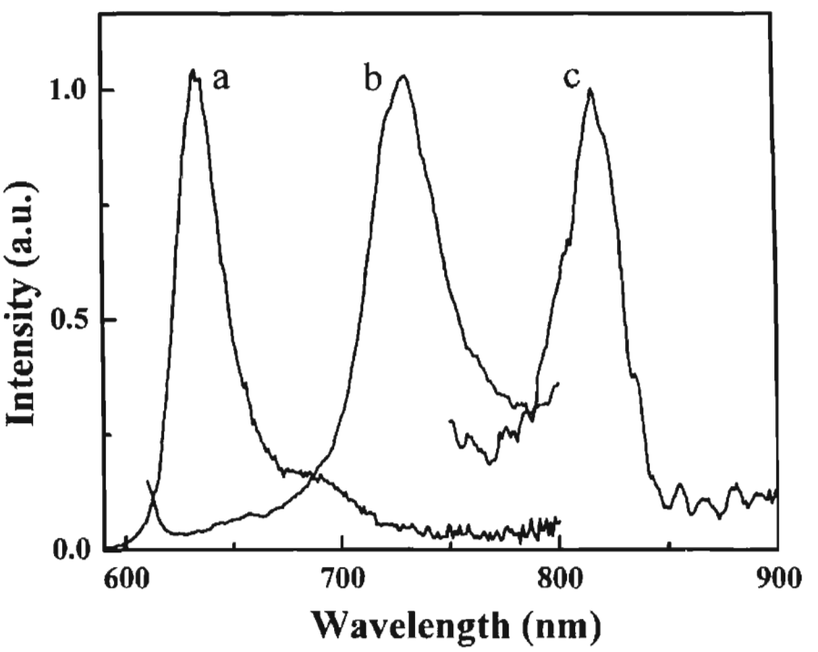

Figure 4.3. Emission spectra of a) **2**; b) **3**; and c) **4** in methanol.

The absorption and emission maxima of **3** as well as the quantum yield of fluorescence measured in different solvents are shown in Table 4.2. The absorption and emission maxima show a hypsochromic shift, with increasing solvent polarity, Figures 4.4 and 4.5 show the absorption and emission bands in various alcoholic solvents. The dependence of the absorption and emission maximum on solvent polarity parameter in protic and non-protic solvents are shown in Figures 4.6 and 4.7, respectively. The hypsochromic shift observed with increasing solvent polarity

is similar to those reported earlier for squaraine dyes, belonging to this class.[12,17] The changes in fluorescence quantum yield, as a function of solvent polarity was however found to depend upon the nature of the solvent. For aprotic solvents, the fluorescence quantum yield was observed to increase slightly with increase in solvent polarity (Figure 4.8), whereas, in protic solvents the quantum yield of fluorescence decreases substantially with increasing solvent polarity.

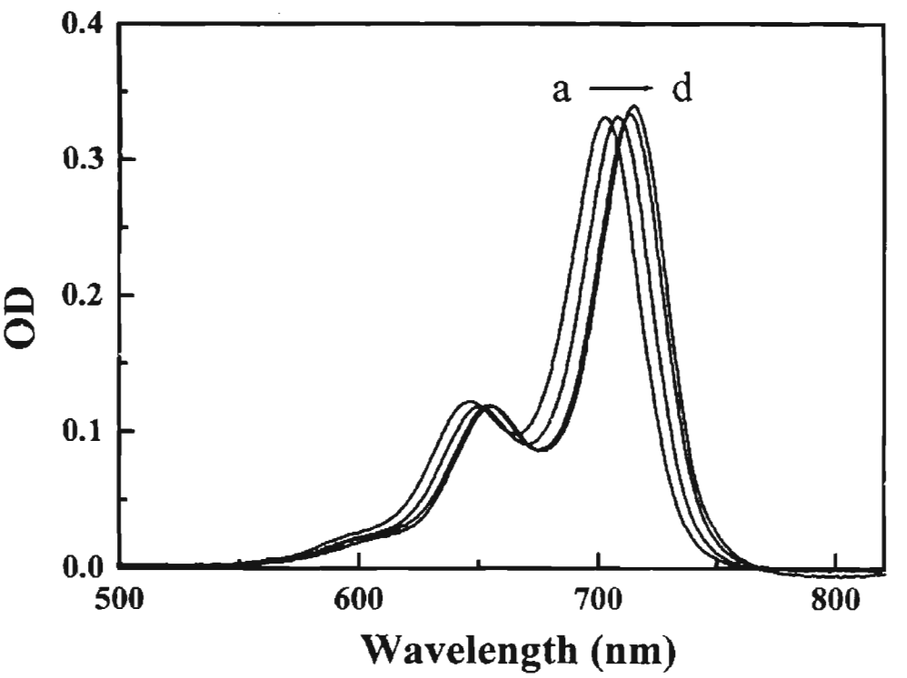

Figure 4.4. Absorption spectra of **3** in alcoholic solvents a) methanol, b) ethanol, c) isopropanol, and d) 1-butanol

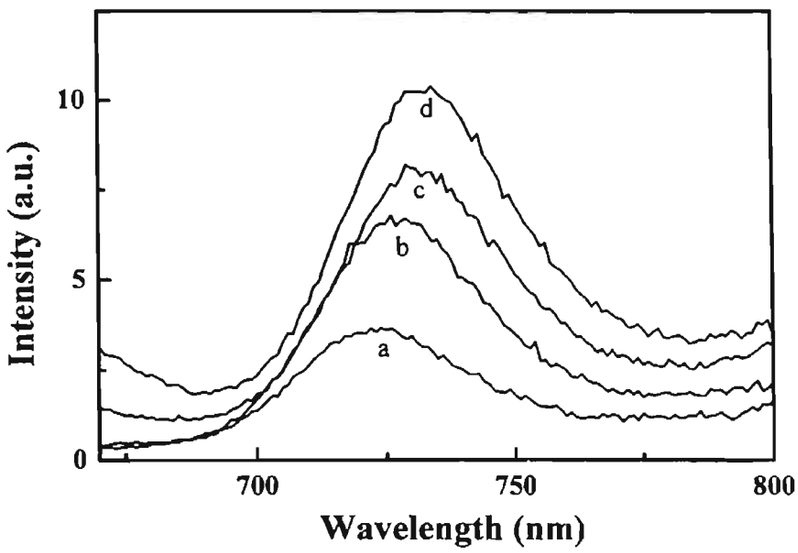

Figure 4.5. Emission spectrum of **3** in a) methanol, b) Ethanol, c) Isopropanol, and d) 1-butanol

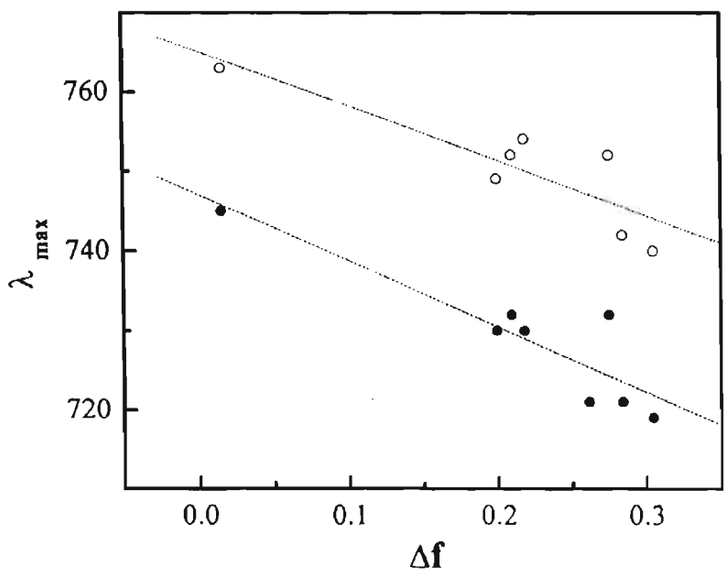

Figure 4.6. Plot of wavelength maxima of (●) absorption and (o) emission of **3** vs Δf in aprotic solvents

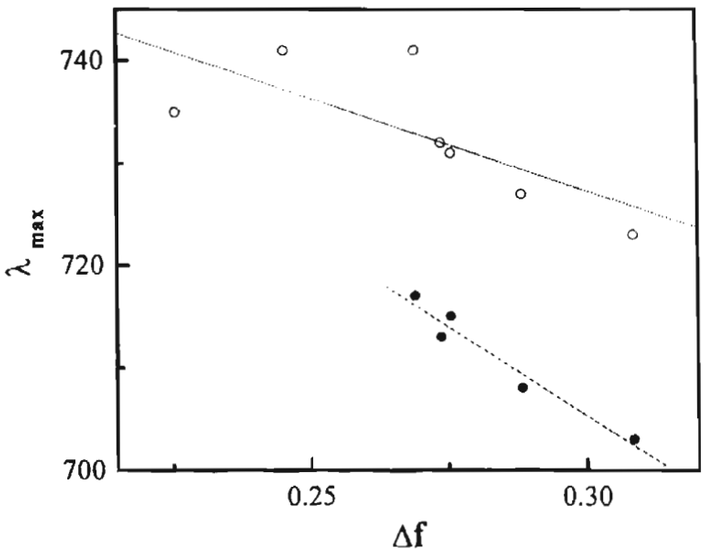

Figure 4.7. Plot of wavelength maxima of (●) absorption and (o) emission of **3** *vs* Δf in protic solvents

The solvent dependence of fluorescence of polycyclic monoazines has been interpreted as involving the interchange of the lowest n-π* singlet excited state in hydrocarbon solvents to the lowest π-π* singlet state in hydroxylic solvents due to hydrogen bonding.[18] It is well known that electronic relaxation of acridine for example, depends on the nature of solvents. Acridine fluoresces in protic solvents such as water and alcohols but not in aprotic solvents such as hydrocarbons, at room temperature. The solvent dependence of the fluorescence quantum yield of acridine was interpreted in terms of hydrogen bond interactions, which causes an interchange of the electronic character in the lowest excited singlet state from π-π* in protic solvents to n-π* in aprotic solvents. The work of Coppens and coworkers on acridines,[19] suggests that the n-π* singlet state is slightly higher than the π-π*

singlet state in polar solvents, in agreement with some other theoretical and experimental studies.[20,21] However, Whitten and Lee[22] proposed lower n-π* states irrespective of polarity.

Table 4.2. Absorption and emission characteristics of compound 3 in various solvents

Solvent	Δf	λmax abs (ε x 10^{-4} $M^{-1}cm^{-1}$)	λ max ems	Quantum yield x 10^3
Toluene	0.01503	745 (6.83)	763	0.098
DMF	0.2753	732 (9.52)	752	0.37
THF	0.20957	732 (8.2)	752	0.38
Acetonitrile	0.30499	719 (5.21)	740	0.096
Methanol	0.30854	703 (12.1)	723	0.37
Ethanol	0.28844	708 (9.18)	727	0.76
2-propanol	0.27387	713 (9.16)	732	0.7
1-Butanol	0.27565	715 (9.16)	731	0.81
Acetone	0.28427	721	742	0.30
Ethyl acetate	0.19964	730	749	0.14
1-Octanol	0.22565		735	2.6

Even in the absence of precise information about relative positions of π-π* and n-π* singlet states, it can be assumed that these two states being very close are strongly mixed by vibronic coupling irrespective of the order of levels. It has been emphasized[23] that vibronic coupling may be more important in deactivation *via* internal conversion of first excited singlet state of nitrogen heterocyclic compounds.

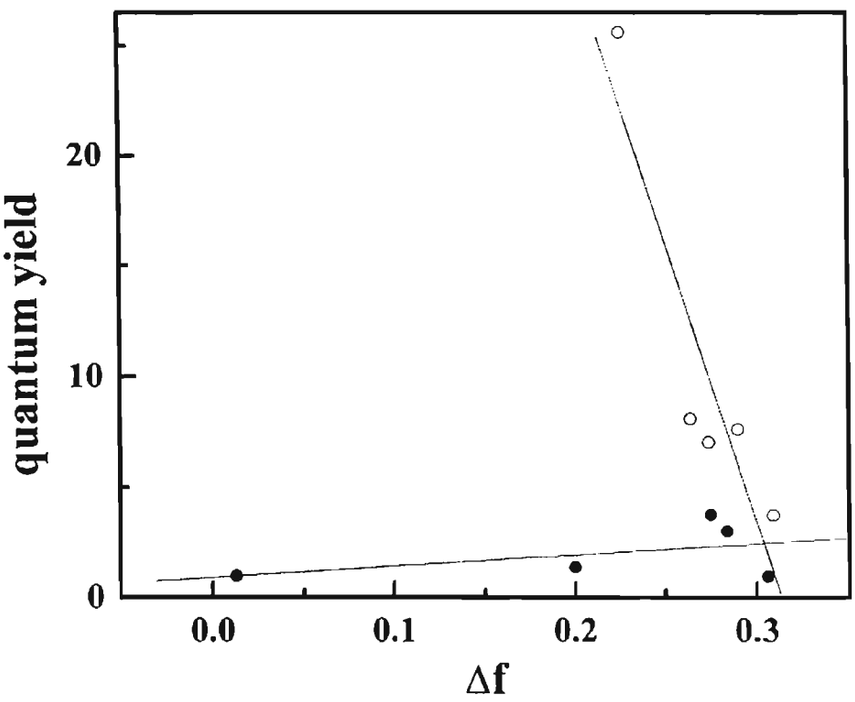

Figure 4.8. Plot of fluorescence quantum yield (●) in aprotic and (o) in protic solvents *vs* Δf for **3**

The dependence of fluorescence quantum yields of **3** in protic and aprotic solvents are also indicative of close lying n-π* and π-π* states. In aprotic solvents the lowest excited state is expected to be an n-π* state where a marginal increase

in fluorescence quantum yield with increase in solvent polarity is observed. In protic solvents the fluorescence quantum yield of **3** decreases substantially with increase in solvent polarity and this may be attributed to the destabilization of the n-π^* state due to hydrogen bonding.

For most of the squaraine dyes which have been reported the lowest excited state is a π-π^* state and in such dyes a systematic decrease in fluorescence quantum yield is observed with increase in solvent polarity, both in protic and aprotic solvents.

4.3. 3. Triplet Excited State Properties

Nanosecond laser flash photolysis experiments were carried out in order to characterize the triplet states of these dyes. Squaraine dyes are generally known to possess very low intersystem crossing efficiencies. The absence of any transient signal following direct excitation of **2** using 355 nm laser pulse is indicative of low triplet quantum yields for this dye as well. In order to characterize the triplet excited state of this dye, its triplet excited state was generated *via* energy transfer from the triplet excited state of pyrene aldehyde. Figure 4.9 shows the transient absorption spectrum obtained following laser pulse excitation of a deaerated methanolic solution of **2** and pyrene aldehyde.

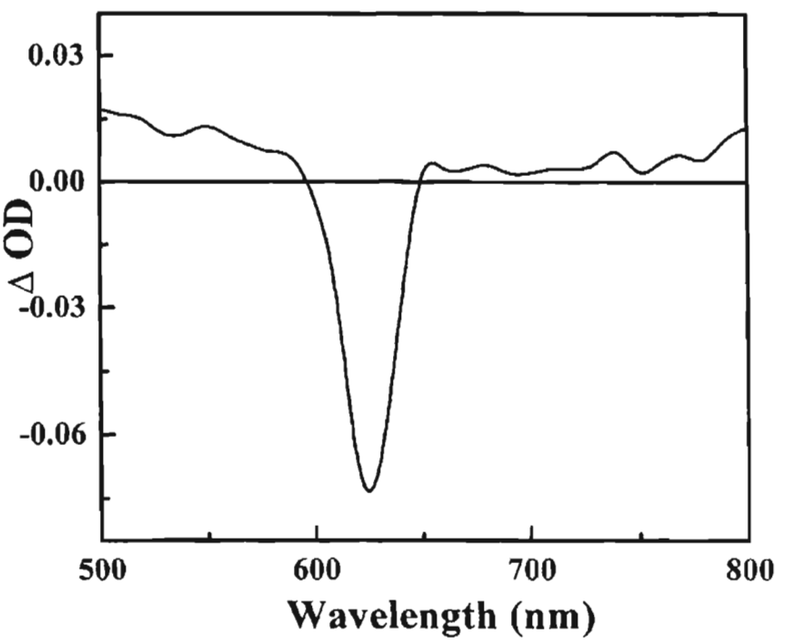

Figure 4.9. Triplet absorption spectrum of **2** generated by energy transfer from the triplet excited state of pyrene aldehyde by laser pulse excitation (355 nm, 10 ns, 60 mJ/pulse) of a deaerated solution containing pyrene aldehyde and **2** in acetonitrile.

A bleach is observed in the region were the ground state of **2** has strong absorption and a transient absorption due to its triplet excited state is observed around 500 – 600 nm. The bleaching of the ground state absorption of the dye and its triplet arising due to energy transfer from pyrene aldehyde, followed at 630 nm is shown in Figure 4.10.

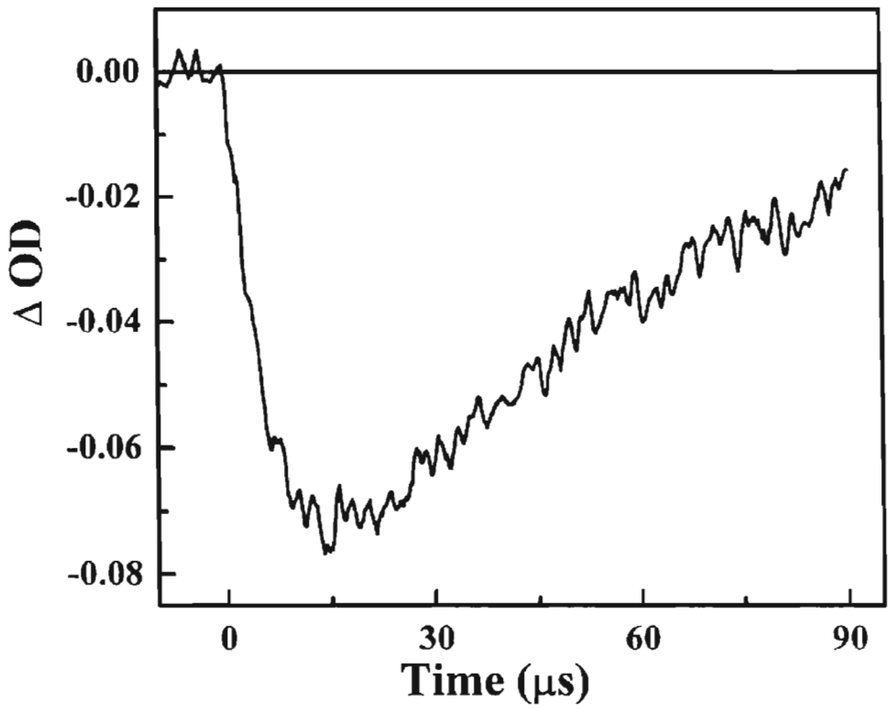

Figure 4.10. Growth and recovery of the bleach at 630 nm on laser pulse excitation of **2** and pyrene aldehyde in deaerated acetronitrile.

The triplet excited states of **3** and **5** were also investigated using nanosecond laser flash photolysis. Unlike **2**, the formation of the triplet excited state could be observed following direct excitation of **3** and **5**. Figure 4.11 shows the transient absorption profile at 690 nm, following laser pulse excitation of **3** in deaerated methanol. A fast depletion occurs within the laser pulse duration. The recovery of the bleach occurs with a lifetime of 1.4 ms. In aerated solutions the recovery is much faster, suggesting that the transient species formed may be the triplet excited state. Due to the weak nature of transient signals, the transient

absorption spectrum could not be recorded. For similar reasons the transient spectra following excitation of **5** could not be recorded.

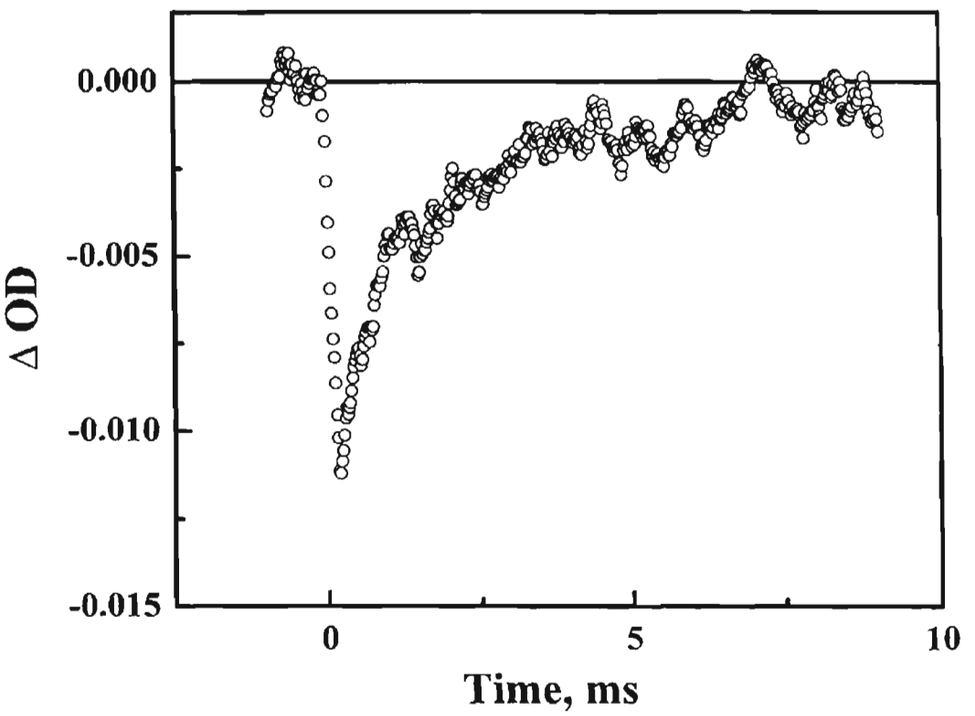

Figure 4.11. Recovery of the bleach measured at 690 nm laser pulse excitation (355 nm, 10 ns, 60 mJ/pulse) of **3** in deaerated methanol.

The formation of triplet excited states, following direct excitation of **3** and **5** was however confirmed *via* triplet energy transfer to β-carotene. Figure 4.12 shows the transient absorption profile, following laser pulse excitation of a deaerated methanolic solution of **3** containing β-carotene at 520 nm where the β-carotene triplet has a strong absorption. The growth and decay of the β-carotene triplet can also be observed on excitation of **5** in the presence β-carotene (Figure

4.13). Since the intersystem crossing efficiency of β-carotene is negligible formation of its triplet state can occur only *via* energy transfer from the triplet excited state of the dyes. Using procedures described in Chapters 2 and 3, the triplet quantum yields of the dyes **3** and **5** were determined to be 0.2 and 0.15, respectively.

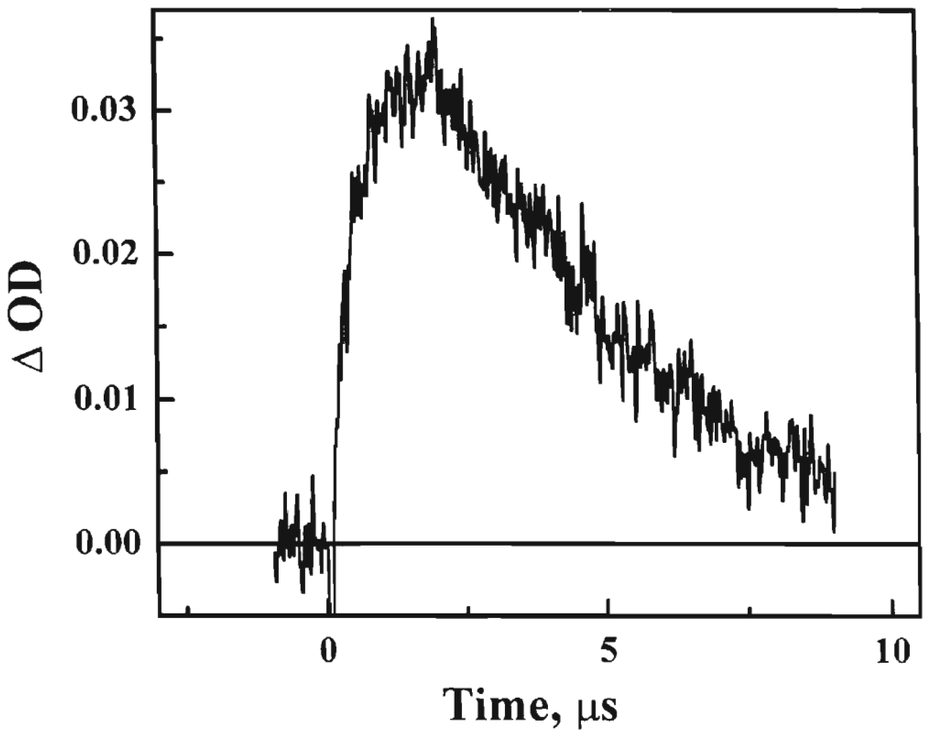

Figure 4.12. Growth and decay of β-carotene triplet excited state observed at 520 nm on laser pulse excitation(355 nm, 10 ns, 60 mJ/pulse) of **3** in deaerated methanol containing 58 μM β-carotene.

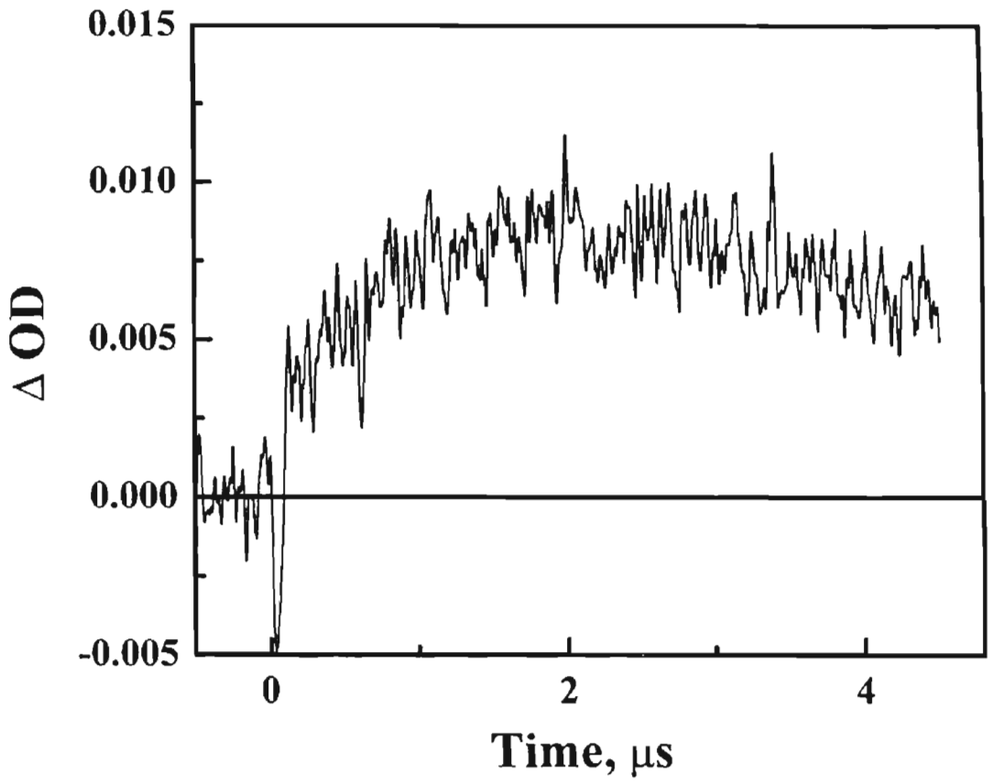

Figure 4.13. Growth and decay of the β-carotene triplet excited state observed at 520 nm on laser pulse excitation (355 nm, 10 ns, 60 mJ/pulse) of **5** in deaerated methanol containing 65 μM β-carotene.

4.4. Conclusion

Preliminary studies on the photophysical properties of squaraine dyes containing nitrogen bearing heterocyclic substituents have been carried out. These studies indicate that the lowest excited state of most of these dyes (**3-5**) have n-π* character in aprotic solvents, whereas it is of π-π* state in polar solvents. The close lying n-π* and π-π* state enhances the intersystem crossing efficiencies and substantial triplet quantum yields could be observed for **3** and **5**.

4.5. Experimental Section

All melting points are uncorrected and were determined using Aldrich Mel-Temp melting point apparatus. The electronic absorption spectra were recorded on Shimadzu 3101 UV-visible-NIR spectrophotometer. Quantum yields of fluorescence were measured by relative methods using optically dilute solutions. DOTC iodide (fluorescence quantum yield $\phi_f = 0.49$) in ethanol was used as standard.[24] Solvents used were purified before use. All experiments were carried out at room temperature.

2,3,3-Trimethylindolinine, 2-Methylquinoline, 4-methylquinoline, and squaric acid (Aldrich) were used without further purification for the synthesis of **2-4**. β-Carotene (Aldrich) was recrystallized from a mixture of benzene and methanol. Benzophenone was used as standard for triplet quantum yield measurements without further purification.

4.5.1. Synthesis

The corresponding salt of the *N*-heterocycles were prepared[14] by heating them with methyl iodide for 20 h in a molar ratio of 2: 3. The products were recrystallized from methanol to give the pure salts.

The squaraine dye (**2-4,** Chart 4.2) were synthesized adopting methods similar to those reported in the literature.[13] These compounds were synthesized by refluxing the appropriate salt (2.95 mmol) and squaric acid (1.5 mmol) in a solvent mixture (1:2.5) of benzene and 1-butanol in presence of quinoline, accompanied by azeotropic distillation of water.

Compound **2**: mp 300-301 ^{0}C, (lit –301.5 ^{0}C), UV λ_{max} (CH_3OH) 630 nm, exact mass cald. for $C_{28}H_{28}N_2O_2$ 424.2151; found, 424.2155

Compound **3**: UV λ_{max}(CH_2Cl_2) 730 nm (90500 $M^{-1}cm^{-1}$); ^{1}H NMR ($CDCl_3$) δ 3.7 (s, 3H, N-CH_3), 5.8 (S, 1H, vinylic), 7.2-7.35 (m, 6H, aromatic); exact mass calculated 392.1525, found 392.1519

Compound **4**: UV λ_{max} (CH_3OH) 806 nm, exact mass calculated 392.1525; found 392.1506

Compound **5** was synthesized by refluxing 6-methylacridinium iodide and squaric acid (1.5 mmol) for 10 h in a solvent mixture (1:2.5) of benzene and 1-butanol in presence of pyridine accompanied by azeotropic distillation of water.

Compound **5**: UV λ_{max} (CH_3OH) 892 nm, IR ν_{max} (KBr) 2937, 1739, 1707, 1633, 1580, 1564, 1499, 1475, 1254, 1253, 1176, 1130, 1051, 756 cm^{-1}. ^{1}H NMR ($CDCl_3$) δ 3.26 (s, N-CH_3), 6.55-7.25 (m, aromatic); exact mass calculated 492.184; found 492

4.5.2. Laser Flash Photolysis

Laser flash photolysis experiments were carried out using the third harmonic (355 mm, 60 mJ) of a Nd: YAG laser GCR-12 series, Quanta Ray of 10 ns pulse width. The kinetic absorption spectrophotometer used to detect the optical density changes after laser excitation (LKS-20, Applied Photophysics) has been described earlier.[25] The analyzing and laser beams were fixed at right angles to each other.

4.6. Reference

1. Tam, A. C., *Appl. Phys. Lett.* **1980**, *37*, 978.
2. Emmelius, M.; Pawlowski, G.; Vollmann, H. W., *Angew. Chem. Int. Ed. Engl.* **1989**, *28*, 1445.
3. Piechowski, A. P.; Bird, G. R.; Morel, D. L.; Stogryn, E. L., *J. Phys. Chem.* **1984**, *88*, 934.
4. Piechowski, A. P.; Bird, G. R.; Morel, D. L.; Stogryn, E. L., *J. Phys. Chem.* **1984**, *88*, 934.
5. Das, S.; Thomas, K. G.; George, M. V., in *Molecular and Supramolecular Photochemistry: Organic Photochemistry Volume 1*, (Ed.: Ramamurthy, V., Schanze, K. S.), **1997**, 467.
6. Liu, D.; Kamat, P. V.; Thomas, K. G.; Thomas, K. J.; Das, S.; George, M. V., *J. Chem. Phys* **1997**, *106*, 6404.
7. Sauve, G.; Kamat, P. V.; Thomas, K. G.; Thomas, K. J.; Das, S.; George, M. V., *J. Phys. Chem.* **1996**, *100*, 2117.
8. Detty, M. R.; Merkel, P. B., *J. Am. Chem. Soc.* **1990**, *112*, 3845.
9. Ramaiah, D.; Joy, A.; Chandrasekhar, N.; Eldho, N. V.; Das, S.; M. V. George, *Photochem. Photobiol.* **1997**, *65*, 783.
10. Turro, N. J. in *Modern Molecular Photochemistry*, The Benjamin/Cummings Publishing Company, California, **1978**, 118.
11. Das, S.; Thomas, K. G.; Thomas, K. J.; Madhavan, V.; Liu, D.; Kamat, P. V.; George, M. V., *J. Phys. Chem.* **1996**, *100*, 17310.

12. Gude, C.; Rettig, W., *J. Phys. Chem. A* **2000**, *104*, 8050.

13. Sprenger, H. E.; Ziegebien, W., *Angew. Chem. Int. Ed. Engl.* **1967**, *6*, 553.

14. Mills, W. H., *J. Chem. Soc.* **1922**, *121*, 455.

15. Matsuoka, M., in *Infrared absorbing dyes*, (Ed.: Matsuoka, M.), Plenum Press, New york, **1990**, 19.

16. Griffiths, J., in *Chemistry of Functional Dyes*, (Ed.: Yoshida, Z., Shirota, Y.), *Vol. 2,* Mita press, Tokyo, **1992**, 1.

17. Das, S.; Thomas, K. G.; Ramanathan, R.; George, M. V.; Kamat, P. V., *J. Phys. Chem.* **1993**, *97*, 13625.

18. Sidman, J. W., *Chem. Rev.* **1958**, *58*, 689.

19. Coppens, G.; Gillet, C.; Nasieski, J.; Donckt, E. V., *Spectrochim Acta* **1962**, *18*, 1441.

20. Wilkinson, F.; Dubois, J. T., *J. Chem. Phys.* **1968**, *48*, 2651.

21. Goodman, L.; Harrell, R. W., *J. Chem. Phys.* **1959**, *30*, 1131.

22. Whitten, D. G.; Lee, Y. J., *J. Am. Chem. Soc.* **1971**, *93*, 961.

23. Li, Y. H.; Lim, E. C., *Chem. Phys. Lett.* **1971**, *9*, 279.

24. *Kodak Laser Dyes*, Eastman Kodak Company, Kodak Publication, New York, **1987**.

25. Ramaiah, D.; Cyr, D. R.; Barik, R.; Gopidas, K. R.; Das, P. K.; George, M. V., *J. Phys. Chem.* **1992**, *96*, 1271.